

**DEVELOPMENT AND BIOLOGICAL EVALUATION OF  
CARBONIC ANHYDRASE MODULATORS AS  
POTENTIAL NOOTROPICS  
AND ANTICANCER AGENTS**

---

**A Dissertation  
Submitted to  
the Temple University Graduate Board**

---

**In Partial Fulfillment  
of the Requirement for the Degree  
DOCTOR OF PHILOSOPHY**

---

**By  
Rajesh Kishore Kumar Sanku  
May 2018**

Examining Committee Members:

Dr. Marc A. Ilies, Advisory Chair

Dr. Ellen A. Walker, Pharmaceutical Sciences

Dr. Daniel J. Canney, Pharmaceutical Sciences

Dr. Reza Fassihi, Pharmaceutical Sciences

Dr. Clementina Mesaros, External member, University of Pennsylvania

©  
Copyright  
2018

by

Rajesh Kishore Kumar Sanku  
All Rights Reserved

## ABSTRACT

Cancer is the second most common cause of death in the world. One of the objectives of this thesis is to biologically evaluate a series of anti-cancer polymeric aromatic/heterocyclic bis-sulfonamides and pyridinium sulfonamides which were synthesized from three established aminosulfonamide carbonic anhydrase (CA, EC 4.2.1.1) inhibitor pharmacophores. Testing of these novel inhibitors and their precursors against a panel of membrane-bound CA isoforms, including tumor-overexpressed CA IX and XII and cytosolic isozymes, identified nanomolar-potent inhibitors against both classes and several compounds with medium isoform selectivity. In the case of pyridinium sulfonamides we used complexes of the inhibitors with cyclodextrins or sulfocalixarene to enhance aqueous solubility for biological testing. The ability of CA inhibitors to kill tumor cells overexpressing CA IX and XII was tested under normoxic and hypoxic conditions, using 2D and 3D in vitro cellular models. The study identified a nanomolar potent PEGylated bis-sulfonamide CA inhibitor (**25**), as well as cyclodextrin and sulfocalixarenes complexes, which were able to significantly reduce the viability of colon HT-29, breast MDA-MB231, and ovarian SKOV-3 cancer cell lines, thus revealing the potential of polymer conjugates in CA inhibition and cancer treatment.

As a different disease state yet still a concern, cognitive dysfunction markedly impacts patients with a host of psychiatric conditions including attention deficit hyperactivity disorder, autism spectrum disorder, drug addiction, schizophrenia, depression, bipolar disorder, obsessive-compulsive disorder, and of course, Parkinson's and Alzheimer's diseases and other types of dementia. Another

objective of this thesis was to profile several series of bis-imidazoles for physicochemical, in-vitro and in-vivo properties as potential memory and learning enhancers (nootropics). Biological testing on eight isozymes of carbonic anhydrase (CA) present in the human brain revealed compounds with nanomolar potency against at least one membrane bound, cytosolic or mitochondrial CA isozymes, combined with good physicochemical properties. We also identified lead compounds with the ability to rescue experimental animals from drug induced memory deficits, using an optimized Novel Object Recognition Task (NORT) procedure.

## DEDICATIONS

To my parents, and to my  
beloved school teacher  
Sr. Princily Paul.

## ACKNOWLEDGMENTS

Finally, I have come to the end of my Ph.D. journey. This experience might not have been rewarding without the help/association of many people.

First and foremost, I would like to express my most profound gratitude to my supervisors, Dr. Marc A. Ilies and Dr. Ellen A. Walker for their guidance into every step of my research. I know that without their encouragement and support this dissertation would not have been possible. They taught me to think freely and work independently. Their contribution to science is of highest standard, and I am proud to be part of their collaborative work. They provided me with guidance and reality checks when I needed them. Besides science, they are my best friends talking about my career outside sciences and other subjects, and they are also like my parents giving me useful suggestions for my personal growth in the USA. I could not have imagined having better PIs for my Ph.D. study.

I owe my sincere thanks to the members of my dissertation advisory committee, Dr. Daniel Canney, Dr. Reza Fassihi and Dr. Clementina Mesaros - without their knowledge and constructive suggestions this thesis would not have been complete. I am also grateful to Dr. John (Jack) Gordon for training me in different aspects of compound profiling and allowing me to use their lab facilities and equipment whenever required. I would like to give a special mention to Almira and Sophon Din, administrative assistants, for taking care of our paperwork precisely so that I was able to focus on my research.

This work became more impactful with the inputs from our collaborators, Dr. Claudiu T. Supuran (University of Florence), Dr. Daniela Vullo (University of Florence),

Dr. Muniswamy Madesh (Temple University), Dr. Mary F. Barbe (Temple University) and Dr. Erik R Swenson (University of Washington).

I address my special thanks to the Temple University School of Pharmacy for a full Ph.D. fee waiver and Teaching Assistantship, being aware that without this funding I would not be able to finish my Ph.D. I would like to thank Graduate student advisor, Dr. Daniel Canney and the Dean, Dr. Peter Doukas, for providing me with an opportunity and the appropriate resources to pursue my graduate studies.

I wish to express my sincere gratitude to Dr. Punna Rao Ravi, Dr. Yogeeswari, Dr. Aditya N, and Dr. Venkata Vamsi Venuganti, my mentors, and professors of my B. Pharm (Hons.) who always encouraged me to seek higher education.

My special thanks to Sr Princily Paul, my school teacher for motivating and inspiring me right from my childhood. She continues to give me strength and always directs me to god despite of all the obstacles life has thrown at me. I would like to thank her for teaching me moral-sciences at my tender age, which helped me be a strong person from inside.

The past five years would not have been as meaningful without the lab mates from Dr. Ilies and Dr. Walker labs. Vishnu, Suleyman, Utpal, Uttam, Ahmed, Iman, Dr. Bogdan Draghici, Dr. Ozlem Karakus, Andy, Matthew, and Chidubem- I cherish my relationship with each one of you and wish all of you success and happiness. I have learned many things from them during the lab meetings and classes. I have a load of memories with them both inside the lab and outside.

I would also like to acknowledge my students, Taylor, Nicole, Antony, Betty, Jonathan, Marvin, Stan, Yang, Weiyu, Besar, Matthew, Andrew, Brendan, Matty,

Shuhuan, Vallabhi, Ashley, and Elaine - all for their extended research support promptly. I have learned a lot from them through their personal and scholarly interactions.

I would like to thank all my close friends across the globe for continually sending me their love and words of support. I am indebted to Hari, Jagadish, Varun, and Chaitanya. They have supported me during the good and bad throughout my Ph.D. studies. I thank all the fellas 2.0s-Ramki, Vinay, Sri Ram, Rahul and Nanda in United States. I cannot imagine my life in the US without them. Trips with them in a timely manner made my stress levels go to zero.

Last, but not least, my love and respect for their unconditional support and patience during my absence and understanding go to my parents, my mother, Kanaka Durga and my father, Satyanarayana. I am also very much indebted to my uncle Satyanarayana (deceased) and aunt Krishnaveni, who supported me all these years with their positive energy.

## TABLE OF CONTENTS

<b>ABSTRACTS.....</b>	<b>iii</b>
<b>DEDICATION.....</b>	<b>v</b>
<b>ACKNOWLEDGEMENTS.....</b>	<b>vi</b>
<b>LIST OF TABLES.....</b>	<b>xi</b>
<b>LIST OF FIGURES.....</b>	<b>xii</b>
<b>LIST OF SCHEMES AND CHARTS.....</b>	<b>xx</b>
<b>ABBREVIATIONS.....</b>	<b>xxi</b>
<b>LIST OF PUBLICATIONS.....</b>	<b>xxiii</b>
<b>LIST OF PRESENTATIONS AND POSTERS.....</b>	<b>xxiv</b>

## CHAPTERS

<b>1 OVERVIEW AND MAIN RESEARCH GOALS.....</b>	<b>1</b>
<b>2 INTRODUCTION.....</b>	<b>4</b>
<b>3 DEVELOPMENT AND BIOLOGICAL EVALUATION OF CARBONIC ANHYDRASE ACTIVATORS AS POTENTIAL NOOTROPICS .....</b>	<b>13</b>
<b>Background and Rationale.....</b>	<b>14</b>
<b>Materials and Methods.....</b>	<b>31</b>
<b>Results and Discussion.....</b>	<b>42</b>
<b>Conclusions.....</b>	<b>70</b>
<b>3. DEVELOPMENT AND BIOLOGICAL EVALUATION OF CARBONIC ANHYDRASE INHIBITORS AS POTENTIAL ANTI-CANCER AGENTS.....</b>	<b>72</b>

<b>Background and Rationale.....</b>	<b>73</b>
<b>Materials and Methods.....</b>	<b>88</b>
<b>Results and Discussion.....</b>	<b>91</b>
<b>Conclusions.....</b>	<b>98</b>
<b>4. SUMMARY AND FUTURE STUDIES OF CA MODULATORS.....</b>	<b>99</b>
<b>BIBLIOGRAPHY.....</b>	<b>101</b>

## LIST OF TABLES

Table	Page
1. The human CA isozymes currently known, with their tissue/organ localization/distribution, catalytic activity, subcellular localization and physiologic role.....	8
2. The human CA isozymes currently known isozymes related to CNS, organ localization, distribution, cellular localization, intensity of expression and catalytic activity.....	15
3. Activation of CA isozymes (mitochondrial in brown, cytosolic in green, membrane-bound in blue) with bis-imidazole derivatives of type <b>18</b> , <b>19</b> and <b>20</b> and histamine 3, by a stopped-flow, CO <sub>2</sub> hydrase assay.....	30
4. Solubility, lipophilicity and TPSA values of different CAAs series <b>19</b> and <b>20</b> investigated, together with their optical properties (absorbance maximums) .....	45
5. Inhibition data of human CA isoforms hCA I, II, IV, IX, XII and XIV with derivatives <b>21-26</b> reported here and the standard sulfonamide inhibitor acetazolamide ( <b>ACZ</b> ) by a stopped flow CO <sub>2</sub> hydrase assay.....	84
6. Inhibition of tumor-associated hCA IX and hCA XII and off-target cytosolic hCA I and hCA II, with selected pyridinium benzenesulfonamides <b>29</b> , and with clinically used CAinhibitor acetazolamide <b>1</b> , using the CO <sub>2</sub> hydration assay.....	86

## LIST OF FIGURES

Figure	Page
<p>1. Picture depiction of subcellular localization and catalytic enzymatic activity of human <math>\alpha</math>-CAs coded as: (devoid of catalytic properties (0), low (+), high (++) activity). The cytosolic CAs, secreted (CA VI) and the mitochondrial CA VA and VB consist only of the CA domain; the membrane-associated CA IV, IX, XII and XIV have a membrane anchor and, except for CA IV, also a cytoplasmic tail, while CA IX is the only isozyme with a N-terminal proteoglycan-like domain. (e, c, m = extracellular, cytosolic and membrane).....</p>	6
<p>2. Representations depicting the X-ray crystal structure of the prototypical CA isozyme, CA II (a) showing a detailed view of its active pocket (b). Within the active site (b), the hydrophobic residues are depicted in red while the hydrophilic amino acid network is depicted in blue. Figure made using PyMol (DeLano Scientific).....</p>	10
<p>3. Schematic illustration of the catalytic mechanism of carbonic anhydrase.....</p>	12
<p>4. Carbonic anhydrase (CA) isozymes present in various CNS cells. Adapted from the reference .....</p>	16
<p>5. Conceptual model of the cognitive continuum, from normal aging to dementia.....</p>	18
<p>6. Schematics of CO<sub>2</sub> flux in hippocampal CA 1 pyramidal cell, revealing the CA isozymes involved in the process and the three different CO<sub>2</sub>/HCO<sub>3</sub><sup>-</sup> pools (extracellular (e), cytosolic (c) and mitochondrial (m)) equilibrated by them. Adapted from reference.....</p>	21

7. Long-term potentiation (LTP) increases the amount of neurotransmitter released at the synapse of the neurons and the number of receptors available for its uptake which is a vital step in the memory formation.....	24
8. Bicarbonate dependent switch of GABA-mediated synapses from excitatory input filter (inhibitory action) into an amplifier (excitatory action) depends on the catalytic activity of CA isozymes present inside and outside the cell .....	25
9. General structure of a carbonic anhydrase activator .....	27
10. Experimental design 2-object Novel Object Recognition test.....	37
11. Absorption spectrum of CA activators <b>19</b> and <b>20</b> investigated in this study. The absorbance maximum $\lambda_{\max}$ was used to determine the concentration of the compounds in different phases.....	45
12. The differentiated SH-SY5Y cell model used for cytotoxicity testing of our novel CAAs. Representative phase contrast images of proliferative (standard, non-differentiated) SH-SY5Y cells in culture medium with 10% of FBS (A) and of differentiated SH-SY5Y cells, cultured for seven days with 10 $\mu$ M RA and BDNF in culture medium with 1% of FBS (B). Note the stellate morphology and neurites in differentiated cells (400 $\times$ magnification, bar = 50 $\mu$ m). .....	47
13. Cytotoxicity of novel CAAs series <b>19</b> and <b>20</b> , assessed via WST-8 assay in differentiated SH-SY5Y cells using acetaminophen as positive control (left scale) and compound calculated lipophilicity (right scale). Each bar represents the mean $\pm$ standard deviation, determined out of 4 individual experiments.....	49

14. Uptake of compound **19e (BD117)** into neuron-like differentiated SH-SY5Y cells does not change the morphology of the cells: DIC image (left top), fluorescence image (left bottom) and superimposed DIC/fluorescence image (right) for neuron-like differentiated SH-SY5Y cells imaged after 30 min incubation time with **19e (BD117)** (10  $\mu$ M)..... 50
15. Comparative fluorescent microscopy revealing the uptake of CAA **19e (BD117)** into the brain of Swiss-Webster male mice. Representative superimposed DIC/fluorescence images of brain slices from **19e (BD117)**-treated animals (right panels) versus saline-treated animals (left panels) in 3 separate slices.....52
16. Microsomal degradation profile of **19e (BD117)** against verapamil as positive control. A half-life of greater than 60 min was observed for **19e (BD117)**. Data represented as a mean  $\pm$  standard deviation out of 3 individual experiments.....54
17. Mice learn and recognize objects one hour after being exposed to the familiar objects in the NORT assay. Time spent exploring objects by saline-treated, Swiss Webster mice (n=40) exposed to two identical objects in the acquisition trial (training phase, acquisition, A) and to one familiar object and one novel object in the retention trial (testing phase, retention, B). Testing was performed 1 h after training. Ordinate: exploration time in sec. Data are shown as mean  $\pm$  S.E. M. Significantly different (\*\*P<0.001) from familiar object as indicated by student's paired t-test.....55
18. Scopolamine, ketamine and acetazolamide produce dose-dependent disruption of memory retrieval in Swiss-Webster mice. Saline (n=40), 1.0 -10 mg/kg Scopolamine (n=6-9, per dose), 10-52 mg/kg ketamine (n=6-9, per dose) and 1.0-10 mg/kg Acetazolamide (n=6-9, per dose) were injected after the training phase (right panel). Saline was injected 30 min prior to training phase (Familiar vs. Familiar) and scopolamine/acetazolamide/ketamine injections occurred immediately after training phase and 1 h prior to testing phase (Familiar vs. Novel). Ordinate:

exploration time in sec. Data are shown as mean  $\pm$  S.E.M. Significantly different (\*, at least  $P < 0.05$ ) from familiar object as indicated by student's paired t-test. Note: the mice did not receive drug until after the training phase, however the legends are matched to data presented in the right panel. ....56

19. Impact of CAA **19e (BD117)** on recognition memory in Swiss-Webster mice, in the absence and in the presence of memory disruptors scopolamine (Sco), ketamine (Ket) and acetazolamide (ACZ), as assessed by NORT procedure (n=6-9, per dose). Upper panel: dose-response curves of **19e (BD117)**; note that doses of 0.03 and 3.0 mg/kg produced similar effects to positive control donepezil at 0.3 mg/kg. Lower panel: CAA **19e (BD117)** is able to reverse the scopolamine-, acetazolamide-, but not ketamine-induced deficits in NORT. Ordinate: exploration time in sec. Data are shown as mean  $\pm$  S.E.M. Significantly different (\*, at least  $P < 0.05$ ) from familiar object as indicated by student's paired t-test.....58

20. Impact of selected CAAs with different isozyme activation profiles on recognition memory in Swiss-Webster mice, at doses of 0.03 mg/kg, each as assessed by NORT procedure (n=6-9, per compound). Note that no adverse effects on motor activity for both training and testing phases of the NORT procedure were observed. Data are shown as mean  $\pm$  S.E.M. Significantly different (\*, at least  $P < 0.05$ ) from familiar object as indicated by student's paired t-test. ....60

21. The CAAs capacity to prevent recognition memory deficits caused by scopolamine, acetazolamide, or ketamine depends on the isozyme activation profile of the tested compounds. Time spent exploring familiar object vs. novel object in the training phase (left panel) and testing phase (right panel) of the 1h-delayed NORT procedure (n=6-9, per dose per compound). CAAs (0.03 mg/kg) were injected 30 min prior to training phase, while the amnesics scopolamine (Sco), ketamine (Ket) and acetazolamide (ACZ) were injected after the training session, at specified doses. Data are shown as mean  $\pm$  S.E.M. Significantly different (\*, at least  $P < 0.05$ ) from familiar object as indicated by student's paired t-test.....62

22. Mice acquire and retrieve a novel nose-poke response using the 1-day procedure. Effects of saline in male, Swiss Webster mice (N = 64) during session 1 (open bars) and during session 2 (closed bars). Vertical axes: (a) mean adjusted latencies calculated as the time in s from the first to the 10th reinforcer; (b) mean reinforced response rates calculated as the total number of center-hole, nose-poke responses over session time in s; (c) mean nonreinforced response rates calculated as the total number of responses in both the left and right nose-poke holes divided by the total session time in s. Total number of mice tested/number of mice completing at least five reinforcers during session 1 (64/63). Horizontal axes: Saline injections, administered intraperitoneally, either 30 min before session 1 or immediately after session 2. Significantly different (\*, at least  $P < 0.05$ ) from session 1 as indicated by paired t-test. Vertical bars represent SEM.....64
23. Scopolamine, ketamine, and acetazolamide produce different patterns of acquisition and retrieval disruption in mice. Vertical axes: (a,d,g) mean adjusted latencies calculated as the time in s from the first to the 10th reinforcer; (b,e,h) mean reinforced response rates calculated as the total number of center-hole, nose-poke responses over session time in s; (c,f,i) mean non-reinforced response rate calculated as the total number of responses in both the left and right nose-poke holes divided by the total session time in s. Horizontal axes: Saline or doses in mg/kg of scopolamine (a–c), ketamine (d–f), or acetazolamide (g–i) injected intraperitoneally immediately after session 1. (a–c) Total number of mice tested/number of mice completing five reinforcers in session 1: Saline (n=16/16), 0.01 mg/kg (n=6/6), 0.1 mg/kg (n= 9/9), 1.0 mg/kg (n= 10/10), 3.2 mg/kg (n=15/15), and 10 mg/kg (n =12/12) scopolamine. Significantly different from saline in session 2 (\*, at least  $P < 0.05$ ); significantly different from 0.01 mg/kg scopolamine in session 2 (^, at least  $P < 0.05$ ) and significantly different from 1.0 mg/kg acetazolamide in session 2 (^, at least  $P < 0.05$ ). Vertical bars represent SEM.....66

24. Dose response curves of **19e (BD117)** and **18c (MAI27)**. Horizontal axes: saline or doses in mg/kg **19e (BD117)** (upper panel), **18c (MAI27)** (lower panel) injected intraperitoneally 30 min before session 1. (upper panel) Total number of mice tested/number of mice completing at least five reinforcers in session 1: Saline (n=23/23), 0.03 mg/kg (n =7/7) and 0.3 mg/kg (n= 8/8) **19e (BD117)**. (Lower panel) Total number of mice tested/number of mice completing at least five reinforcers in session 1: Saline (n=8/6), 3.0 mg/kg (n =14/12), 10 mg/kg (n= 9/5), 18 mg/kg (n =9/9), and 30 mg/kg (n =6/5) **18c (MAI27)**. Significantly different from saline (\*, at least P<0.05).....68
25. Co-administration of **18c (MAI27)** or Pretreatment of **19e (BD117)** partially protected the retention of a newly learned operant response when administered prior to the memory disrupters' ketamine and acetazolamide respectively. Horizontal axes, (upper panel): Saline, doses of 30 mg/kg **18c (MAI27)** and 10 mg/kg ketamine alone after session 1, or in combination injected together after session 1. Total number of mice tested/number of mice completing five reinforcers in session: Saline (n= 8/6), 30 mg/kg **18c (MAI27)** (n =6/6), 18 mg/kg ketamine (n =11/11), and 30 mg/kg **18c (MAI27)**+18 mg/kg ketamine (n =8/8). Significantly different from saline (\*, at least P<0.05) or 18 mg/kg ketamine (^, at least P<0.05) in session 2. Horizontal axes, (lower panel): Saline, doses of 0.03 mg/kg **19e (BD117)** injected 30 min prior to session 1, 1 and 10 mg/kg ACZ injected immediately after session 1, or in combination injected 30 min before session 1 **19e (BD117)** and immediately after session 1 (ACZ). Total number of mice tested/number of mice completing five reinforcers in session: Saline (n= 23/23), 0.03 mg/kg **19e (BD117)** (n =7/7), 1 mg/kg ACZ (n =12/12), 10 mg/kg ACZ (n=17/17), 0.03 mg/kg **19e (BD117)**+ 1 mg/kg ACZ (n=11/11) and 0.03 mg/kg **19e (BD117)** + 10 mg/kg ACZ (n=12/12). Significantly different from saline (\*, at least P<0.05) in session 2.....69
26. Differences between metabolisms of normal cells (A), as compared to tumors (B).  
Normal cells in the presence of oxygen perform oxidative phosphorylation, while the

cancer cells either in the presence or absence of oxygen overexpress glycolysis for their energetic and biosynthetic needs. ....	76
27. Uncontrolled proliferation and poor vasculature of cancer cells leads to the hypoxia. Hypoxia upregulates the HIF pathway which in turn upregulates the expression of transmembrane CA isozyme CA IX. ....	78
28. The central role played by overexpressed transmembrane CA isozymes CA IX, CA XII in tumor cells metabolism. H <sup>+</sup> ions produced via glycolysis are transported outside the cell with the help of cytosolic CA Isozymes (CA I and CA II) and transmembrane, tumor overexpressed CA isozyme CA IX. ....	79
29. Overview of the distribution of CA IX and CA XII in normal human tissues and in corresponding tumors. The intensity of the gray color reflects the presence of that particular CA isoform and its expression level .....	81
30. Schematic representation of <i>p</i> -sulfonated calix[n]arenes (H1, H2, H3, n = 4, 6, 8) selected as hosts in our complexation study, together with the three pyridinium CAIs <b>29a</b> = G1, <b>29d</b> = G2 and <b>29m</b> = G3 used as complexation guests in this study and the proposed structure of the inclusion complex between <b>H1</b> and <b>G2</b> . ....	87
31. Effect of <b>PEGylated bis-sulfonamide carbonic anhydrase inhibitors 21-26</b> and acetazolamide (ACZ), at different concentrations, on the viability of colon HT-29, breast MDA-MB231 and ovarian SKOV-3 cancer cell lines under a) normoxic (b) hypoxic and (c) 3D cell cultures (tumor spheroids) conditions. P values were determined by one-way ANOVA, comparing the value with the acetazolamide (ACZ) (*P < 0.05, **P < 0.01, ***P < 0.001). Only the statistical significant differences were shown. ....	94
32. Comparative cytotoxicity of complexes generated from calixarenes <b>H1-H3</b> and cyclodextrins <b>H4-H6</b> with guest CAIs <b>29 G1-G3</b> against normoxic (left panels), and	

hypoxic (right panels) 2D cell cultures. Acetazolamide (ACZ) was used as control..... 96

33. Comparative cytotoxicity of complexes generated from calixarenes **H1-H3** and cyclodextrins **H4-H6** with guest CAIs **29 G1-G3** against tumor spheroids. Acetazolamide (ACZ) was used as control.....97

## LIST OF SCHEMES AND CHARTS

Scheme	Page
1. Synthesis of new pyridinium 3-aminobenzene sulfonamide series.....	85

Chart	Page
1. Evolution of CA activators design and the activation potency of compounds <b>1-17</b> tested or developed previously. The specific series of CA activators <b>18</b> and <b>19-20</b> (boxed) developed for this section are used in this CA activation project to triangulate on key CA isozymes involved in learning and memory.....	28
2. CA inhibitors in clinical use, designed either for systemic use ( <b>ACZ-BZA</b> ) or for topical administration into the eye ( <b>ZNP</b> and <b>TPM</b> ).....	74
3. Bis-sulfonamide CA Inhibitors <b>21-26</b> synthesized for this study.....	83

## ABBREVIATIONS

AE:	Anion exchanger
ATP:	Adenosine triphosphate
ACZ:	Acetazolamide
BDNF:	Brain derived neurotrophic factor
BZA:	Benzolamide
CA:	Carbonic anhydrase
CAI:	Carbonic anhydrase inhibitor
CARP:	Carbonic anhydrase related proteins
DCP:	Dichlorphenamide
DDS:	Drug delivery systems
DMEM:	Dulbecco's modified eagle medium
DMSO:	Dimethyl sulfoxide
ETZ:	Ethoxzolamide
FBS:	Fetal Bovine Serum
GLUT:	Glucose transporters
HIF:	Hypoxia inducible factor
HPLC:	High performance liquid chromatography
HR-MS:	High resolution mass spectrometry
LC-MS:	Liquid chromatography-mass spectrometry
LTP:	Long term potentiation
MCI:	Mild cognitive impairment
MCT:	Monocarboxylate transporters
MTZ:	Methazolamide
NMR:	Nucleic Magnetic Resonance
NORT:	Novel object recognition test
PBS:	Phosphate buffer saline
PEG:	Polyethylene glycol
PFK-1:	Phosphofructokinase 1
RA:	Retinoic acid

SA: Sulfonamide  
SAR: Structure activity relationship  
SPR: Structure property relationship  
TPM: Topiramate  
TPSA: Topological polar surface area  
TFA: Trifluoroacetic acid  
TFE: 2,2,2-Trifluoroethanol  
UV-Vis: Ultraviolet-visible spectroscopy  
VEGF: Vascular endothelial growth factor  
VHL: Von Hippel–Lindau  
ZNA: Zonisamide

## LIST OF PUBLICATIONS

**Sanku, R.K.K.**, John, J.S., Salkovitz, M., Ilies, M.A., and Walker, E.A. Potential learning and memory disruptors and enhancers in a simple, one-day operant task in mice. *Behavioural Pharmacology* 2018, doi: 10.1097/FBP.0000000000000400 (published online March 21, 2018).

Akocak, S., Alam, M.R., Shabana, A.M., **Sanku, R.K.K.**, Vullo, D., Thompson, H., Swenson, E.R., Supuran, C.T., and Ilies, M.A. PEGylated bis-sulfonamide carbonic anhydrase inhibitors can efficiently control the growth of several carbonic anhydrase IX-expressing carcinomas. *Journal of Medicinal Chemistry* 2016, 59 (10): 5077–5088.

## LIST OF PRESENTATIONS AND POSTERS

### PRESENTATIONS

#### Extramural, peer-reviewed:

**Sanku, R.K.K.**, Karakus, O.O., Mondal, U.K., Lemon, N., and Ilies, M.A. Anti-tumor activity of several host-guest complexes of pyridinium carbonic anhydrase IX inhibitors. Abstracts of Papers AAPS National Meeting, San Diego, CA, November 11-15, 2017.

Lemon, N., **Sanku, R.K.K.**, Chung, A., Ilies, M.A., and Walker, E.A. Profiling a novel series of carbonic anhydrase activators in mouse memory assays. Mid-Atlantic Pharmacology Society, Philadelphia, PA, October 26, 2017. (2nd Place Undergraduate Poster Award).

Elezi, B., Xie, W., **Sanku, R.K.K.**, Lemon, N., Rico, M., Barrero, C., and Walker, E.A. Mouse strain comparisons in the novel location recognition test. Mid-Atlantic Pharmacology Society, Philadelphia, PA, October 26, 2017.

**Sanku, R.K.K.**, Draghici, B., Yan, P., Ilies, M.A., and Walker, E.A. Novel lipophilic carbonic anhydrase activators protect mice from recognition memory deficits produced by scopolamine” American Society of Pharmacology and Experimental Therapeutics at Experimental Biology, Chicago, IL. April 22-26, 2017.

Spoon, T., **Sanku, R.K.K.**, Ilies, M.A., and Walker, E.A. Discriminative stimulus effects of novel carbonic anhydrase activator BD117. American Society of Pharmacology and Experimental Therapeutics at Experimental Biology, Chicago, IL, April 22-26, 2017 (Undergraduate Student Travel Award winner and 1<sup>st</sup> Place Undergraduate Poster Award, Behavioral Pharmacology Division).

**Sanku, R.K.K.**, Draghici, B., Pan, P., Ilies, M.A., and Walker, E.A. Novel lipophilic carbonic anhydrase activators protect mice from recognition memory deficits produced by scopolamine. 36th Annual Meeting of the Philadelphia Area Chapter of the Society for Neurosciences, University of Pennsylvania, Philadelphia, PA, May 2017.

**Sanku, R.K.K.**, Draghici, B., Mondal, U.K., Walker, E.A., Supuran, C.T., and Ilies, M.A. Development of efficient carbonic anhydrase activators for memory impairments. 252nd ACS National Meeting, Philadelphia, PA, August 21 – 25, 2016.

Karakus, O.O., **Sanku, R.K.K.**, Mondal, U.K., and Ilies, M.A. Host-guest formulations of novel isozyme-selective carbonic anhydrase inhibitors for colon cancer detection and treatment. 252nd ACS National Meeting, Philadelphia, PA, August 21 – 25, 2016.

Akocak, S., Alam, M.R., Shabana, A.M., **Sanku, R.K.K.**, Thompson, H., Supuran, C.T., and Ilies, M.A. PEG-conjugated aromatic and heterocyclic sulfonamides as potent carbonic anhydrase inhibitors with antitumor activity. 252nd ACS National Meeting, Philadelphia, PA, August 21 – 25, 2016.

Walker, E.A., **Sanku, R.K.K.**, Salkovitz, M., Draghici, B., and Ilies, M.A. Carbonic anhydrase activation: An exploration of a novel nootropic mechanism. American Psychological Association, Denver, CO, August, 2016.

Karakus, O.O., **Sanku, R.K.K.**, Mondal, U.K., and Ilies, M.A. Toxicity of host-guest formulations of isozyme-selective carbonic anhydrase inhibitors. 44th Middle Atlantic Regional Meeting of the American Chemical Society, Riverdale, NY, United States, June 9-12, 2016, MARM-553.

**Sanku, R.K.K.**, Draghici, B., Satyal, U., Walker, E.A., and Ilies, M.A. Activation of carbonic anhydrase and its role in enhancing memory and learning. 251st ACS National Meeting, San Diego, CA, March 13–17, 2016.

**Sanku, R.K.K.**, Satyal, U., and Ilies, M.A. Structure–toxicity correlations in a series of carbonic anhydrase activators. AAPS National Meeting, Orlando, FL, October 25 – 29, 2015.

Walker, E.A., Salkovitz, M., Draghici, B., **Sanku, R.K.K.**, and Ilies, M.A. Effects of carbonic anhydrase inhibition and activation on learning and memory in mice. European Behavioral Pharmacology Society, Verona, Italy, September 2015.

**Sanku, R.K.K.**, Akocak, S., and Ilies, M.A. Anti-tumor activity of carbonic anhydrase inhibitors AAPS National Meeting, San Diego, CA, November 2-6, 2014.

**Intramural:**

Lemon, N., **Sanku, R.K.K.**, Chung, A., Ilies, M.A., and Walker, E.A. Profiling a novel series of carbonic anhydrase activators in mouse memory assays. Undergraduate Research Program Symposium, Temple University, Philadelphia, PA, October 6th, 2017.

**Sanku, R.K.K.**, Draghici, B., Pan, P., Ilies, M.A., and Walker, E.A. Novel lipophilic carbonic anhydrase activators protect mice from recognition memory deficits produced by scopolamine. Research Recognition Day, Temple University School of Pharmacy, Philadelphia, PA, February 17th, 2017.

Douek, J.S., Lu, B., Pan, Y., **Sanku, R.K.K.**, Ilies, M.A., and Walker, E.A. Effects of a carbonic anhydrase activator with memantine on memory in mice using novel object recognition testing. Research Recognition Day, Temple University School of Pharmacy, Philadelphia, PA, February 17th, 2017.

**Sanku, R.K.K.**, Draghici, B., Satyal, U., Walker, E.A., and Ilies, M.A. Effects of efficient carbonic anhydrase activation on learning and memory in mice. Research Recognition Day, Temple University School of Pharmacy, Philadelphia, PA, February 19th, 2016.

Klar, B.R., Pathrose, M.T., **Sanku, R.K.K.**, Jiao, Y., Ilies, M.A., and Walker, E.A. Implementation of the novel object recognition test for mice to test novel carbonic anhydrase activators. Research Recognition Day, Temple University School of Pharmacy, Philadelphia, PA, February 19th, 2016.

Salkovitz, M., Draghici, B., **Sanku, R.K.K.**, Ilies, M.A., and Walker, E.A. Acetazolamide's detrimental effects on memory are partially reversed with novel carbonic anhydrase activator BD117 in mice. Research Recognition Day, Temple University School of Pharmacy, Philadelphia, PA, February 19th, 2016.

Karakus, O.O., **Sanku, R.K.K.**, and Ilies, M.A. Comparative toxicity of several nanocarriers for drug delivery. Research Recognition Day, Temple University School of Pharmacy, Philadelphia, PA, February 19th, 2016.

Depuy, A.M., **Sanku, R.K.K.**, Merali, S., and Walker, E.A. Effects of the flavonoid Apigenin on learning and memory in mice. Research Recognition Day, Temple University School of Pharmacy, Philadelphia, PA, February 19th, 2016.

**Sanku, R.K.K.**, Akocak, S., and Ilies, M.A. Anti-tumor activity of carbonic anhydrase inhibitors. Research Recognition Day, Temple University School of Pharmacy, Philadelphia, PA, February 20th, 2015.

## CHAPTER 1

### OVERVIEW AND MAIN RESEARCH GOALS

Carbonic anhydrase (CA, EC 4.2.1.1) is a zinc metalloprotein which catalyzes the reversible hydration of  $\text{CO}_2$  to  $\text{HCO}_3^-$  and  $\text{H}^+$ . CA is involved in respiration and  $\text{CO}_2$  transport from metabolizing tissues to lungs,  $\text{CO}_2$  and pH homeostasis, electrolyte secretion in various tissues and organs, bone resorption/calcification, biosynthetic reactions, etc. In mammals, 15 isozyme or CA-related proteins have been described to date, with different catalytic activity, sub-cellular localization, and tissue distribution. Their dysfunction can cause diseases such as edemas, glaucoma, osteoporosis, obesity, cancer and several neurological disorders.

Activation of CA isozymes in the brain has the potential to alleviate mild dementias and therefore suggest that CA activators could act as potential nootropics or memory enhancers. On the other hand, over the last decade of cancer research, a relation was established between tumor cells and the expression of specific CA isozymes. Published studies show that to support the malignant tumor cell's metabolism specific membrane-bound carbonic anhydrases, CA IX and CA XII, are over-expressed and upregulated significantly. Pharmaceutical agents which can selectively bind, inhibit CA IX and CA XII, may have therapeutic value in imaging and the treatment of a large variety of hypoxic tumors.

Our **long-term goal** is to treat mild dementias and cancer by modulating CA isozymes responsible for those disease states. The **objective** of this project is to evaluate the set of CA activators and CA inhibitors, validate their ability to act as nootropics or anticancer agents respectively, and to establish structure property and structure-activity

relationships in order to identify the most efficient scaffolds and substituents for development as lead compounds in subsequent libraries.

Our **central hypothesis** is that we can generate potent nootropics and anti-cancer agents by modulating the activity of carbonic anhydrase isozymes. The rationale of this research is that small drug molecules with optimal physicochemical properties and nanomolar potency against their corresponding CA isozyme targets will be able to generate the desired biological effect – either tumor cell killing (for CA inhibitors) or nootropic action (for CA activators).

Thus, in the third chapter our goal was to correlate the structure of a set of CAAs with their specific physicochemical properties, biochemical and biological properties, including toxicity, and to determine the best CAAs for eliciting nootropic action. For testing the nootropic action of CAAs, I assessed cytotoxicity, cell uptake, brain uptake, and microsomal stability of a set of newly synthesized CAAs and I tested their specific biological activity in vivo using learning and memory assays like Novel Object Recognition Task (NORT) and simple operant task in mice. Conclusions of these studies will allow the identification of lead compounds with nootropic activity to be further developed into future drugs for efficient management of mild cognitive impairment (MCI) and other, more advanced, forms of dementia such as Alzheimer's disease (AD).

In the fourth chapter I correlated the potency of several series of CA inhibitors with their ability to kill tumor cells in vitro. More specifically, for testing the anticancer action of CAIs I have performed cytotoxicity assays on 2Ds and 3D cell models of different cancer cell lines, under normoxic or hypoxic conditions. Optimization of physicochemical properties was made either through drug delivery systems (DDS) or by using medicinal

chemistry approach, where we changed the structures to improve physicochemical characteristics without diminishing their potency. Pyridinium sulfonamides, which have a limited solubility, were delivered using cyclodextrins or sulfocalixarenes and I optimized these formulations. The study allowed us to identify the main structural and physicochemical properties responsible for increased CAI potency to kill cells in the selected cancer models expressing CA IX.

## CHAPTER 2

### INTRODUCTION

#### 2.1 Carbonic anhydrase: background, distribution, physiologic role, structure

Carbon dioxide is the main by-product of cellular respiration in living organisms. This non-polar molecule must be transported from mitochondria to the external environment. CO<sub>2</sub> in water is in equilibrium with carbonic acid, which is water-soluble [1]. However, the uncatalyzed reaction is too slow to match the demand of living cells. Therefore, a class of ubiquitous metalloenzymes named carbonic anhydrases (CAs, E. C. 4.2.1.1) have evolved to efficiently catalyze this reaction [2]. CA enzymatic activity was first observed in the late 1920s, where experiments performed with hemolyzed blood samples demonstrated that the rate of carbon dioxide release from the hemolyzed blood was higher than expected, indicating that blood could contain a catalyst [3]. Carbonic anhydrase (CA) was later extracted from erythrocytes in 1933 by Meldrum and Roughton [4]. This enzyme efficiently catalyzes the reversible hydration of carbon dioxide (CO<sub>2</sub>) to yield a bicarbonate ion (HCO<sub>3</sub><sup>-</sup>) and a proton (H<sup>+</sup>) [5].



It has been known since 1940s that CA is ubiquitous in plants [6], where it is used for CO<sub>2</sub> fixation [7]. CA and its isozymes are found virtually in all living organisms, from the unicellular ones to higher vertebrates including humans. Their structure is encoded by

five evolutionary unrelated gene families, generating the  $\alpha$ -,  $\beta$ -,  $\gamma$ -,  $\delta$ -,  $\zeta$ -CAs and  $\eta$ -CA [8-10].

- $\alpha$ -CAs are expressed in vertebrates, algae, protozoa (e.g. Plasmodium),
- $\beta$ -CAs can be present in bacteria, chloroplasts of mon-/dicotyledons.
- $\gamma$ -CAs are present in some bacteria and archaea [11].
- $\delta$ -CAs are present in and marine diatoms [12].
- $\zeta$ -CAs were identified only in some marine diatoms [12, 13].
- $\eta$ -CA were recently identified in Plasmodium's, the malaria-provoking pathogens [9, 10].

### **2.1.1 Carbonic anhydrase isozymes**

To date, fifteen different CA (hCAs) isozymes, are currently known in humans, all belonging to the  $\alpha$ -class [5, 8, 14]. CAs have different organ and tissue distribution, subcellular localization and catalytic activities to meet the demands of a living organism [15]. Through these different isozymes CAs are maintaining the  $\text{CO}_2/\text{HCO}_3^-$  pools in the interior and exterior of cells [15]. Based on their subcellular localization, the CA enzymes found in mammals can be divided into four broad subgroups [16, 17]:

- Secreted CAs (CA VI).
- Membrane-bound CAs (CA IV, CA IX, CA XII, CA XIV and CA XV).
- Cytosolic CAs (CA I, CA II, CA III, CA VII, and CA XIII).
- Mitochondrial CAs (CA VA and CA VB).

Different isozymes are structurally adapted to perform this reaction in diverse environments encountered in the body and therefore their kinetic properties are adapted to

these environments. Typical turnover numbers for different isozymes range between  $10^4$  and  $10^6$  molecules per second. Some of these isozymes are catalytically very fast (CA II, CA IV, CA VII, CA IX, CA XII and CA XIII), while some isoforms are slower (CA I, CA III, CA V, CA VI and CA XIV) [5, 17]. Notably, three human CA-related proteins (CARPs) were also identified (CA VIII, CA X and CA XI), which do not possess any catalytic activity (acatalytic). Their subcellular localizations and relative enzymatic activity are illustrated in Figure 1 [5, 18, 19].

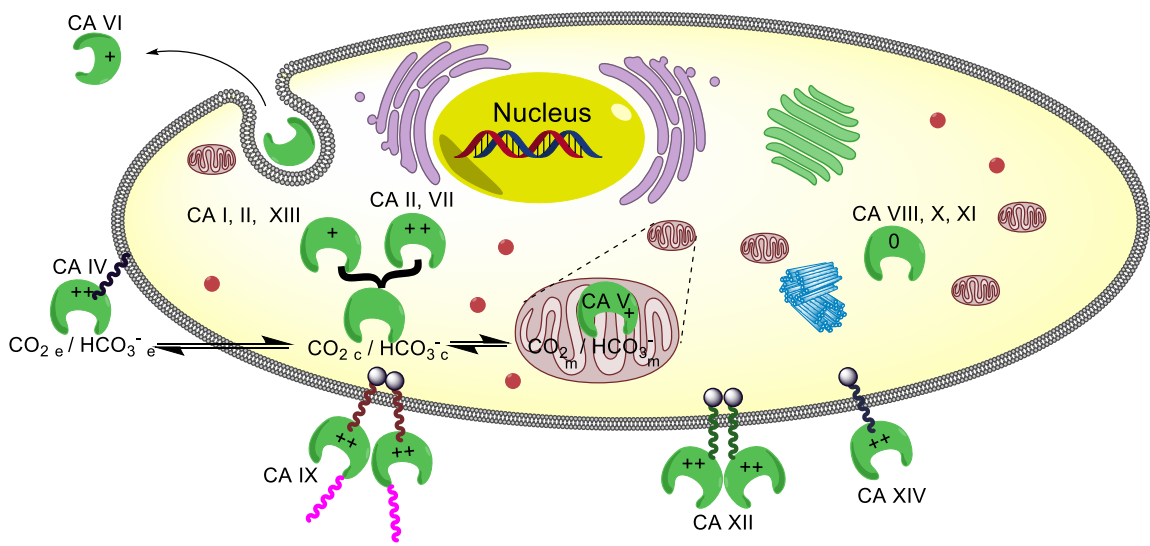


**Figure 1:** Picture depiction of subcellular localization and catalytic enzymatic activity of human  $\alpha$ -CAs coded as: (devoid of catalytic properties (0), low (+), high (++) activity) [18]. The cytosolic CAs, secreted (CA VI) and the mitochondrial CA VA and VB consist only of the CA domain; the membrane-associated CA IV, IX, XII and XIV have a membrane anchor and, except for CA IV, a cytoplasmic tail, while CA IX is the only isozyme with a N-terminal proteoglycan-like domain. (e, c, m = extracellular, cytosolic and membrane) [5].

### 2.1.2 Physiologic roles of carbonic anhydrases

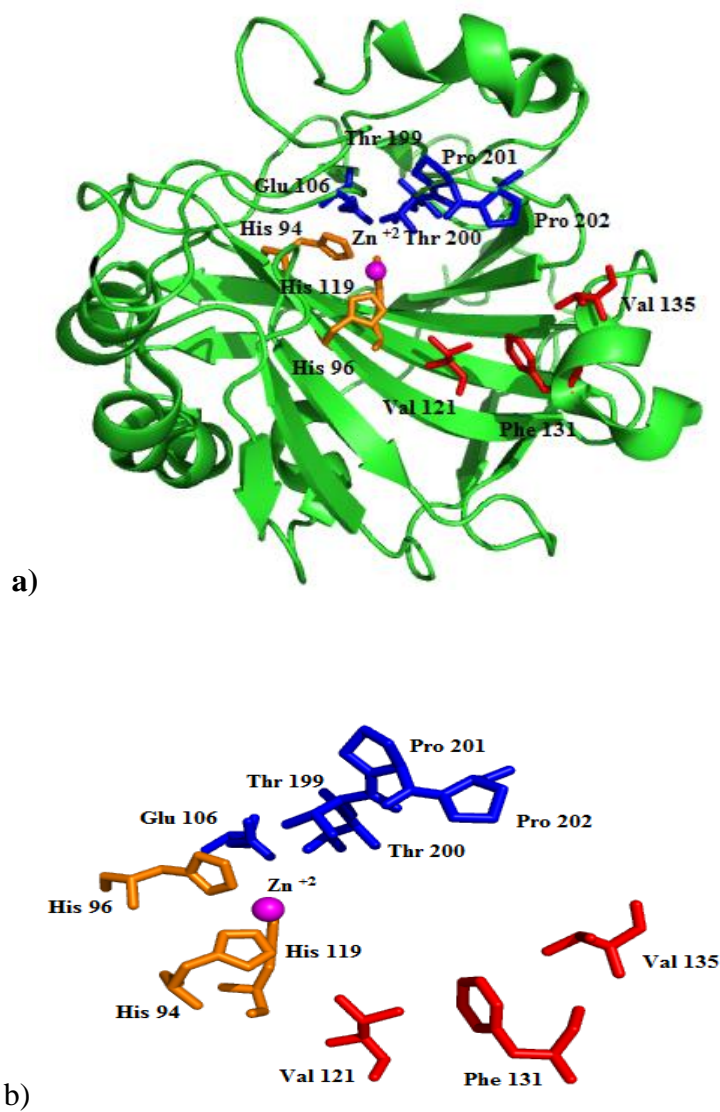
The main function of the carbonic anhydrase isoforms in human tissues is to interconvert carbon dioxide and bicarbonate to maintain pH homeostasis in blood and different tissues [19]. The  $\text{CO}_2/\text{HCO}_3^-$  buffer is the main buffer in the interstitial/extracellular space of different organs and the main buffer in blood and cerebrospinal fluid [20]. Tight control of pH inside and outside mammalian cells is essential, as small variations can trigger protein degradation. CAs are also involved in very important physiologic and pathologic processes in the human body, which include respiration and transport of  $\text{CO}_2$  from tissues to lungs, electrolyte secretion in various tissues and organs, bone resorption/calcification, turnover of cerebrospinal fluid, biosynthetic reactions such as gluconeogenesis, lipogenesis and ureagenesis, tumorigenicity and cerebrospinal fluid secretion [20-22]. The brain is an important  $\text{CO}_2$  producer, oxidizing about a quarter of body's glucose. In order to maintain ionic gradients and homeostasis in brain, CAs located at different subcellular locations in brain play a central role [15, 23]. About 85% of total  $\text{CO}_2$  produced in the body is transported to lungs in bicarbonate form, after hydration by CAs [15, 22]. CAs dysfunction can cause diseases. Thus, some of these isoforms are over-expressed in pathological conditions such as edemas, glaucoma, obesity, epilepsy, osteoporosis, altitude sickness, gastric ulcer, diabetes, cerebral edema, idiopathic intracranial hypertension, oxidative stress, respiratory disorder, circulatory disorder and cancer, making CA important targets for research [5, 8, 14, 24]. Table 1 depicts the currently known human CA isozymes, their tissue and organ localization/distribution, catalytic activity, sub-cellular localization and physiologic impact [19, 24-30].

Table 1: The human CA isozymes currently known, with their tissue/organ localization/distribution, catalytic activity, subcellular localization and physiologic role

Human CA isozyme	Tissue/organ localization	Catalytic activity/ $K_{cat}(s^{-1})$	Subcellular localization	Dysfunction disease
hCA I	erythrocytes, GI tract, eye	moderate / $2.0 \times 10^5$	cytosol	respiratory, circulatory
hCA II	erythrocytes, GI tract, eye, bone, osteoclasts, kidney, lung, testis, CNS (oligodendrocytes, astrocytes, dorsal root ganglia and neurons)	high / $1.4 \times 10^6$	cytosol	glaucoma, edema, altitude sickness epilepsy, osteoporosis, gastric ulcer, diabetes, cerebral edema, idiopathic intracranial hypertension.
hCA III	skeletal muscle, adipocytes, liver	low/ $3.0 \times 10^5$	cytosol	oxidative stress
hCA IV	kidney, eye, heart muscle, lung, pancreas, brain capillaries, colon	high/ $1.1 \times 10^6$	membrane-attached	glaucoma, retinitis pigmentosa, stroke
hCA VA	liver, mitochondria of neuronal and glial cells	moderate/ $2.9 \times 10^5$	mitochondria	obesity
hCA VB	pancreas, kidney, GI tract, spinal cord, mitochondria of neuronal and glial cells	high/ $9.5 \times 10^5$	mitochondria	obesity
hCA VI	salivary and mammary glands	moderate / $3.4 \times 10^5$	secreted (saliva, milk)	cariogenesis
hCA VII	CNS, colon, liver, skeletal muscle, duodenum, stomach	high/ $9.5 \times 10^5$	cytosol	epilepsy
hCA-related protein VIII	CNS	acatalytic (0)	cytosol	neurodegenerative cancer
hCA IX	tumors, GI mucosa, CNS	high/ $3.8 \times 10^5$	trans membrane	cancer
hCA-related protein X	CNS	acatalytic (0)	cytosol	Not Determined
hCA-related protein XI	CNS	acatalytic (0)	cytosol	Not Determined
hCA XII	renal, intestinal, eye, tumors, reproductive epithelia, CNS	high/ $4.2 \times 10^5$	trans membrane	cancer, glaucoma
hCA XIII	kidney, CNS, lung, gut, reproductive tract	moderate / $1.5 \times 10^5$	cytosol	sterility
hCA XIV	kidney, liver, eye, neurons, axons, medulla oblongata, pons, corpus callosum, pyramidal tract, hippocampus, choroid plexus and cerebral white matter.	moderate/ $3.1 \times 10^5$	trans membrane	retinopathy, epilepsy

### 2.1.3 Structure of Carbonic Anhydrases

X-ray crystallographic data revealed that the active site of the  $\alpha$ -carbonic anhydrase is conically-shaped, with the zinc ion placed at the bottom of a 15 Å deep active-site cleft [5]. This zinc atom (pink sphere in Figure 2) is coordinated by three histidine residues (His-94, His-96 and His-119, Figure 2), with the fourth ligand of the metal being either a water molecule or a hydroxyl ion in the enzymatic inactive and enzymatically active forms. The deprotonation of the metal bound water is assisted by a proton shuttling group, which is His-64 in CA II, assisted by a histidine cluster His-4, His-3, His-17, His-15 and His-10 in CA II. This deprotonation process of the Zn-bound water transform the enzyme from its inactive form (Zn-OH<sub>2</sub>) into its active form (Zn-OH). The hydroxyl moiety of Thr-199, which is bridged to the carboxylate moiety of Glu-106 orients the Zn-bound OH group for optimum nucleophilic attack on the CO<sub>2</sub> molecule. As shown in the figure below, half of the active site is made with hydrophilic amino acids, while the other half is lined up with hydrophobic amino acids [5, 8]. Many of these amino acids are conserved across different CA isoforms with a high degree of structural homology. This makes the design of isozyme selective modulators a challenging task [24].



**Figure 2:** Representations depicting the X-ray crystal structure of the prototypical CA isozyme, CA II (a) showing a detailed view of its active pocket (b). Within the active site (b), the hydrophobic residues are depicted in red while the hydrophilic amino acid network is depicted in blue. Figure made using PyMol (DeLano Scientific)

#### 2.1.4 Catalytic mechanism of Carbonic Anhydrase

CA enzymes typically use a metal ion ( $\text{Zn}^{2+}$  in  $\alpha$ -,  $\beta$ - and  $\gamma$ -CAs,  $\text{Fe}^{2+}/\text{Co}^{2+}/\text{Zn}^{2+}$  in  $\delta$ -CAs and  $\text{Cd}^{2+}$  in  $\zeta$ -CA) which favors in the reduction pKa of  $\text{H}_2\text{O}$  from 15.7 to 7 [8, 11-14, 24, 31-33]. Human CAs use a  $\text{Zn}^{2+}$  ion to decrease the pKa of  $\text{H}_2\text{O}$  bound with  $\text{Zn}^{2+}$  ion which is also bound to histidine residues (His-94, His-96 and His-119). This reduction of pKa favors in the removal of  $\text{H}^+$  from the Zn-bound  $\text{H}_2\text{O}$  in the inactive form of the enzyme (Form D in Figure 3) to its catalytically active form (Form A in Figure 3). This is the rate-limiting step for the enzyme. Deprotonation is further assisted by the proton shuttle of the enzyme ( $\text{BH}^+$  between form A and D, below figure). In CA II, His-64 acts as a proton shuttle for rapidly moving the  $\text{H}^+$  from the active site to the external milieu [34, 35]. The metal bound  $\text{OH}^-$  (Form B in Figure 3) is a very powerful nucleophile which readily attacks the  $\text{CO}_2$  molecule, present in the hydrophobic pocket of the enzyme, to form the tetragonal  $\text{Zn-HCO}_3^-$  ion complex (Form C in Figure 3). The bicarbonate ion is subsequently displaced from  $\text{Zn}^{2+}$  by another  $\text{H}_2\text{O}$  molecule, thus closing the catalytic cycle (Form D in Figure 3).

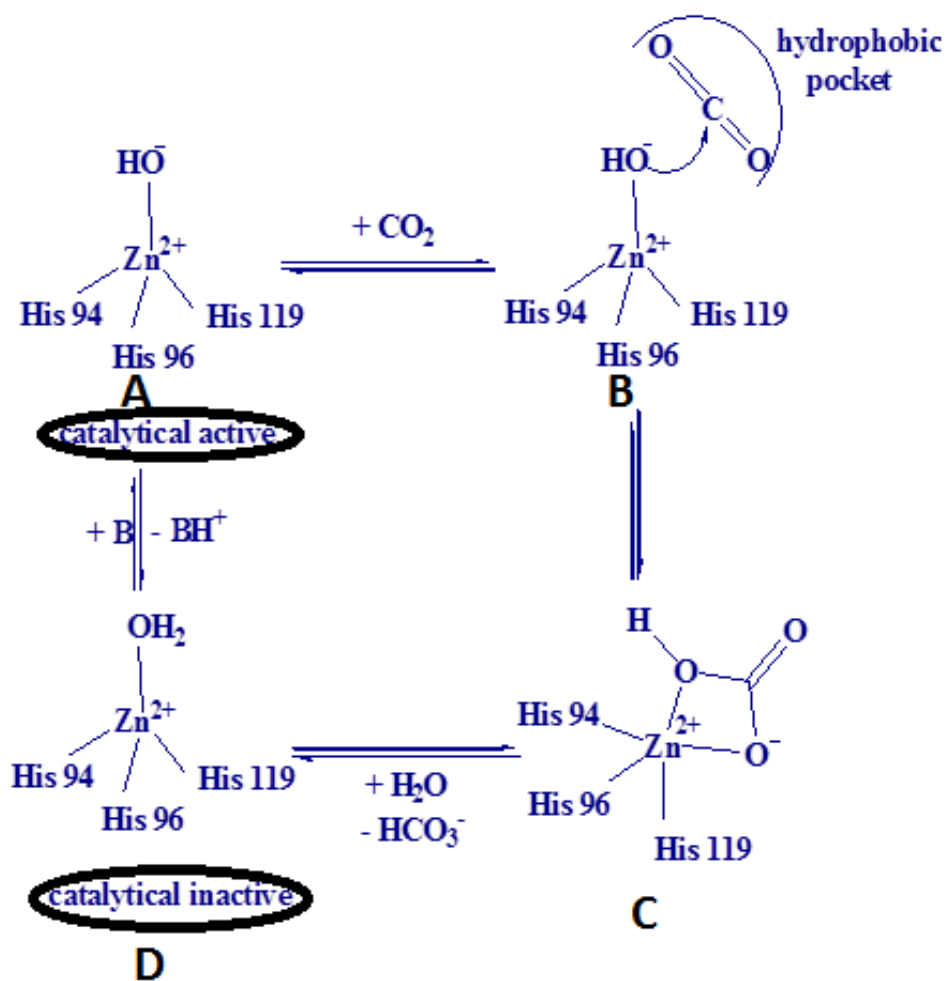


**Figure 3:** Schematic illustration of the catalytic mechanism of carbonic anhydrase.

The removal of the  $HCO_3^-$  ion is facilitated by hydrophilic amino acid residues lining half of the active site of CA (blue in Figure 2). The other half of the active site is hydrophobic (comprised by Val-143, Val-121 shown in red in Figure 2), facilitating the diffusion of non-polar substrate  $CO_2$  to the active site. The amphiphilicity (both hydrophobic and hydrophilic linings) of the active site of CA enzyme is dictated by the nature of the reaction catalyzed and plays a very important role in the design of the CAs inhibitors and activators [24].

## **CHAPTER 3**

### **DEVELOPMENT AND BIOLOGICAL EVALUATION OF CARBONIC ANHYDRASE ACTIVATORS AS POTENTIAL NOOTROPICS**

The goal of the studies included in this chapter was to correlate the structure of the latest generation of CA activators synthesized in our lab with their physicochemical and biological properties such as topological surface area, lipophilicity, solubility, CAs activation profile, neurotoxicity and ability to enhance learning and memory. Our working hypothesis was that CAs play an important role in learning and memory and activation of CA isozymes can improve these processes, with the potential to treat mild cognitive impairments (MCIs) and dementias. Although a range of molecular and clinical approaches imply a role for CA in learning, memory, and perhaps cognition, the hypothesis that activation of brain CA isozymes improves all these processes could not be tested experimentally until very recently due to lack of efficient CA activators with appropriate pharmacokinetic and toxicity profiles that will allow them to cross the blood-brain barrier (BBB) efficiently and to activate different CA isozymes present in the brain. Improving on our previous designs, our lab recently introduced new series of CAAs with structures that confer physicochemical properties within the optimal range for blood-brain barrier penetration.

### **3.1 Background and rationale**

#### **3.1.1 CAs and brain homeostasis**

As mentioned above, the hydration reaction of CO<sub>2</sub> is critical for many physiologic and pathologic processes [36, 37], with about 85% of total CO<sub>2</sub> produced in the body being transported to lungs in bicarbonate form, after hydration by CA. Brain is a major CO<sub>2</sub> producer. It oxidizes about a quarter of body's glucose in order to maintain homeostasis and ionic equilibrium. CAs are directly involved in cerebrospinal fluid (CSF) secretion at the level of the choroid plexus, generating HCO<sub>3</sub><sup>-</sup> from CO<sub>2</sub> and H<sub>2</sub>O, and regulating, through ion hydration, the volume, buffering properties, and turnover of CSF [21, 23, 38]. Currently, known human CA isozymes related to CNS, brain distribution, cellular localization, intensity of expression and catalytic activity are tabulated below (Table 2).

**Table 2:** The human CA isozymes currently known isozymes related to CNS, organ localization, distribution, cellular localization, intensity of expression and catalytic activity.

Isozymes	CNS region	Type of brain cells	Intensity of expression	Location*	Catalytic activity (% CA II) <sup>†</sup>	References
<b>I</b>	cerebral tissue, CSF, spinal cord	neurons	low	C	14.3	[5, 39-41]
<b>II</b>	hippocampal CA1 pyramidal neurons, medulla, brain stem, cerebellum, choroid plexus,	neurons, microglial cells, epithelial cells, oligodendrocytes, astrocytes, choroid plexus cells	high	C	100	[36, 42-58]
<b>III</b>	choroid plexus	epithelial cells, microglial cells	low	C	21.4	[44, 56, 57]
<b>IV</b>	hippocampal pyramidal , luminal surface of cerebral capillaries	neurons , glia and capillary endothelial cells	high	E	78.6	[26, 44, 59, 60]
<b>V</b>	hippocampus, cerebrum, spinal cord, cerebellum, Purkinje cell perikarya	pericytes, neurons, glial cells	high	M	20.7	[44, 61-63]
<b>VII</b>	hippocampus CA1 region	neuron (not in glial cells)	high	C	67.9	[58, 62, 64]
<b>VIII</b>	hippocampus, medulla, brain stem, cerebellum, choroid plexus	neural cells, astrocytes, epithelial cells of the choroid plexus, Purkinje cells	high	C	0	[44, 62, 65-67]
<b>IX</b>	choroid plexus, ventricle, cerebrum, cerebellum,	neuronal axons and Purkinje cells	low	E	27.1	[68-71]
<b>X</b>	medulla, brain stem, cerebellum, choroid plexus, myelin sheath	myelin sheath and neural cells	low	E	0	[44, 66, 67]
<b>XI</b>	medulla, brain stem, cerebellum, choroid plexus	neural cells, astrocytes, epithelial cells of the choroid plexus	medium	C	0	[44, 66, 67]
<b>XII</b>	cerebellum, cerebrum, corpus striatum, choroid plexus, cortex, brain ventricles	neurons of the cerebellum and cerebrum	low	E	30	[69, 72]
<b>XIV</b>	hippocampus, corpus callosum, cerebellar white matter and peduncles, pyramidal tract, and choroid plexus, Pons and medulla oblongata	neurons, astrocytes, endothelial cells of the brain capillaries	high	E	22.1	[26, 44, 73, 74]

<sup>†</sup>Catalytic activity of each isozyme is presented as percentage of CA II catalytic activity;

\*C = cytosolic, E = extracellular, M = membrane bound

CAs maintains ionic equilibrium and brain homeostasis at the cellular level through different CA isozymes located in the neural, oligodendrocytes, endothelial cells, astrocytes and glial cells (Figure 4) [19, 25, 26].

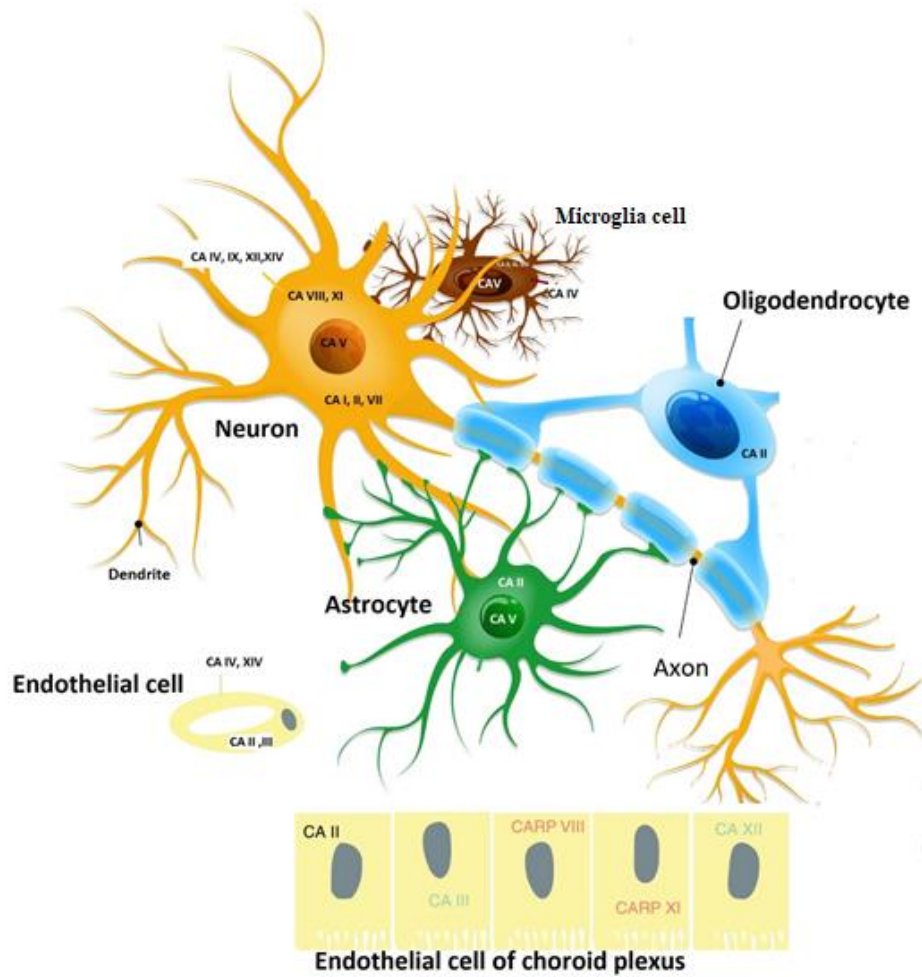


**Figure 4:** Carbonic anhydrase (CA) isozymes present in various CNS cells. Adapted from the reference [75].

### **3.1.2 CA role in CNS related disease states**

The critical role played by CAs in brain homeostasis and normal cerebral function is emphasized in CA deficiency syndrome [36, 37]. This distinct genetic disorder is characterized by severe pathological modifications of the lungs, kidney, brain and bone metabolism [37]. Clinical data revealed that absence of CA II in these organs and blood is associated with mental retardation, cerebral calcification, respiratory and renal tubular acidosis, and inherited osteoporosis [37]. In patients with Alzheimer's disease, the expression level of CA was found to be significantly diminished compared to a healthy adult [76]. Other recent redox proteomics studies demonstrate that isoforms CA I and CA II are oxidized or nitrosylated, which reduces the catalytic activity in the frontal cortex and hippocampus of Alzheimer patients [77-79]. These modifications reduce the catalytic power for hydration of CO<sub>2</sub> in different areas of the brain and indicate a direct connection between reduced CA activity and impaired brain function. Similarly, there is a decrease in level of CA expression was observed in the brain of older rats relative to younger rats [76].

### **3.1.3 Mild Cognitive Impairment (MCI)**

MCI is an intermediate stage between cognitive decline with normal aging process and dementia, with symptoms such as loss of long-term and short-term memory. MCI is an important clinical condition that is increasing in prevalence within western societies [80]. The study of MCI is further advancing in the future through subtyping MCI by cognitive decline, domain and etiology. A special place may be reserved for early Alzheimer's disease diagnosis at the MCI stage [80, 81]. Sometimes, MCI remains stable over time or further deteriorates to dementia. Causation of this disease remains

unknown [81]. Over the past decades, classification of MCI disease and the description of the subtypes have been built up. Currently, there are a variety of reference terms, which are important for understanding the prevalence, incidence, and outcomes that exist for MCI and its best-studied subtypes [80]. Figure 5 illustrates the subtypes of MCI, along the continuum from normal functioning to dementia.

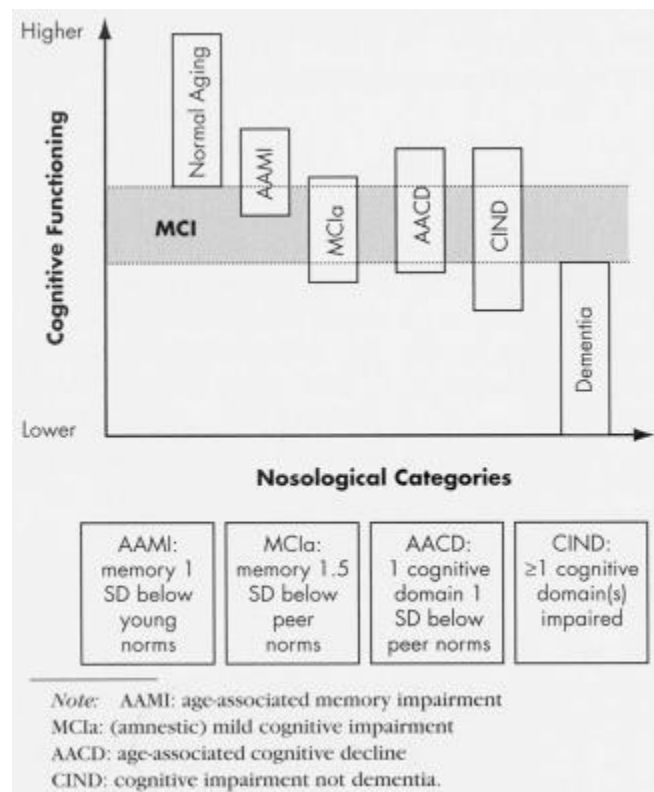


**Figure 5.** Conceptual model of the cognitive continuum, from normal aging to dementia [80].

Currently, there is no cure for MCI [82]. As MCI is considered a prodromal state to Alzheimer’s disease, treatments proposed for Alzheimer’s disease, such as antioxidants and cholinesterase inhibitors, are currently used for therapy of MCI [83].

Unfortunately, all marketed drugs in use proved inefficient in treating MCI. The main reason is that etiology of this disease is not fully understood. However, CA has a profound involvement in the general activity of the brain with a potential significant contribution to memory and learning. The use of CA inhibitors was clearly associated with cognition impairments. Therefore, in order to develop a drug candidate against MCI we have decided to study the effects of CA activation and to assess its role towards improving learning and memory.

### **3.1.4 Hippocampal CA 1 pyramidal cells and learning and memory**

Cognition can be broadly seen as a set of complex cerebral networks. Synaptic plasticity, strengthening, or modulating of signaling pathways can occur through long-term potentiation, elicited by a short period of high-frequent stimulations. One of the critical areas for learning and memory formation is the hippocampal region, with CA1 pyramidal cells playing a vital role [84, 85].

The CA1 pyramidal neurons receive three major inputs: cholinergic, glutamatergic inputs and GABAergic [86, 87]. Of the three inputs, the glutamatergic and cholinergic inputs elicit an excitatory action, while the GABAergic input is inhibitory.

In CA1 pyramidal cells, one can find mitochondrial isoform CA V, cytosolic CA II, CA VII isozymes and the membrane-bound isoforms CA IV and CA XIV (Figure 6) [19, 25, 26]. These isozymes actively transport CO<sub>2</sub>, the by-product of oxidative phosphorylation, from mitochondria to the exterior of the cell, and also neutralize the pH gradients in mitochondria, cytosol and external milieu of cells [15]. Mechanisms that govern H<sup>+</sup> ions concentration in the intracellular and extracellular fluid are especially

important in the brain, because electrical activity can elicit rapid pH changes in both compartments. These acid-base transients may in turn influence neural activity either directly or indirectly by affecting a variety of ion channels, receptors and neurotransmitters [22]. A slight change in extracellular pH often accompanies synchronous change in neural activity. Significant pH change would likely have a major influence over neural activity, over ionization of neurotransmitters and therefore, learning and memory [22]. Steep pH gradients, as high as 0.1 pH units, which are generated by neuronal discharge can be superimposed on the normal flux of protons caused by aerobic metabolism [22]. A very tight pH control is critical in this case, since small pH variations can significantly affect the membrane polarization and the ionization of key neurotransmitters, such as glutamate, GABA, and dopamine [88]. Protons compete for the channel flux of NMDA (N-methyl-D-aspartate) receptors and thereby reduce channel conductance to other cations into the cell [89, 90]. Thus, NMDA receptors are strongly modulated by changes in extracellular pH [91-94]. An increase in extracellular pH facilitates the activation of postsynaptic NMDA receptor responses in hippocampal CA1 pyramidal neurons, whereas a decrease in extracellular pH inhibits the ion channel function [88].

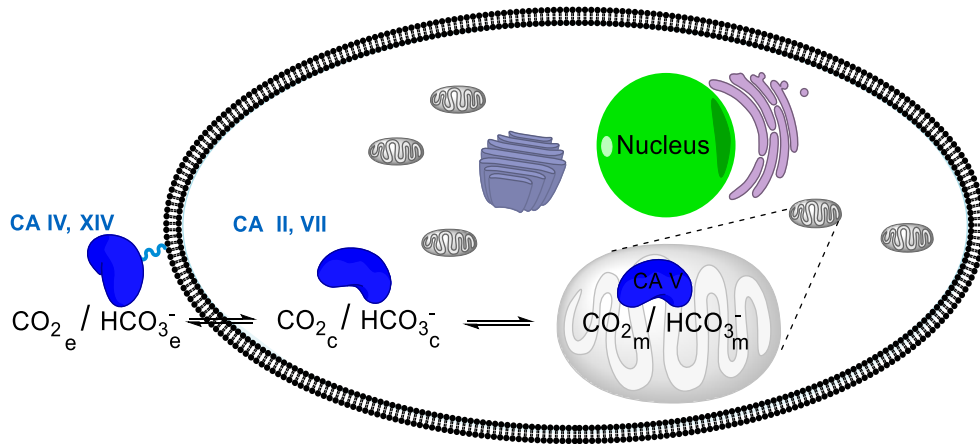


**Figure 6:** Schematics of CO<sub>2</sub> flux in hippocampal CA 1 pyramidal cell, revealing the CA isozymes believed to be involved in the process and the three different CO<sub>2</sub>/HCO<sub>3</sub><sup>-</sup> pools (extracellular (e), cytosolic (c) and mitochondrial (m)) equilibrated by them. Adapted from reference [15].

### 3.1.5 CA role in learning and memory

Focusing on the role of CAs in hippocampus and CA 1 pyramidal cells, the expression of cytosolic CA VII isozyme was suggested to act as a molecular switch within the rat hippocampus in the second postnatal week. This event was found to correspond to synchronous gamma-frequency firing of hippocampal CA1 pyramidal cells, which aids synaptic plasticity [64]. Moreover, NMDA receptor-dependent raise of extra cellular pH of CA 1 pyramidal neurons was found to be regulated by extracellular CA XIV in wild type, but not in CA XIV-knockout mouse, suggesting that a change in extracellular pH modulated by this particular isozyme have impacted pH-sensitive NMDA receptors responses [95]. In particular the, 2B subunit (NR2B) of NMDA receptor, which is necessary for long term potentiation (LTP), showed an overexpression in NR2B transgenic mice but not in the wild type mice. This over-expression of NR2B

resulted in increasing concentrations of CA II isozyme, showing an indirect relationship between CA II isozyme and LTP [96, 97]. Another observation of the role of CA in learning and memory was the finding that CA IX-deficient (Car 9<sup>-/-</sup>) mice performed poorly in acquisition and retrieval tasks on the Morris water maze (MWM) model [68]. These mice also had reduced motor activity in a T-maze test, without changes in their locomotor activity, in open/dark field, or balance beam tests compared to wild-type control mice [68] suggesting that the loss of CA had more selective effects on memory. CA inhibitor methazolamide infused nasally in rats impaired CO<sub>2</sub> discrimination in an operant learning task by reducing the CO<sub>2</sub> detection threshold, suggesting that CA activity influences olfactory neurons, perhaps through a role in the transduction mechanism of CO<sub>2</sub> chemoreceptors [98] or perhaps by disrupting the discrimination in the operant task. These studies in rodents suggest a role of CA in learning and memory.

There is less evidence available in humans, however, acetazolamide, a CA inhibitor which is used to treat acute mountain sickness, showed signs of reduced mental alertness [99]. Topiramate, an antiepileptic and a strong CA inhibitor, showed cognition deficits in humans upon regular use [100]. Taken together, these observations support a connection between reduced CA activity and impaired learning and memory. In this context, our findings that CA activation can prevent memory deficits is not very surprising.

### 3.1.6 Mechanism of action of CAAs in learning and memory enhancement

A class of pharmaceuticals that increase the catalytic activity of carbonic anhydrase enzyme are called carbonic anhydrase activators (CAAs). Although CA inhibition was being extensively studied and several compounds have made it into the clinic for the treatment of various diseases, the field of CAAs was largely unexplored for decades (*vide infra*). In early 2000's, Alkon et al. suggested that **GABAergic synaptic responses could be switched from inhibitory to excitatory and demonstrated that this synaptic switching depends on the increased  $\text{HCO}_3^-$  conductance and CA activity through the  $\text{GABA}_A$  receptor channel complex** [101, 102]. As mentioned above, we currently know that several CA isozymes are present in hippocampus CA1 pyramidal cells and the CA inhibitor acetazolamide was effective in blocking the GABAergic response in these neurons [103]. In their studies, Sun and Alkon showed that CA activator phenylalanine changed the function of GABAergic synapses from excitation filter to amplifier, which facilitates depolarization of the neurons, synchronous firing and thereby Long-term Potentiation (LTP) (Figure 7) [101].

LTP represents a persistent increase in synaptic strength following high-frequency stimulation of a chemical synapse, which increases the amount of neurotransmitter released at the synapse of the neurons and the number of receptors available for its uptake. Rats injected with the CA activators phenylalanine or imidazole had significantly faster latencies to escape in the Morris Water maze. The CA inhibitor acetazolamide prevented these improvements [101]. A very recent study by Canto de Souza et al. shows that mice injected with CAA phenylalanine have shown improved learning compared with a saline control group. Phosphorylation of extracellular signaling kinase in cortex

and hippocampus was advanced as molecular consequences of the use of CAAs [104]. Phosphorylation of extracellular signaling kinase (Erk) is a known pathway that mediates gene transcription and translation in neurons and plays an important role in synaptic plasticity and LTP in cortex and hippocampus.

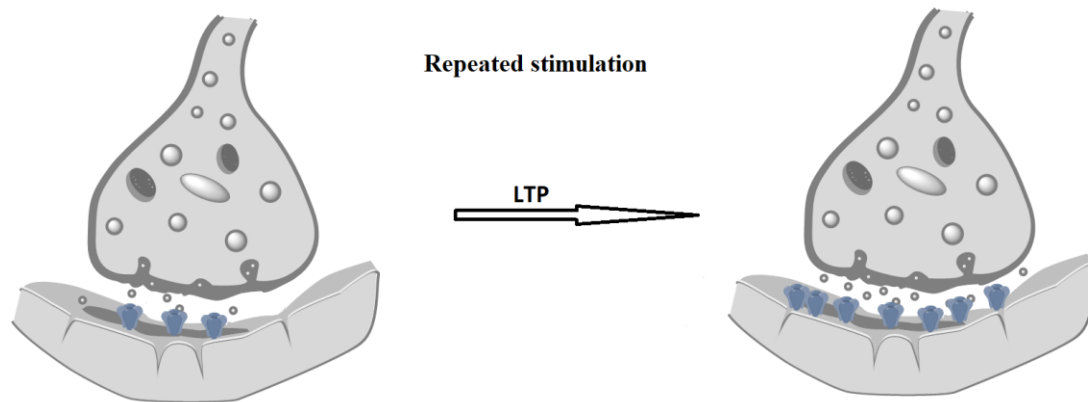


**Figure 7:** Long-term potentiation (LTP) increases the amount of neurotransmitter released at the synapse of the neurons and the number of receptors available for its uptake which is a vital step in the memory formation.

In terms of mechanism, LTP produced by CA1 pyramidal neurons and neurons from the frontal cortex involved in learning and memory can be conceptually achieved by switching the GABA synapse from inhibitory to excitatory, as described by Sun and Alkon [102, 105, 106]. Thus, **inhibitory action of GABA** is caused by binding of GABA neurotransmitter to GABA<sub>A</sub> receptors (GABA<sub>A</sub>Rs), which open up and allow Cl<sup>-</sup> to move inside the neuron, causing a drop-in membrane potential from -70 mV (resting membrane potential) to -85 mV. Once a membrane potential ( $V_m$ ) of -85 mV is reached, no Cl<sup>-</sup> inward flux is possible; however, the GABA<sub>A</sub>Rs are permeable to HCO<sub>3</sub><sup>-</sup> too, in both

senses (similarly to  $\text{Cl}^-$ ), with  $\text{Cl}^-$  having five times higher affinity for GABA<sub>A</sub>Rs as compared with  $\text{HCO}_3^-$ . Since the  $\text{HCO}_3^-$  equilibrium potential is -12.5 mV,  $\text{HCO}_3^-$  can freely flow out from the neuron through the open GABA<sub>A</sub>Rs, depolarizing the membrane towards the -55 mV firing threshold (excitatory action). This flow though of  $\text{HCO}_3^-$  is dependent on the activity of intracellular/extracellular CAs, which can produce/consume  $\text{HCO}_3^-$  inside/outside the cell (Figure 8). Thus, the activation of these CA isozymes can move  $V_m$  towards the threshold potential required for the neuron to fire (-55 mV) via the  $\text{HCO}_3^-$  flux and accomplish the GABA<sub>A</sub>Rs switch from inhibitory to excitatory. As a direct consequence, the overall stimulation of the neuron can generate more downstream action when CAs are activated, thus favoring LTP.

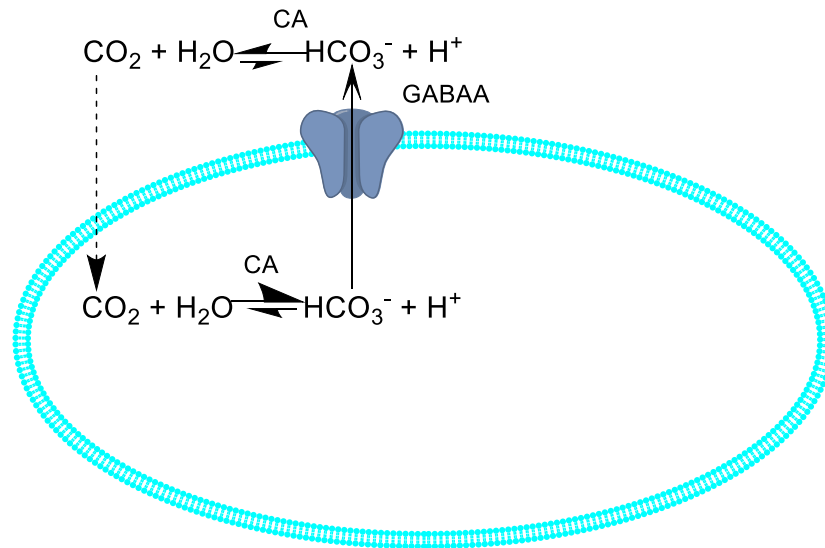


**Figure 8.** Bicarbonate dependent switch of GABA-mediated synapses from excitatory input filter (inhibitory action) into an amplifier (excitatory action) depends on the catalytic activity of CA isozymes present inside and outside the cell [102].

**Since the activity of CAs can be modulated by CAAs, this mechanism constitutes, together with the other indirect evidence presented above, the basis for considering CAAs as enhancing memory and learning (nootropic action) and potentially toward their use in treating various cognitive impairments or dysfunctions such as MCI.**

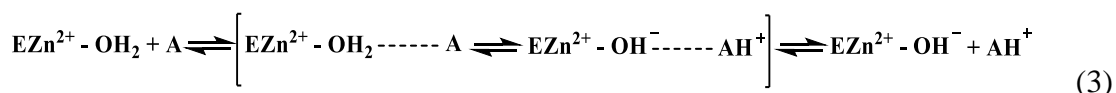
### **3.2. CA activators investigated: design evolution and rationale**

Despite the fact that activation of CA was reported [107] almost simultaneously with its inhibition [108], the field of CAAs remained rather unexplored for decades. The first activators identified were usually small molecules such as EDTA [109], histamine [110], imidazole, phosphate, histidine and hemoglobin [111-113], which are close structures to the biological proton shuttling group His-64 of CA II. Coleman [114] demonstrated CA activation with lysine, polylysine, imidazole, glycine, and histamine. Other natural molecules with basic moieties, such as amino acid phenylalanine **1**, tyrosine **2**, biogenic amines histamine **3**, serotonin **4**, and various peptides were also investigated and found to be CA activators with various potencies [115]. A structure-activity relationship (SAR) study revealed that efficient CA activators possess a proton-shuttling group attached to a hydrophobic/amphiphilic aromatic/heterocyclic anchor via a short, flexible linker (Figure 9) [115]. It was understood that CA activators act by speeding up the deprotonation of zinc bound water (the rate-determining step, equation (2) in the

catalytic mechanism) [115, 116], with generation of the active form of the enzyme [111] (see equations below):



In the presence of an activator 'A', equation (2) becomes (3):



### enzyme-activator complex

Comprehensive structure-activity relationship (SAR) studies, done by our team, revealed that efficient CA activators (CAAs) possess a proton-shuttling group attached to a hydrophobic/amphiphilic aromatic/heterocyclic anchor via a short, flexible linker (Figure 9) [15].

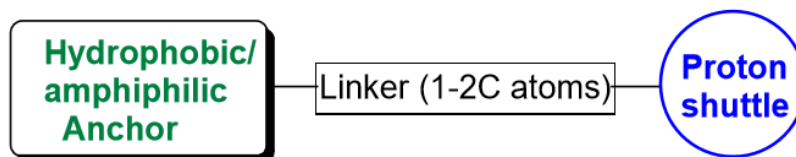


**Figure 9.** General structure of a carbonic anhydrase activator

Subsequent CAA designs using amino group as proton shuttling group (5-7) identified pyridinium moiety as an efficient heterocyclic amphiphilic anchor (Chart 1) [117]. Activation of CA with bis-(N1)-azoles such as bis-(N1)-imidazole **8** had been discovered almost simultaneously. In these compounds, one imidazole ring acts as hydrophobic anchor and the other one as proton shuttle (Chart 1) [118, 119].

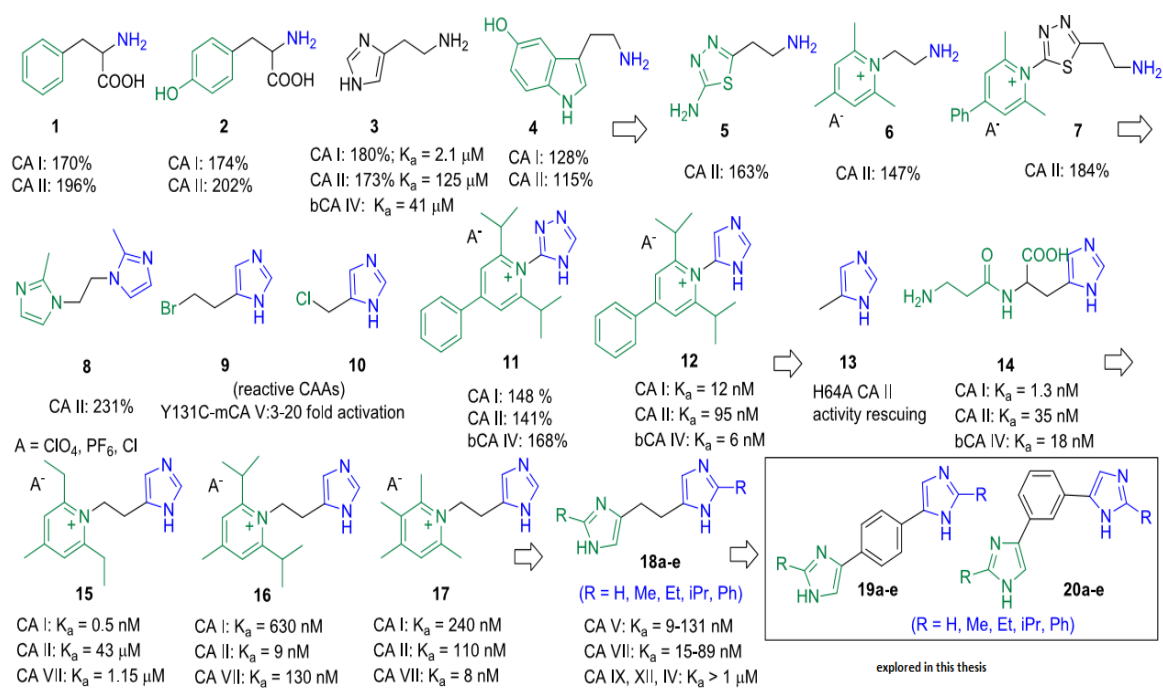


**Chart 1.** Evolution of CA activators design and the activation potency of compounds **1-17** tested or developed previously [115, 118, 120-124]. The specific series of CA activators **18** and **19-20** (boxed) developed for this section are used in this CA activation project to triangulate on key CA isozymes involved in learning and memory.

Amino and azole proton-shuttling groups were used extensively in early CAA design, in combination with various anchors (Chart 1) [115]. Several key SAR studies from our team, [110, 121] supported by X-ray crystallography studies [125-132] clearly established imidazole moiety as one of the most efficient proton-shuttling groups available. It was successfully used in the design of potent CAAs in combination with pyridinium, [121, 124] peptidyl [122] and other anchors.

Structural analyses of available CA activators (Chart 1) reveals that most CAAs are polar compounds with a limited ability to pass the BBB. Therefore, our group recently

developed novel bis-imidazole CA activators (**18**) that proved nanomolar potent against mitochondrial CA VA and cytosolic CA VII [15]. The new compounds were derived from their pyridinium histamine predecessors **15-17**, with whom shared the flexible and compact ethyleneimidazole moiety but used a second imidazolic ring as amphiphilic heterocyclic anchor. This retained the potency against CA isozymes but made the new compounds **18** less polar, allowing them to cross the BBB.

However, the brain penetration of the most potent compounds from series **18** (CAAs **18a-c**) was found to be suboptimal, so our group replaced the ethylene linker in **18** with a more lipophilic phenylene one (1,3- or 1,4 disubstituted), generating bis-phenylene-imidazoles **19** and **20** (Chart 1). Their structure was confirmed by <sup>1</sup>H- and <sup>13</sup>C-NMR and high-resolution mass spectrometry (HRMS). The full activation profile of series **19** and **20** against mitochondrial CA VA, cytosolic CA I, CA II, CA VII, and membrane-bound CA IV, CA IX, CA XII, and CA XIV was conducted at University of Florence by Dr. Claudiu Supuran (Table 3).

**Table 3:** Activation of CA isozymes (mitochondrial in brown, cytosolic in green, membrane-bound in blue) with bis-imidazole derivatives of type **18**, **19** and **20** and histamine **3**, by a stopped-flow, CO<sub>2</sub> hydrase assay. \*

No.	K <sub>a</sub> (μM)							
	hCA I	hCA II	hCA IV	hCA VA	hCA VII	hCA IX	hCA XII	hCA XIV
Histamine <b>3</b>	2.1	125			37.5			
<b>18a</b>	16.4	68.5	1.25	0.021	0.015	9.51	8.63	13.9
<b>18b</b>	23.5	69.3	4.51	0.009	0.020	13.1	5.40	10.2
<b>18c (MAI 27)</b>	1.13	76.8	2.37	0.037	0.071	24.7	6.13	18.5
<b>18d</b>	4.81	80.4	9.50	0.131	0.054	20.1	9.85	24.6
<b>18e</b>	5.96	78.7	12.4	0.052	0.089	18.5	12.6	25.9
<b>19a</b>	12.5	42.3	0.090	0.098	18.5	1.02	7.81	6.54
<b>19b</b>	34.2	44.5	0.14	0.007	23.4	0.84	6.23	14.1
<b>19c</b>	8.10	50.2	0.061	0.005	20.7	0.79	9.50	10.2
<b>19d</b>	6.42	49.3	0.040	0.013	21.9	0.013	9.21	18.5
<b>19e (BD 117)</b>	5.50	51.7	0.029	0.010	30.7	0.010	12.4	24.6
<b>20a</b>	1.13	36.8	7.58	0.004	24.6	0.009	10.5	13.9
<b>20b</b>	1.42	38.0	12.3	0.002	26.8	0.005	10.7	14.1
<b>20c</b>	3.21	35.3	5.04	0.027	20.4	0.012	14.4	10.2
<b>20d</b>	4.97	27.1	8.93	0.013	31.7	0.031	21.5	18.5
<b>20e</b>	6.20	40.2	15.6	0.009	25.1	0.028	28.7	24.6

\* Mean from 3 different assays, by a stopped flow technique (errors were in the range of ± 5-10 % of the reported values). Monomeric (recombinant) human enzymes were used in all cases.

### **3.3. Materials and methods**

#### **Materials**

Solvents (methanol, ethanol, dichloromethane, acetone, acetonitrile, trifluoroethanol, all HPLC quality) were purchased from EMD (Gibbstown, NJ), Fisher Scientific (Hampton, NH) or VWR International (Radnor, PA) and were used as received. Deionized water produced from a Millipore MilliQ system (Burlington, MA) was used in all experiments that required it. Drugs were purchased from various vendors: Ketamine from Fort Dodge Animal Health (Parsippany-Troy Hills, NJ), scopolamine from Tocris Bioscience (Minneapolis, MN), acetazolamide, verapamil and retinoic acid from Sigma-Aldrich (St. Louis, MO). Human neuroblastoma cell line (SH-SY5Y) was purchased from ATCC (Manassas, VA). Propafenone was purchased from LKT laboratories (Saint Paul, MN). Mouse CD 1 liver microsomes from Life technologies (Carlsbad, CA). Dulbecco's Modified Eagle's medium (DMEM), RPMI-1640, and McCoy's 5A media was purchased from Mediatech-Corning (Manassas, VA) and fetal bovine serum (FBS), brain derived neurotrophic factor (BDNF) was from Fisher Scientific (Pittsburgh, PA). The 3-(4,5-Dimethylthiazol-2-yl)-2,5-diphenyltetrazolium bromide (MTT), phosphate-buffered saline (PBS), dimethyl sulfoxide (DMSO) and water-soluble tetrazolium salt-8 (WST-8) were purchased from VWR International (West Chester, PA).

#### **Methods**

##### **3.3.1 TPSA and Log P calculation**

Topological Polar Surface Area (TPSA) and Log P were calculated for all compounds using the ChemDraw software.

### **3.3.2 Determination of solubility**

The solubility assay was performed as reported using a shake well method [133, 134]. To determine solubility, an initial stock solution (10 mM) for each CAA was made in DMSO. An amount of 40  $\mu$ L of each stock solution was diluted with PBS to 2 mL to give a final DMSO concentration of 2 % and a theoretical drug concentration of 200  $\mu$ M. Vials were vortexed for 1 min each and shaken for 48 h on a mechanical shaker. Each CAA drug solution was subsequently filtered into a new vial using a 0.2  $\mu$ m nylon filter to remove the undissolved drug. Subsequently, 800  $\mu$ L of the filtrate was moved to a new vial containing 200  $\mu$ L of methanol or an organic solvent.

Separately, the  $\lambda_{\text{max}}$  for the absorbance of the individual CAA compounds were found using a solution of drug in an amphiphilic solvent (MeOH, EtOH, TFE) via a UV-Vis spectrophotometer. The drug concentration in the filtrate was determined by absorbance at their  $\lambda_{\text{max}}$  via a UV-Vis spectrophotometer against a calibration curve constructed with drug solution of known concentration in a good solvent (organic) [134].

### **3.3.2 TPSA and Log P calculation**

Topological Polar Surface Area (TPSA) and Log P were calculated for all compounds using the ChemDraw software.

### **3.3.3 Cytotoxicity assay**

The cytotoxicity assay was performed on differentiated SH-SY5Y cells, using an adaptation of an existing procedure [135-138]. Thus, SH-SY5Y cells were plated at the density of 5000 cells per well using 1:1 of Ham's F12 and DMEM media mixture

supplemented with 10% fetal bovine serum, 1% non-essential amino acids, 1% L-glutamine, 100 U/mL penicillin-G, and 100 µg/mL streptomycin on 96 well collagen coated plates. Plates were placed in the incubator for 24 h to allow cells to attach. After 24 h of cell plating, cell differentiation into neuron-like cells was induced by treatment with retinoic acid (5 µM in media) and brain derived neurotrophic factor (BDNF, 10 ng/ml in media) at 37 °C and 5% CO<sub>2</sub>. Five days later cells were washed with serum free media and treated with 10 % WST-8 solution for 1.5 h in incubator and read at 450 nm with reference 650 nm. Cells were then washed with PBS and treated with media containing different concentrations of drugs and placed back in the incubator for 24 h. After a day, cells were washed with PBS and treated with 10 % WST-8 solution for 1.5 h in an incubator and read at 450 nm with reference 650 nm.

### **3.3.4 Cell uptake and morphological studies of 19e (BD117)**

The uptake of the lead drug candidate, **19e (BD117)** was investigated by confocal microscopy, using a similar procedure as stated in the cytotoxicity assay of this chapter [135-138]. Briefly, SH-SY5Y cells were seeded on gelatin/collagen coated glass slides in 6 well plates at density of 150 k cells/well using 1:1 of Ham's F12 and DMEM media mixture supplemented with 10% fetal bovine serum, 1% non-essential amino acids, 1% L-glutamine, 100 U/mL penicillin-G, and 100 µg/mL streptomycin on a 6 well plate. Plates were incubated for 24 h to allow cells to attach. After a day, differentiation was induced by treating cells with retinoic acid (RA) 5 µM and 10 ng/ml BDNF in media. After 5 days in the incubator, cells were washed with serum free media and treated with **19e (BD117)** at a concentration of 10 µM for 30 min. Cells were then washed with PBS

and examined under the confocal microscope for any differences in morphology post treatment.

### **3.3.5 In vivo uptake of 19e (BD117) determined via mouse brain imaging**

In vivo uptake of selected CAA candidates was investigated by confocal microscopy, using an established procedure [139]. Swiss-Webster male mice, weight 20-25 g were dosed with 30 mg/kg of **19e (BD117)** compound or saline. Animals were euthanized 30 min after injection by CO<sub>2</sub> asphyxiation, followed by decapitation. Brains were extracted and stored at -70°C. Microscopy slides with brain slices (30 µm thickness) were made from all areas of the frozen brains using a microtome cryostat operating at -20° C. Brain slices were fixed by incubating the microscopy slides into 10 % paraformaldehyde for fixation. Fixation terminates any ongoing biochemical reactions and increases the mechanical strength of the treated tissues with paraformaldehyde. Approximately 15 microscopy slides containing various areas of the brain were made following this procedure. Prepared slides were subsequently imaged using confocal microscopy (dual excitation 405, 561 nm, emission above 565 nm, optical parameters tuned to minimize tissue autofluorescence). Same optical parameters were used for all imaging (saline/CAA injections).

### **3.3.6 Microsomal stability**

Microsomal stability was determined by a standard procedure [133, 140, 141]. The clearance of test compounds in mouse liver microsomes was determined at 37 °C, using 96-deep well polypropylene plates. Each drug candidate was tested in triplicates. A

volume of 1  $\mu\text{M}$  of the test compound was made in 0.5 mL of a solution containing 100 mM potassium phosphate buffer (pH 7.4) with 0.5 mg/mL liver microsomes from male CD-1 mice, 2 mM tetra-sodium NADPH (co-factor) and 3 mM magnesium chloride incubated for 60 min, at 37  $^{\circ}\text{C}$ , with gentle shaking using shaker plate. At five different time points, 75  $\mu\text{L}$  of reaction mixture was transferred to 96-shallow well stop plates on ice containing 225 mL of acetonitrile with 0.1  $\mu\text{M}$  propafenone as internal standard. Control reactions lacking NADPH, which is a cofactor, were performed in a similar manner to demonstrate NADPH dependency of compound loss. Verapamil was used as a positive control as it has rapid clearance. Standard curves for test compounds were generated using 5 concentrations in duplicate which were processed as above but with no incubation time with microsomes. Stop plates were centrifuged at 2000g for 10 min and then 170  $\mu\text{L}$  of the supernatants were transferred to a Waters Aquity UPLC 700  $\mu\text{L}$  96-well sample plate with cap mat. The amount of compound remaining in the supernatant was quantified by LC/MS/MS based on the internal standard. GraphPad Prism v 5.04 was used for nonlinear fitting of time course data [133].

### **3.3.7 Novel Object Recognition Test (NORT)**

The NORT was performed using Swiss-Webster male mice, weight 25-45 g based on the procedure developed previously [142-144]. For NORT, transparent polycarbonate cages of dimensions 16  $\frac{3}{4}$ 'L x 11  $\frac{7}{8}$ 'W x 7'H were selected. The objects used during testing were a 4'' Lego figure and a plastic bottle of same height and dimension but different in color and design. The entire cage was spread uniformly with corn cob bedding and was placed in a ventilated sound-attenuated box. This was illuminated with

lights from inside. Trials were video recorded and later coded by an experimenter [142-144].

As prerequisites, the objects to be used were first assessed to ensure that the mice neither inherently preferred nor averted these objects, and that both objects would be explored for similar duration upon initial exposures. All cages were disinfected before and after each trial. Exploration was defined as directing the nose to the object at no more than 2 cm and/or touching the object with the nose or mouth. Rearing up on the object was not counted unless the mice faced towards, but not away from, the object [145].

Procedure. The procedure involves three steps. In the initial habituation phase, an individual mouse which was naïve to behavioral testing, was habituated to the testing cage for 5 min, within a sound-attenuated box. Subsequently, the animal was returned to the home cage. After 1 h, the first trial (training phase) was started and the mouse was placed again in the testing cage that contained two identical objects, placed on the left and right of the mouse entrance (Figure. 10). The animals were placed in the testing cage facing away from two objects equidistantly. The amount of time spent exploring each object was recorded over a 5 min period. At the end of training phase, mice were returned to the home cage for 1 h. Each animal was placed back to the same testing cage for second trial (testing phase), which now contained one of the prior objects and a novel object, which replaced the second (familiar) object in the same location (Figure 10). The amount of time spent exploring each object was recorded over a 5 min period. Familiar and novel objects, cage locations, object locations were counterbalanced between the subjects. Control mice were individually injected with isotonic sterile saline 30 min after cage habituation. Another group of mice were injected with drug 30 min after cage

habituation. After analyzing the videos, the average time used by animals to explore each object was plotted and compared for the drug-treated mice vs. saline treated mice, in both training phase and testing phase. These parameters were recorded and plotted at different drug concentrations, in order to construct a dose-response curve. Once the dose response curve was developed, an optimal dose was used for subsequent experiments.

To test for a disruption of recognition memory, scopolamine, ketamine, and acetazolamide were examined as previously described [104, 143, 146]. In these studies, after training phase, mice were injected IP with a dose of 1-10 mg/kg scopolamine, or 1-56 mg/kg of ketamine or 1-10 mg/kg acetazolamide immediately after the training phase. One hour later, mice were returned to testing cages for testing phase, as described above. Once a disruption dose was established, we have assessed the ability of the CAA to prevent the memory disruption generated by scopolamine/ketamine/acetazolamide.

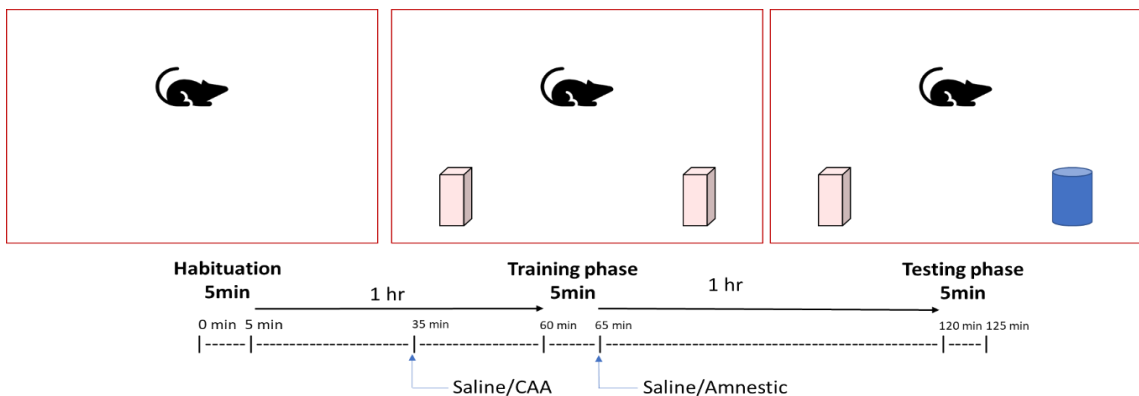


**Figure 10.** Experimental design for the 2-object Novel Object Recognition test.

Data and statistical analysis. In order to measure differences in exploration of the two objects in the training phase or between the familiar versus a novel object in the testing phase, a two-tailed, paired Student's t-test was run on exploration times of all animal groups (n specified in each case). Significance was set at  $P < 0.05$  for all statistical tests.

### 3.3.8 Simple 1-day operant task

Simple 1-day operant task was performed on Swiss-Webster male mice, weighting 25-45 g, based on the procedure developed in Dr. Walker's laboratory [142, 147-149].

**Apparatus.** Twelve experimental chambers ( $21.6 \times 17.8 \times 12.7$  cm, Model ENV-307W; MED Associates, St. Albans, Vermont, USA) were used, each located in a sound attenuating enclosure. One side wall of the operant chamber contained three receptacles: one large dipper hole in the center (ENV-313M) and two smaller nosepoke holes on the left and right (ENV-313W). A dipper well and a food delivery arm driven by a motor were located behind the center dipper hole. The opposite wall had a house light that illuminated the chamber during the session in progress. Nose-poke responses into each hole were detected by photocell head entry detectors (ENV303HD) and were recorded. Each chamber was equipped with an audible tone device (Sonalert, 2900 Hz; Mallory Sonalert, Indianapolis, Indiana, USA). The chambers were connected to a computer-driven interface (Model SG-502; MED Associates), which controlled the experimental conditions and collected the data [142, 147-149].

**Procedure.** Mice were separated into individual cages, weighed, and food-restricted for 24 h before day 1 of acquisition. Water was left available ad libitum. An acquisition session (session 1) and after 1 h later a retrieval session (session 2) were performed. To study the effect of the selected drug candidate on the acquisition and retrieval of a simple 1-day operant task, mice were injected with saline control or with drug (at a dose optimized based on the NORT) 30 min before the start of the session. At the start of session 1, mice were placed in the experimental chamber, the house light was

lit, and a tone occurred on a variable-time schedule (mean of 45 seconds; range, 4–132 seconds). The tone remained on for 6 sec or until a nose-poke response occurred. If a nose-poke response occurred in the center receptacle during the tone, a 0.01 cm<sup>3</sup> dipper filled with a vanilla-flavored liquid nutritional drink Ensure Plus/water (50:50) solution was presented for 3 sec in the center-hole nose-poke area, and the tone was turned off. This reinforce was counted as a reward. Nose-poke responses in the absence of the tone were counted but had no programmed consequences. Session 1 lasted for 1 h or until 10 rewards were obtained. Mice were returned to their home cages for 1 h. After 1 h, mice were tested in session 2 (retrieval) using the same set of contingencies, although the procedure lasted for 2 h or until 20 reinforcers are made. To test the effects of either saline, a dose of scopolamine, acetazolamide, or ketamine on consolidation and/or retrieval, mice were injected immediately after session 1. To test for enhancement of acquisition, mice were injected 30 min before session 1 with saline or a dose of **19e (BD117)** or **18c (MAI27)**. To evaluate whether the administration of **19e (BD117)** would alter the effects of ketamine, mice were injected with **19e (BD117)** 30 min before session 1 and acetazolamide immediately after session 1. To evaluate whether the administration of **18c (MAI27)** would alter the effects of ketamine, both **18c (MAI27)** and ketamine were injected after session 1 to prevent disruption from **18c (MAI27)** in session 1. Nose-poke responses in the left and right poke (inactive pokes) were counted but responses had no consequences. Session 1 lasted 1 h or until 10 reinforcers were obtained. If mice completed the session before 1 h, the houselight was turned off and the mouse remained in the darkened, experimental chamber until a full 1 h had expired. Mice were then removed from the experimental chamber, injected with drug or saline, and returned to

their homepage for 1 h. In session 2 (retrieval), the procedure was repeated as described above, except that the session lasted 2 h or until 20 reinforcers were obtained.

Data and statistical analysis. The acquisition (session 1) and retrieval (session 2) of the nose-poke responses were measured using mean adjusted latency, calculated as the lapsed time in seconds to the 10<sup>th</sup> reinforced response minus the latency to the first reinforced response ( $L_{10} - L_1$ ). As the tone was presented on a variable time schedule, this adjustment corrected for the different times of exposure from 4 to 132 s for the first tone presentations. The reinforced response rate was calculated as the total number of reinforced nose-pokes over the entire session divided by the total time in seconds, regardless of the presence or absence of auditory tone. The reinforced response rate served as an indicator of overall activity, motivational responses, and an assessment for motor response deficits on the measure of adjusted latency. The left and right nose-pokes were recorded even though there were no programmed consequences. The nonreinforced response rate was calculated as the total number of left and right nose-pokes over the entire session divided by the total time in seconds, regardless of the presence or absence of auditory tone.

Data from all the mice were included in the acquisition and retrieval response rate measures from session 1. However, mice that failed to achieve at least five reinforcers during session 1 were excluded from the mean adjusted latency measure for both sessions 1 and 2, as it was deemed inappropriate to evaluate the retrieval of a response from which the mouse was insufficiently reinforced or not reinforced at all. The number of mice that failed to reach the data inclusion criteria is reported in the figure legends.

A set of control mice injected with saline were tested alongside each drug or drug combination. To compare the ability of mice to learn and retrieve a novel nose-poke response after saline injections, paired t-tests were used to compare session 1 and session 2 adjusted latencies, reinforced response rates, or nonreinforced response rates in all the mice injected with saline across all the experiments (n=64). To examine the effect of drug dose and session 1 versus 2 on adjusted latencies, reinforced response rates, or nonreinforced response rates, a mixed model, two-way analysis of variance (ANOVA) was used with Bonferroni post-hoc tests for each measure. Significance was set at P less than 0.05 for all analyses.

### **3.4 Results and discussion**

The objective of these studies were to determine if the synthesized CAAs series 19 and 20 can pass the BBB based on their specific physiochemical properties and if these compounds were able to elicit positive effects on learning and memory in mice. Ideally, CNS drugs must efficiently pass the blood-brain barrier and reach the brain in a significant concentration to alter learning and memory. From there, drugs can partition back into the blood or might be metabolized over time, and their metabolites can be eliminated from the brain. Therefore, in our research, the physicochemical properties of the synthesized compounds are important factors to be determined. It is also important to establish structure-property relationship for these compounds based on their pharmacophore substitution to continue to design better compounds and understand their relationship to our functional outcome of learning and memory.

#### **3.4.1 LogP**

Lipophilicity of a molecule is defined as its ability to dissolve in hydrophobic phases such as organic solvents (oils, hexane or toluene). Lipophilicity can be evaluated using the partition coefficient  $P$ , defined as the ratio between concentrations of compounds in two immiscible solvents of opposite polarities. Lipophilicity can be determined experimentally and expressed as  $\log P$  or calculated by using *in silico* methods ( $\text{clog}P$ ). The lipophilicity of a compound is usually revealed by its partition coefficient ( $P$ ), defined by the ratio of the compound's concentration in a hydrophobic, organic layer and an aqueous polar layer [150]. A typical pair of solvents used for determination of  $P$  is *n*-octanol and water. Other pairs, such as  $\text{CHCl}_3$ /water (of different

buffers) are also used in P/logP determination. These two solvents are chosen because they are immiscible, and the compound being analyzed will partition into both solvents at different concentrations due to its specific physicochemical properties. It can be determined experimentally and expressed as log P or calculated by using in silico methods (clogP). Nowadays, chemistry software such as ChemUltra suite can predict the lipophilicity and partition coefficient of a compound quite accurately, generating a calculated P or calculated log P (clogP) values. Using this software, we obtained the cLogP values, which are tabulated in Table 4. The optimal range for the partition coefficient of the compound to pass the blood brain barrier is between 1.5 and 2.7. The upper limit of this range is about 3, while the lower is 1 [151]. Compounds with clogP between 1-5 were selected for subsequent in vitro and in vivo tests.

Based on pharmacophore substitution for these two series of CAA, one would predict the order of lipophilicity of the calculated log Ps, from most hydrophilic (**19a**, **20a**) to the most lipophilic compounds (**19e (BD117)**, **20e**). These clog P values obtained suggest that these novel molecules should possess excellent BBB penetration and allow testing of learning and memory.

### 3.4.2 TPSA

The polar surface area (PSA) of a compound is the summation of surface area overall polar atoms, primarily nitrogen and oxygen, together with their attached hydrogens [152]. Topological polar surface area (TPSA) of a molecule is the sum of tabulated surface contributions of polar fragments [153]. Tabulated PSA values for various fragments are available online [153]. In order to penetrate the BBB and thus act

on targets in the central nervous system, a PSA of less than  $90 \text{ \AA}^2$  is usually needed for a drug candidate [154]. PSA was calculated for all our compounds using the ChemDraw software and was found to be about  $49 \text{ \AA}^2$  for all representatives. These calculated values also suggest the two series of CAAs would possess suggesting a good BBB penetration profile (Table 4).

### **3.4.3 Solubility**

The solubility of the drug represents a critical Adsorption Distribution Metabolism and Elimination (ADME) characteristic. A high enough concentration of drug in the blood is needed to produce an optimal level of drug to reach its target and elicit an action. The purpose of this assay is to quantitatively determine the aqueous solubility of CAAs. This is important for many reasons. Specifically, for CNS drug candidates, the compound must have a high enough concentration in plasma to be able to pass the BBB. Diffusion across the BBB is a kinetic process, therefore a significant concentration of drug in the blood is needed in order to produce an optimal concentration of drug at its receptor in the brain.

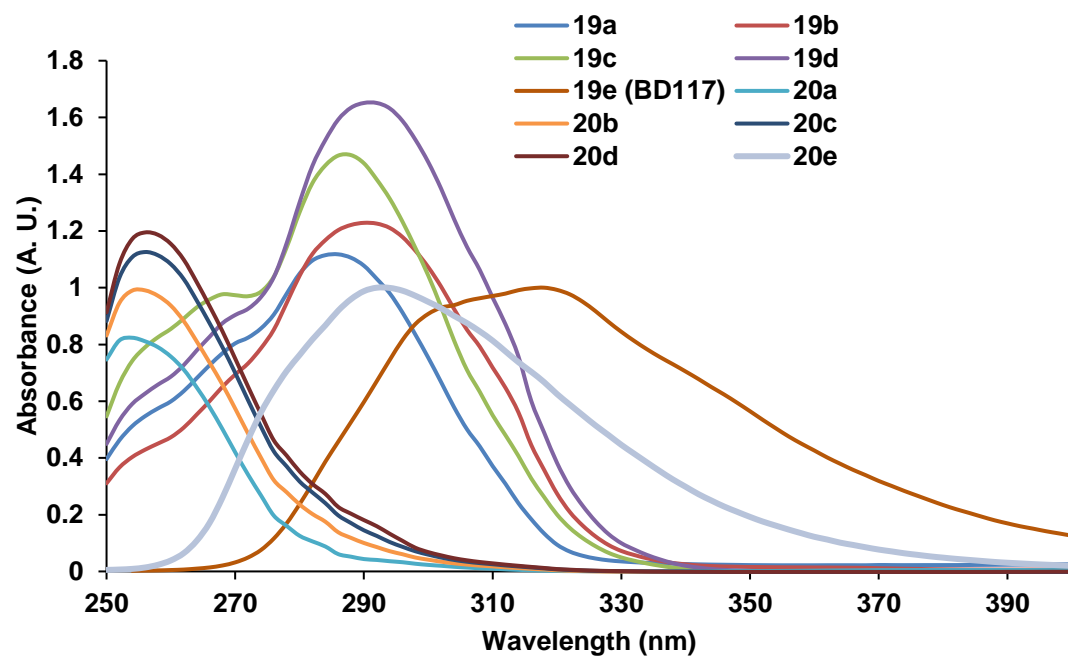


**Figure 11.** Absorption spectrum of CA activators **19** and **20** investigated in this study. The absorbance maximum  $\lambda_{\text{max}}$  was used to determine the concentration of the compounds in different phases.

**Table 4:** Solubility, lipophilicity and TPSA values of CAAs series **19** and **20** investigated, together with their main optical properties (absorbance maximums).

<b>Compound</b>	<b>Absorbance maximum</b> ( $\lambda_{\text{max}}$ , <b>nm</b> )	<b>Solubility</b> ( $\mu\text{M}$ )	<b>TPSA</b> ( $\text{\AA}^2$ )*	<b>CLogP*</b>
<b>19a</b>	286	43.85	48.78	0.83
<b>19b</b>	290	32.41	48.78	2.17
<b>19c</b>	288	30.86	48.78	3.32
<b>19d</b>	290	4.12	48.78	4.29
<b>19e (BD117)</b>	318	1.03	48.78	4.94
<b>20a</b>	254	24.53	48.78	0.83
<b>20b</b>	256	24.05	48.78	2.17
<b>20c</b>	256	22.21	48.78	3.32
<b>20d</b>	256	18.58	48.78	4.29
<b>20e</b>	292	4.03	48.78	4.94

TPSA and ClogP determined with ChemDraw Ultra v. 12.0

Absorbance spectrums and the position of absorbance maximum for various CA activators are depicted Figure 11 and are tabulated in Table 4 respectively. The solubility of each CAA was determined at the absorbance maximum, as presented in the experimental section. Ideally, plasma concentration of a CNS drug candidate has to be higher than 60  $\mu\text{g}/\text{mL}$  [154]. It is difficult to design a potent CAA that is lipophilic enough to cross the BBB and at the same time that has a good aqueous solubility. Efforts to balance the two parameters are required in drug design. In drug development practice,

a solubility lower than 60  $\mu\text{g}/\text{mL}$  can be observed for many CNS drugs in current clinical use as the lipophilicity is a more important parameter for these kinds of drugs than aqueous solubility. [155].

#### 3.4.4 Cytotoxicity

Any drug candidate that is expected to be able to penetrate the BBB easily and to remain in the brain for a significant amount of time must be devoid of any toxic effects. In order to test the toxicity of our CAAs, we adapted a validated assay that simulated the brain microenvironment in vitro [135-138]. Thus, we have differentiated the neuroblastoma SH-SY5Y cells into neuron-like cells by treating them with retinoic acid and BDNF. Once differentiated, these cells mimic the neuronal structures of the human brain (Figure 12) [135-138] and allow the evaluation of CAA cytotoxicity with high sensitivity using a formazan-based viability assay [156].

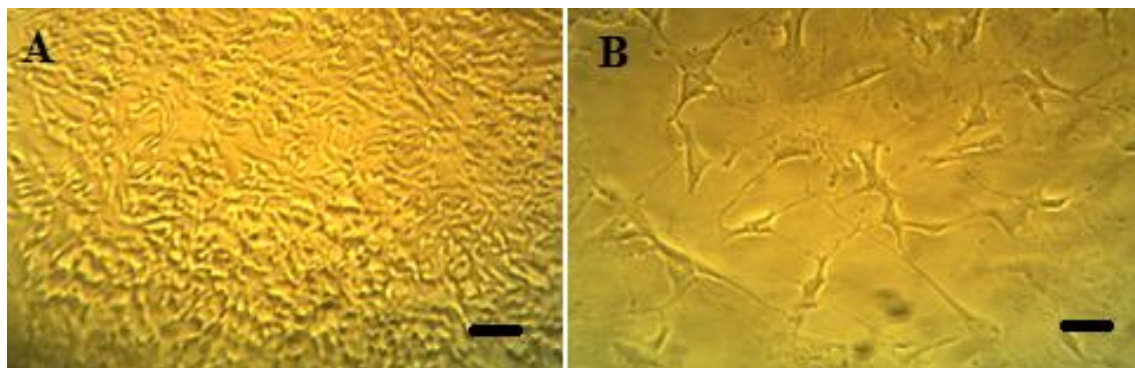


**Figure 12.** The differentiated SH-SY5Y cell model used for cytotoxicity testing of our novel CAAs. Representative phase contrast images of proliferative (standard, non-differentiated) SH-SY5Y cells in culture medium with 10% of FBS (A) and of differentiated SH-SY5Y cells, cultured for seven days with 10  $\mu\text{M}$  RA and BDNF in culture medium with 1% of FBS (B). Note the stellate morphology and neurites in differentiated cells (400 $\times$  magnification, bar = 50  $\mu\text{m}$ ).

We selected the WST-8 formazan-type assay due to its very low toxicity, after conducting a direct toxicity comparison with the more popular WST-1 and MTT assays based on the same formazan technology, on several cell lines (data not shown) [156, 157]. We assessed the cytotoxicity of CAAs series **19** and **20** using WST-8 assay at a concentration of 10  $\mu$ M, against acetaminophen (a frequently used drug for benchmarking CNS compounds on this cell line) at the same concentration (Figure 13). Data from Figure 13 revealed that that our new compounds were essentially non-toxic, with cell viability around or exceeding 100% in all cases. There was no correlation between the lipophilicity and the cytotoxicity of the CAAs as all the CAA proved to be nontoxic in these cultures. Profiting from the fluorescence of selected compounds (**19e** (**BD117**), **20e**) within the two CAA series, we also assessed the morphology of the differentiated SH-SY5Y post-treatment with **19e** (**BD117**).

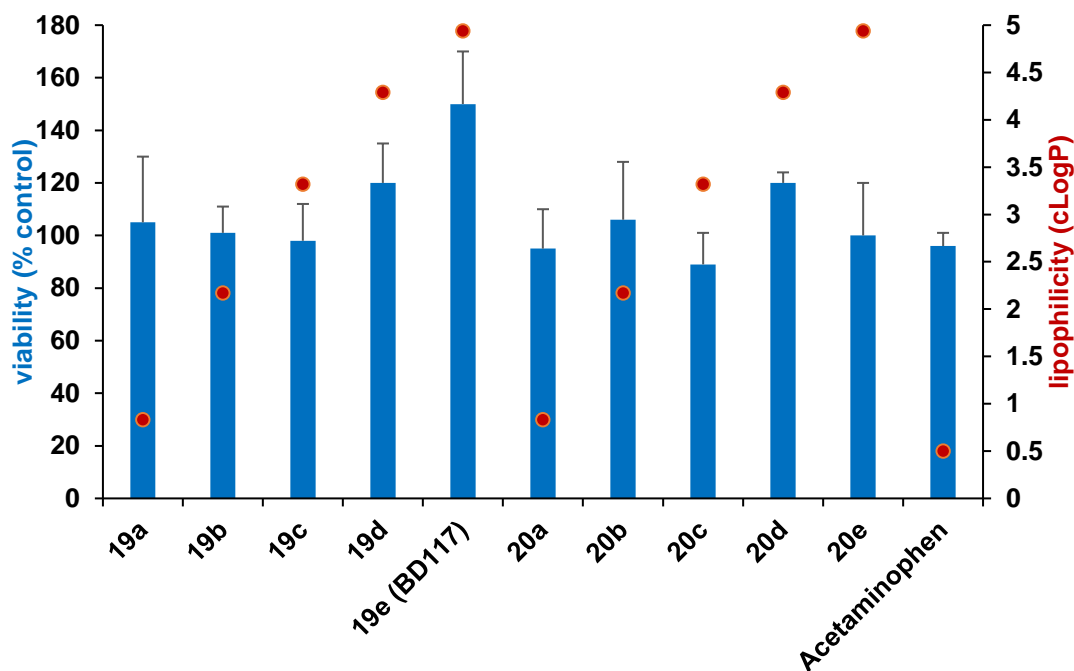


**Figure 13.** Cytotoxicity of novel CAAs series **19** and **20**, assessed via WST-8 assay in differentiated SH-SY5Y cells using acetaminophen as positive control (left scale) and compound calculated lipophilicity (right scale). Each bar represents the mean  $\pm$  standard deviation, determined out of 4 individual experiments.

### 3.4.5 Cell uptake of **19e** (BD117) and morphological studies

The morphology of neuron-like SH-SY5Y cells differentiated with retinoic acid was investigated post-treatment with compound **19e** (BD117) at 10  $\mu$ M (Figure 14). We have selected **19e** (BD117) as lead CAA due to its optimum physicochemical properties, doubled by an excellent cytotoxicity and activation profile (three isozymes activated simultaneously). While examining Figure 14 one can appreciate that the morphology of differentiated SH-SY5Y cells did not change with the drug treatment. Mention must be made that this cellular model is quite sensitive to toxicity, with toxic drugs affecting the morphology of neuron-like cells [135-138]. Since **19e** (BD117) is fluorescent, the

technique also allowed us to reveal the significant drug uptake by these cells within the relative short incubation time (30 min, Figure 14, panels A, B, C).

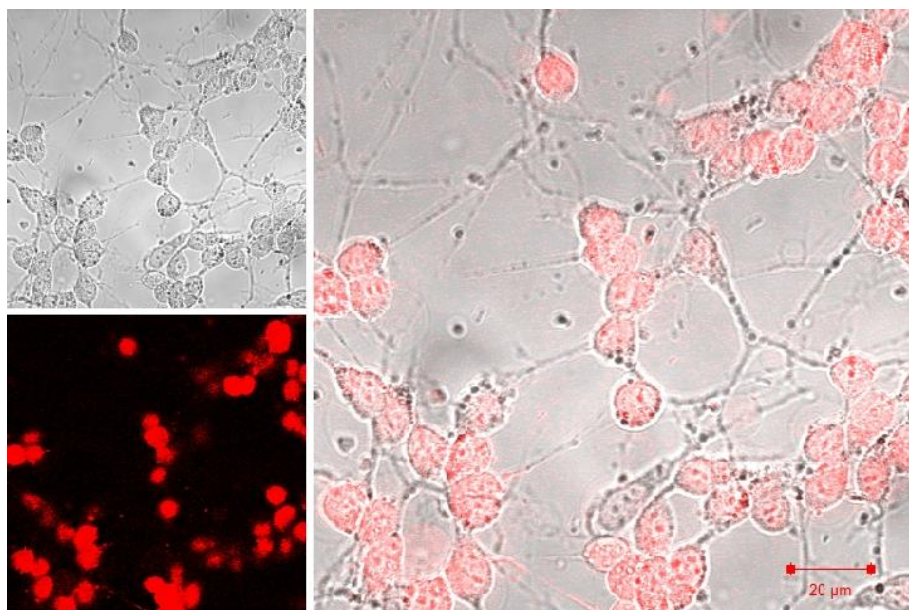


**Figure 14.** Uptake of compound **19e (BD117)** into neuron-like differentiated SH-SY5Y cells does not change the morphology of the cells. DIC image (left top), fluorescence image (left bottom) and superimposed DIC/fluorescence (right) image for neuron-like differentiated SH-SY5Y cells imaged after 30 min incubation time with **19e (BD117)** (10  $\mu$ M).

#### **3.4.6 In vivo uptake of 19e (BD117) and brain imaging**

In order to validate the brain penetration and accumulation of novel lipophilic CAAs series **19** and **20**, we treated Swiss-Webster male mice with the same fluorescent CAA **19e (BD117)** used in the SH-SY5Y imaging. Mice (n=3) were euthanized 30 min post administration of CAA **19e (BD117)**, brains were harvested, sliced via microtome and imaged for fluorescence of **19e (BD117)**. Saline-injected mice (n=3) were subjected to the same procedure and were used as reference. A lipophilic CAA such as **19e (BD117)** was expected to efficiently cross the BBB and to accumulate into the brain in a

significant amount. We confirmed the brain accumulation of **19e (BD117)** via comparative confocal fluorescent microscopy (Figure 15). For the confocal images of Figure 15, one can immediately distinguish the drug-treated brains from control ones, as **CAA 19e (BD117)** fluorescence adds significantly to the background fluorescence of the brain tissue. Mention must be made that no side-effects were observed on experimental animals while injected with high doses of **19e** and no toxicity was observed at the level of the mouse brains sampled, as revealed by microscopy images of histochemical samples collected (Figure 15). Considered together, the last set of experiments confirmed the good brain penetration of CAAs series **19** and **20** and the lack of toxicity associated with their use. These premises are essential for the development of any potential drug to treat a dysfunction in the brain and provide a solid base for subsequent in vivo assessment of nootropic action.

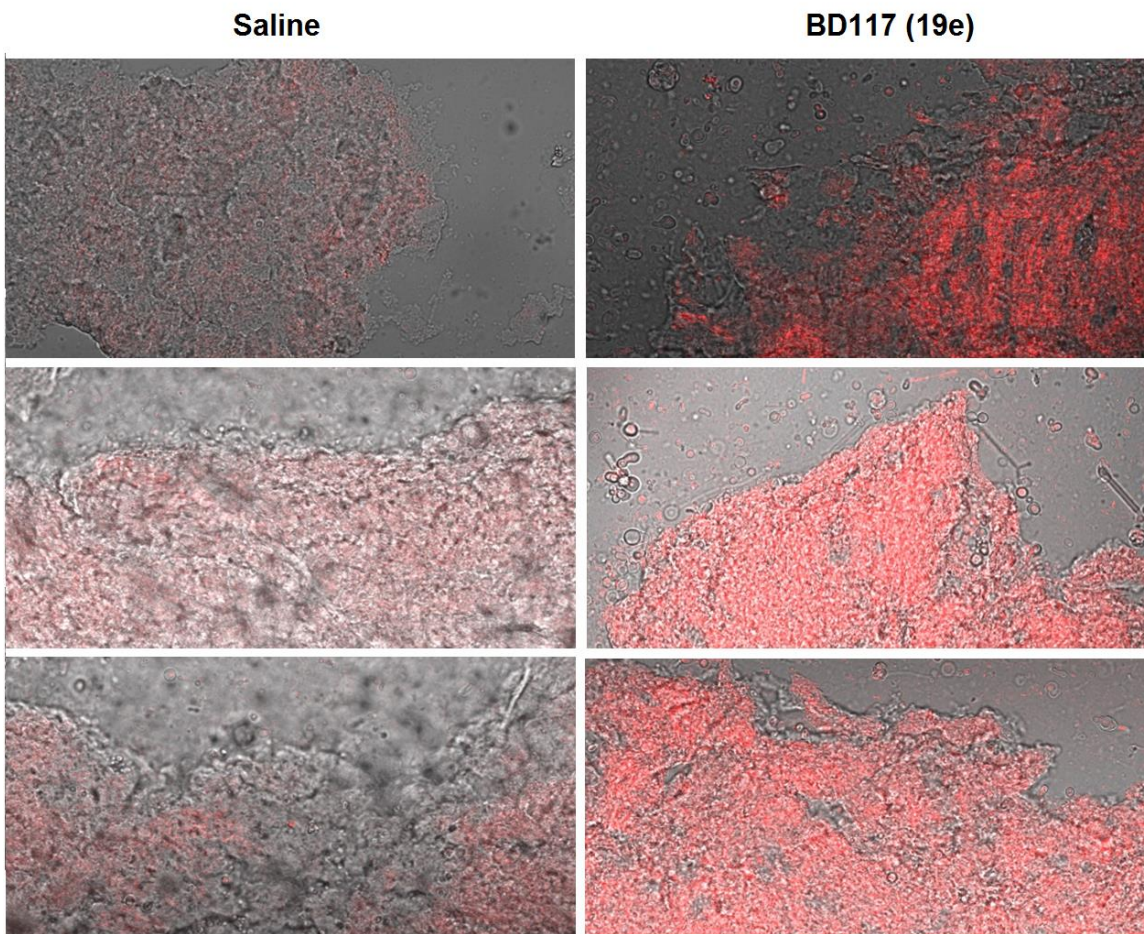


**Figure 15.** Comparative fluorescent microscopy revealing the uptake of CAA **19e** (**BD117**) into the brain of Swiss-Webster male mice. Representative superimposed DIC/fluorescence images of brain slices from **19e** (**BD117**)- treated mice (right panels) versus saline-treated mice (left panels) in 3 separate slices.

### 3.4.7 Microsomal stability

Liver metabolism is one of the major routes for drug elimination in humans. Around 60% of marketed drugs are eliminated by hepatic cytochrome P450 (CYP)-mediated metabolism [141]. A microsomal stability assay provides a means to measure the rate of clearance of a test drug candidate over time in microsomal incubation, and these data are used to calculate intrinsic drug clearance. Microsomal metabolic assays

primarily assess metabolism of drug candidates by the cytochrome P450 systems, relying on the use of liver microsomes that contain subcellular fractions of drug metabolizing enzymes, including many a large variety of CYPs.

Low microsomal stability of a given compound may translate into a high clearance and short half-life  $t_{1/2}$  of respective compound *in vivo*. A  $t_{1/2}$  greater than 15 mins is considered as an important parameter/threshold to be passed by CNS drug candidates [155]. Therefore, we tested our primary CAA candidate **19e (BD117)** for its stability on mouse liver microsomes. This is our lead drug candidate which has passed all the physicochemical filters and was further validated to be nontoxic *in vitro*. Results (Figure 16) revealed that **19e (BD117)** has a good microsomal stability, with about 80 % being recovered intact after 1 h incubation with CD-47 mouse liver microsomes. This means **19e (BD117)** is having a  $t_{1/2}$  of more than 1 h, which ensures the availability of compound in the mouse systemic circulation for enough time to reach the brain and to elicit its potential nootropic action. The assay was validated with the positive control drug verapamil, known for its rapid clearance via CYP-mediated metabolism (Figure 16).

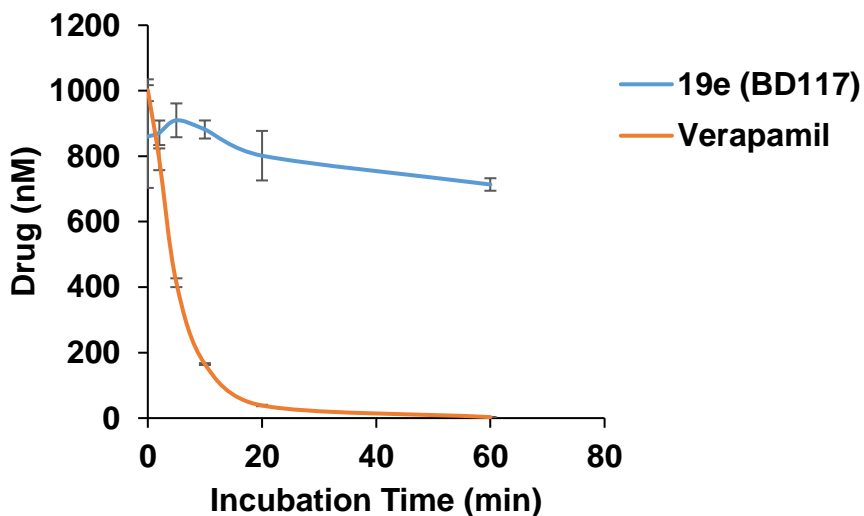


**Figure 16.** Microsomal degradation profile of **19e (BD117)** against verapamil as positive control. A half-life of greater than 60 min was observed for **19e (BD117)**. Data represented as a mean  $\pm$  standard deviation out of 3 individual experiments.

### 3.4.8 Novel Object Recognition Test

NORT is a validated assay and a primary screen to evaluate recognition memory. NORT is frequently used to test the efficacy of both memory-enhancing compounds (nootropics), as well as memory disruptors [158-164]. We established this procedure in our laboratory and the data from Figure 17 demonstrate that mice treated with saline explored both (identical) objects in training phase (acquisition) for approximately the same time. The same mice recognized the familiar object one hour later in testing phase (retrieval) and spent more time to examine the novel object. Therefore, similar to other published experiments, [158-164] the mice in these experiments demonstrated novel object recognition memory.

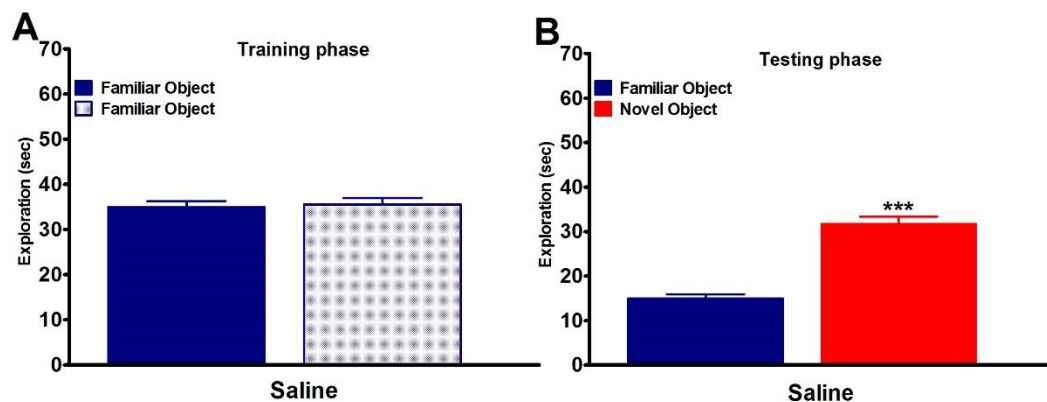


**Figure 17. Mice learn and recognize objects one hour after being exposed to the familiar objects in the NORT assay.** Time spent exploring objects by saline-treated, Swiss Webster mice (n=40) exposed to two identical objects in the acquisition trial (training phase, acquisition, A) and to one familiar object and one novel object in the retention trial (testing phase, retention, B). Testing was performed 1 h after training. Ordinate: exploration time in sec. Data are shown as mean  $\pm$  S.E. M. Significantly different (\*\*\*) $P < 0.001$ ) from familiar object as indicated by student's paired t-test.

To further validate the procedure and to test for recognition memory deficits, we used three known drugs, namely scopolamine, ketamine, and acetazolamide that can disrupt memory in other assays [104, 147, 160, 165]. Mice were injected after the training phase with either scopolamine (1 or 10 mg/kg, i.p.), ketamine (10, 20, 32 or 56 mg/kg) and acetazolamide (1 or 10 mg/kg). Groups of 6-9 mice were used for each dose point (Figure 18). Data from Figure 18 revealed that recognition memory impairments were induced with scopolamine (both 1 and 10 mg/kg doses), ketamine (only at high dose of 56 mg/kg) and acetazolamide (only at high dose 10 mg/kg), as shown by almost equal exploration time for both familiar and novel object during the testing phase (retrieval phase).

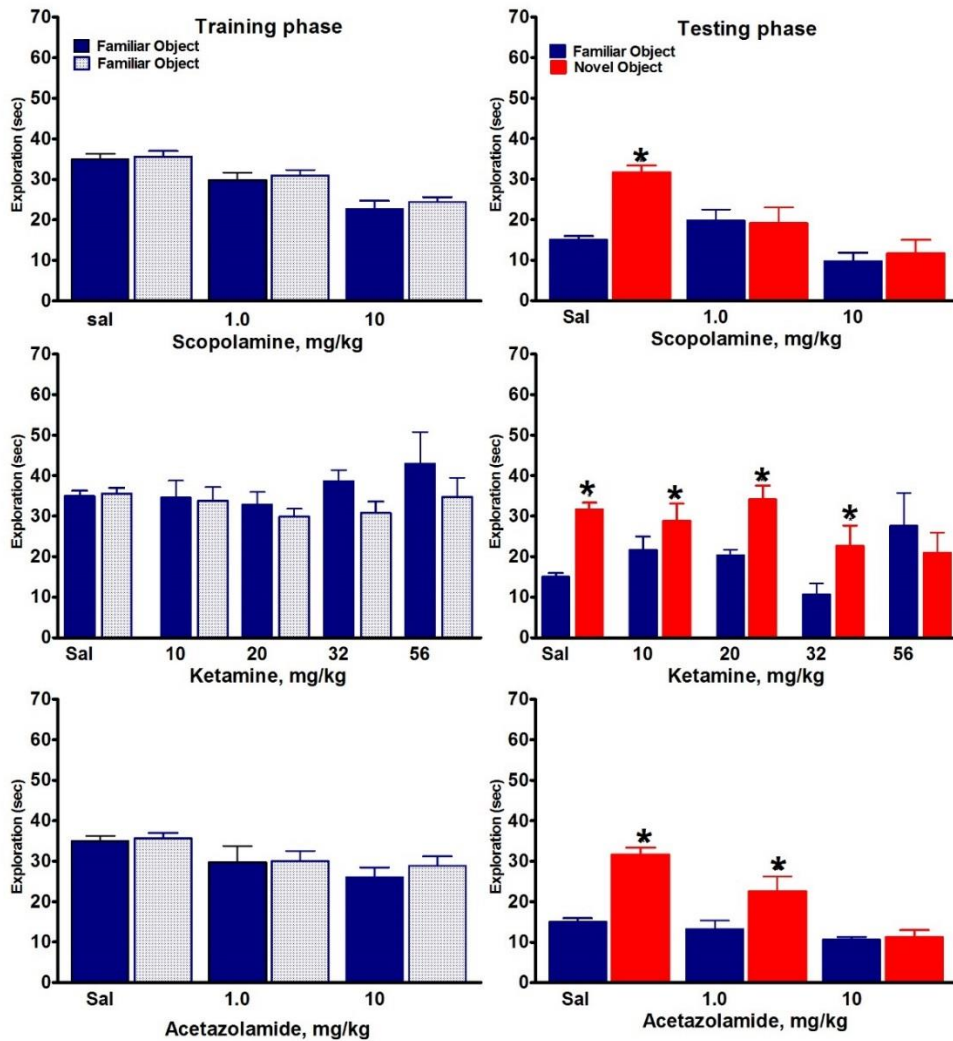


**Figure 18.** Scopolamine, ketamine and acetazolamide produce dose-dependent disruption of memory retrieval in Swiss-Webster mice. Saline (n=40), 1.0 -10 mg/kg Scopolamine (n=6-9, per dose), 10-52 mg/kg ketamine (n=6-9, per dose) and 1.0-10 mg/kg Acetazolamide (n=6-9, per dose) were injected after the training phase (right panel). Saline was injected 30 min prior to training phase (Familiar vs. Familiar) and scopolamine/acetazolamide/ketamine injections occurred immediately after training phase and 1 h prior to testing phase (Familiar vs. Novel). Ordinate: exploration time in sec. Data are shown as mean  $\pm$  S.E.M. Significantly different (\*, at least  $P < 0.05$ ) from familiar object as indicated by student's paired t-test. Note: the mice did not receive drug until after the training phase, however the legends are matched to data presented in the right panel.

A dose-response curve was determined for **19e (BD117)** (0.03-3.0 mg/kg) to evaluate the efficacy and safety profile of the novel CAA. The CAA, **19e (BD117)** was injected i.p. at doses of 0.03, 0.3 and 3.0 mg/kg 30 min before the acquisition session within the standard one hour delayed NORT procedure. Donepezil (DP), a mild cognitive enhancer, was used as positive control [166] at 0.3 mg/kg (Figure 19, upper panels). Data from Figure 19 revealed that CAA **19e (BD117)** did not impair or improve acquisition and retrieval phases and that the pattern of response for the BD117-inject mice was similar to the trend observed for saline-treated mice. Similarly, donepezil did not impair or improve recognition memory as compared to saline-treated mice. At higher doses of **19e (BD117)**, the time dedicated to the exploration of the novel object in the retrieval phase was diminished. These data confirm that **19e (BD117)** treatment had no significant adverse effects on exploration activity in the NORT over a wide range of doses (Figure 19). We selected the lower dose of 0.03 mg/kg to be used in subsequent experiments designed to evaluate of the ability of **19e (BD117)** to protect mice from recognition memory deficits caused by scopolamine, ketamine and acetazolamide.

We have tested lead CAA **19e (BD117)**, which activates mitochondrial CA V and membrane-bound CA isozymes CA IV and CA IX (see activation profile in Table 3), for the ability to protect the mice from drug-induced recognition memory deficits. The lead CA activator **19e (BD117)** was injected 30 min prior to acquisition phase, at a dose of 0.03 mg/kg, followed by 1 mg/kg scopolamine or 56 mg/kg ketamine or 10 mg/kg acetazolamide, administered after the end of acquisition phase. Results (Figure 19, bottom panels) revealed that CAA **19e (BD117)** prevented scopolamine and acetazolamide from disrupting recognition memory and also induced an improved

overall exploration time (familiar object + novel object) when compared with the same parameter recorded for the animal group treated just with the corresponding memory disruptor. This observation suggests that our lead CAA activator, **19e (BD117)** can protect the drug induced recognition memory deficits caused by scopolamine.

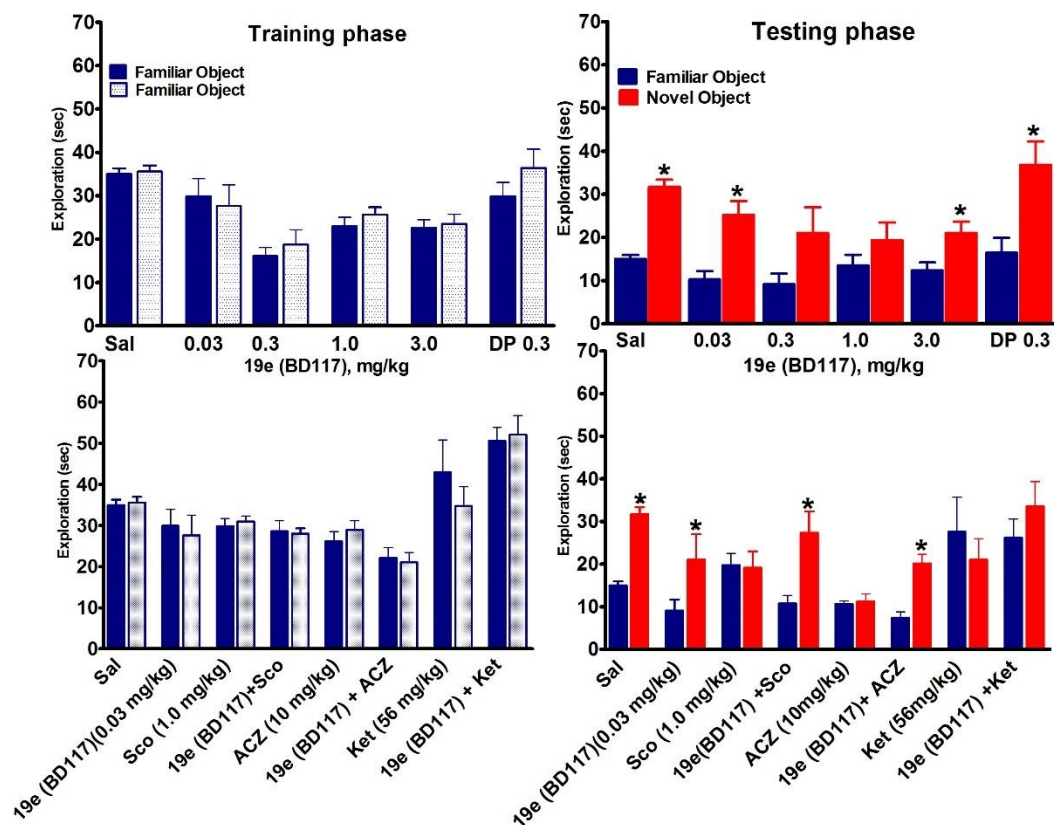


**Figure 19.** Impact of CAA **19e (BD117)** on recognition memory in Swiss-Webster mice, in the absence and in the presence of memory disruptors scopolamine (Sco), ketamine (Ket) and acetazolamide (ACZ), as assessed by NORT procedure (n=6-9, per dose). Upper panel: dose-response curves of **19e (BD117)**; note that doses of 0.03 and 3.0 mg/kg produced similar effects to positive control donepezil at 0.3 mg/kg. Lower panel: CAA **19e (BD117)** is able to reverse the scopolamine-, acetazolamide-, but not ketamine-induced deficits in NORT. Ordinate: exploration time in sec. Data are shown as mean  $\pm$  S.E.M. Significantly different (\*, at least  $P < 0.05$ ) from familiar object as indicated by student's paired t-test.

### **3.4.9 Triangulation of CA isozyme potentially involved in learning and memory using CAAs and NORT**

In order to determine the CA isozymes responsible for the learning and memory in mammal brain, we have decided to tested 5 more CAAs from series **19** and **20**, each having different CA isozyme activation profiles (Table 3), using the same NORT procedure. We considered that we might need to selectively activate one, two or more different CA isozymes simultaneously with our CAAs in order to generate a nootropic effect. We compared these results with the ones obtained with our multi CA isozyme-activator **19e** (**BD117**) (Figure 20). We have selected **19a**, **19b**, **19c**, since they are nanomolar potent against CA IV and CA VA. Their direct comparison with **19e** was expected to reveal if CA IX activation simultaneously with CA IV and VA, which can be achieved only by **19e**, is important for the nootropic effect. At the same time CAAs **19a-c** would allow us to test the impact of lipophilicity on the nootropic action, since they have a similar CA isozyme activation profile. We have also selected compounds **20a** and **20e**, with nanomolar potency against CA VA and CA IX. These CAAs are isomers of **19a** and **19e**, with almost similar physicochemical properties, allowing a direct comparison of effects associated with activation of CA IV (by **19** series) versus CA IX (by **20** series), besides CA VA, activated by both series. Moreover, by directly comparing the effects of CAAs **20a** and **20e** with **19e**, one could evaluate the impact of activating CA IV, simultaneously with CA VA and CA IX, to the nootropic effect.

Data from Figure 20 revealed that CA activators **19a**, **19b**, **19c**, **19e** (**BD117**), **20a** and **20e**, tested at a constant dose of 0.03 mg/kg, administered 30 min before the acquisition session, had no adverse effects on exploration activity of the mice in both

the training and testing phase of NORT. Data from Figure 20 revealed that CAAs treatment did not impair or improve acquisition or retrieval alone and that the pattern of exploration was similar to the trend observed for saline-treated mice. Mice spent time exploring an object during the training session after treatment with above-mentioned CAAs indicating that the CAAs did not disrupt normal exploratory behavior. Mice consistently recognized the familiar object an hour later, in the retrieval session, and spend statistically significant more time exploring the novel object after testing all CAAs (Figure 20, right panel,  $p < 0.01$ ). These preliminary evaluations confirmed that all CA activators at a dose of 0.03 mg/kg produced no obvious adverse effects in terms of motor activity or exploration in the NORT.

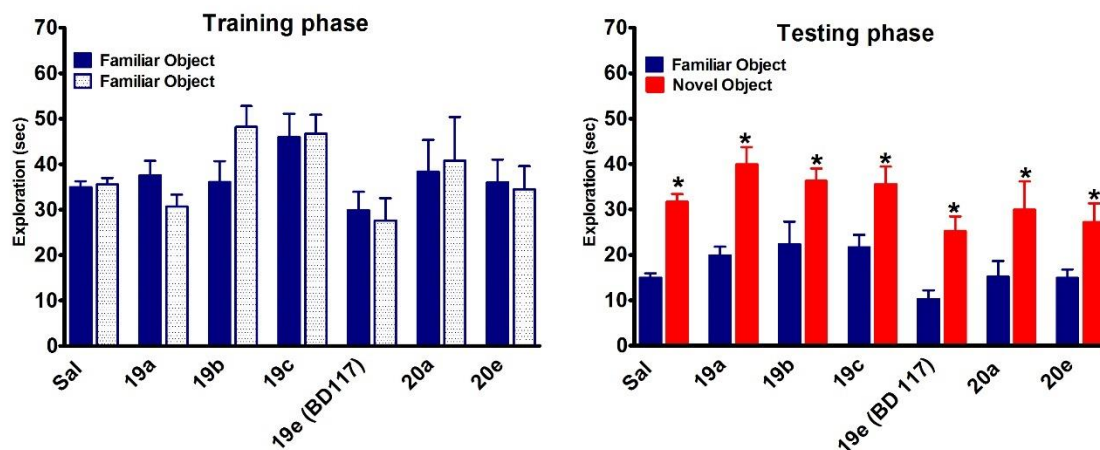


**Figure 20:** Impact of selected CAAs with different isozyme activation profiles on recognition memory in Swiss-Webster mice, at doses of 0.03 mg/kg, each as assessed by NORT procedure ( $n=6-9$ , per compound). Note that no adverse effects on motor activity for both training and testing phases of the NORT procedure were observed. Data are shown as mean  $\pm$  S.E.M. Significantly different (\*, at least  $P < 0.05$ ) from familiar object as indicated by student's paired t-test.

Subsequently, we tested the same CAA set for their capacity to prevent recognition memory deficits induced by scopolamine, ketamine or acetazolamide, similar to the procedure with **19e (BD117)** (Figure 21). Data from Figure 21 revealed that **19a, 19b, 19c** and **19e (BD117)**, at doses of 0.03 mg/kg, prevented the memory deficits induced by scopolamine (1.0 mg/kg), while **20a** and **20e** did not. Since scopolamine is a muscarinic antagonist that acts on the cholinergic pathway, these data suggest that activation of both CA IV and CA VA are required to prevent memory deficits generated through this pathway. Activation of CA VA and CA IX alone (by CAAs **20a** and **20e**) does not seem to be sufficient to prevent recognition memory deficits induced by scopolamine, indicating a key role played by the missing CA IV in modulating cholinergic responses. The confirmed presence of CA IV in hippocampal pyramidal CA 1 cells (Table 2) and the absence of CA IX from the same region seems to suggest a key role of CA IV in recognition memory and learning via cholinergic pathway in this assay.

On the other hand, acetazolamide-induced memory impairments (at 10 mg/kg) could be prevented only by **19e (BD117)**, **20a**, **20e**, revealing the importance of co-activation of CA VA and CA IX in preventing recognition memory deficits generated by this CA inhibitor. These deficits may be related with general  $\text{CO}_2/\text{HCO}_3^-$  imbalances in the whole brain, as acetazolamide is non-selective potent CA inhibitor [5]. Furthermore, since CA IX is present in large amounts in the choroid plexus that secretes the cerebrospinal fluid, CA IX has the potential to compensate for these  $\text{CO}_2/\text{HCO}_3^-$  concentration imbalances as cerebrospinal fluid is the main buffering fluid in the brain and serves as a bicarbonate source for proton neutralization catalyzed by CA isozymes.

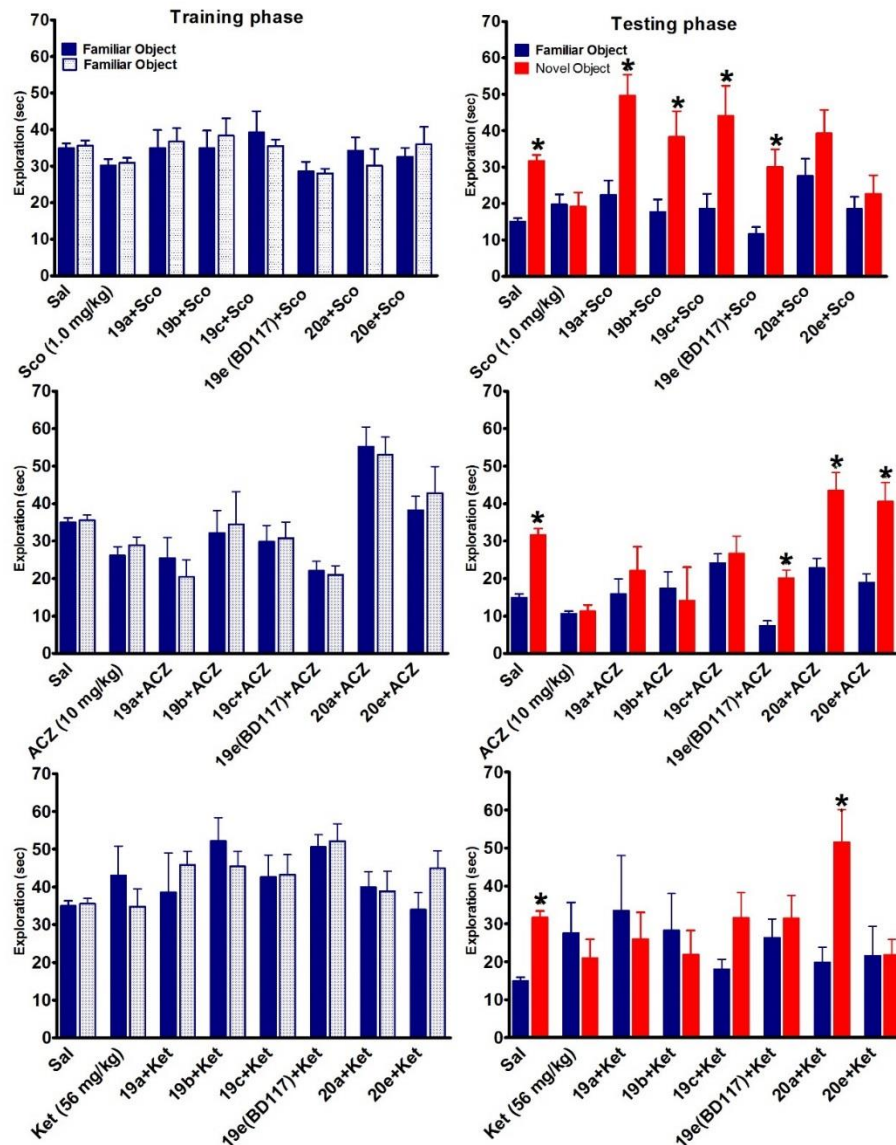


**Figure 21: The CAAs capacity to prevent recognition memory deficits caused by scopolamine, acetazolamide, or ketamine depends on the isozyme activation profile of the tested compounds.** Time spent exploring familiar object vs. novel object in the training phase (left panel) and testing phase (right panel) of the 1h-delayed NORT procedure (n=6-9, per dose per compound). CAAs (0.03 mg/kg) were injected 30 min prior to training phase, while the amnesics scopolamine (Sco), ketamine (Ket) and acetazolamide (ACZ) were injected after the training session, at specified doses. Data are shown as mean  $\pm$  S.E.M. Significantly different (\*, at least  $P < 0.05$ ) from familiar object as indicated by student's paired t-test.

The bicarbonate basal concentration also influences the ionic balance of neurons, their membrane potential and excitability. Interestingly, only **20a** was able to reverse the memory deficits caused by ketamine. In this case, we cannot advance a clear-cut hypothesis, possibly due to the complex mechanism of memory disruption by ketamine and its particular metabolism (Figure 21).

#### **3.4.10 Simple 1-day operant task**

Another relatively rapid-throughput learning and memory assay developed in our laboratory is the 1-day operant task procedure which is based off a series of assays of combined Pavlovian and Instrumental conditioning called autoshaping. In the first description of autoshaping, the repeated pairing of a light stimulus with the delivery of food led to the emergence of responses from pigeons that could be differentiated and maintained by its consequences [167]. The autoshaping procedure combines both Pavlovian and instrumental conditioning and requires an intact neuronal system, specifically the hippocampus, septum, and cortex [168, 169]. An advantage to using variations of this simple procedure is that effects on acquisition, consolidation, and/or retention can be measured by administering drugs at different time points, and drug effects on motivation or motor responses can also be detected [170-172]. Our laboratory has published on three different variations of a two-day operant task procedure with different proportions of Pavlovian and/or Instrumental conditioning to study drugs in adult and adolescent male and female mice [148, 149, 173, 174]. For the current study, we further modified the two-day autoshaping task to more rapidly assess acquisition and retention using a one-day procedure more reliant on instrumental conditioning. We

reduced our acquisition session from two to one hour and removed the non-contingent food presentations as in previous studies [175]; however, we tested the mice for retrieval 1 h after the acquisition session instead of 24 h, similar to a procedure in rats, in order to focus more on short-term memory processes [165] and increase the throughput of the assay. To validate the procedure, we used two known amnesics, scopolamine and ketamine that have worked in the 2-day procedure [147, 165].

Saline control. In the current study, using a single day acquisition and retrieval procedure, mice injected with saline decreased the average latency to earn 10 rewards ( $t(63)=3.74$ ,  $p<0.0004$ ), increased the reinforced response rate ( $t(64)=9.15$ ,  $p<0.0001$ ), and decreased the non-reinforced response rate (errors) ( $t(64)=4.0$ ,  $p<0.0002$ ) indicative of learning and subsequently retrieving the nose-poke response (Figure 22).

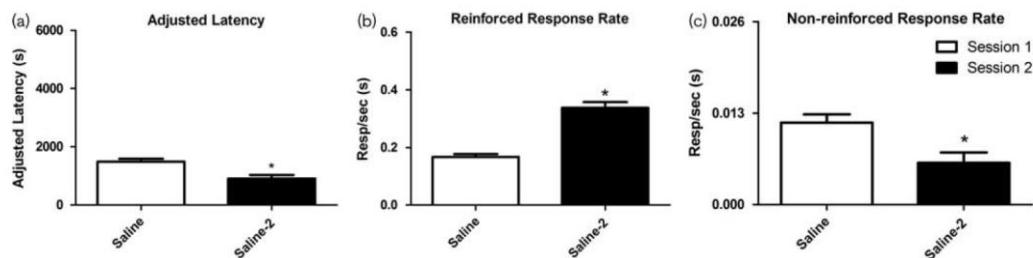


**Figure 22.** Mice acquire and retrieve a novel nose-poke response using the 1-day procedure. Effects of saline in male, Swiss Webster mice (N = 64) during session 1 (open bars) and during session 2 (closed bars). Vertical axes: (a) mean adjusted latencies calculated as the time in s from the first to the 10th reinforcer; (b) mean reinforced response rates calculated as the total number of center-hole, nose-poke responses over session time in s; (c) mean nonreinforced response rates calculated as the total number of responses in both the left and right nose-poke holes divided by the total session time in s. Total number of mice tested/number of mice completing at least five reinforcers during session 1 (64/63). Horizontal axes: Saline injections, administered intraperitoneally, either 30 min before session 1 or immediately after session 2. Significantly different

(\* , at least  $P < 0.05$ ) from session 1 as indicated by paired t-test. Vertical bars represent SEM.

Multiple doses of scopolamine (0.01-10 mg/kg), ketamine (3.2-18 mg/kg), and acetazolamide (1 and 10 mg/kg) were tested for the capacity to disrupt learning or retrieval of the nose-poke response (Figure 23). Memory impairments were observed for scopolamine treatment at doses ranging from 0.1 to 10 mg /kg, for ketamine at 18 mg/kg and for acetazolamide at both 1 and 10 mg/kg administered after the training phase. A number of 6-10 mice were used for each dose point. An effective disruptive dose was selected from the graph and was combined with one of our CAAs to test for reversal of retrieval deficits.

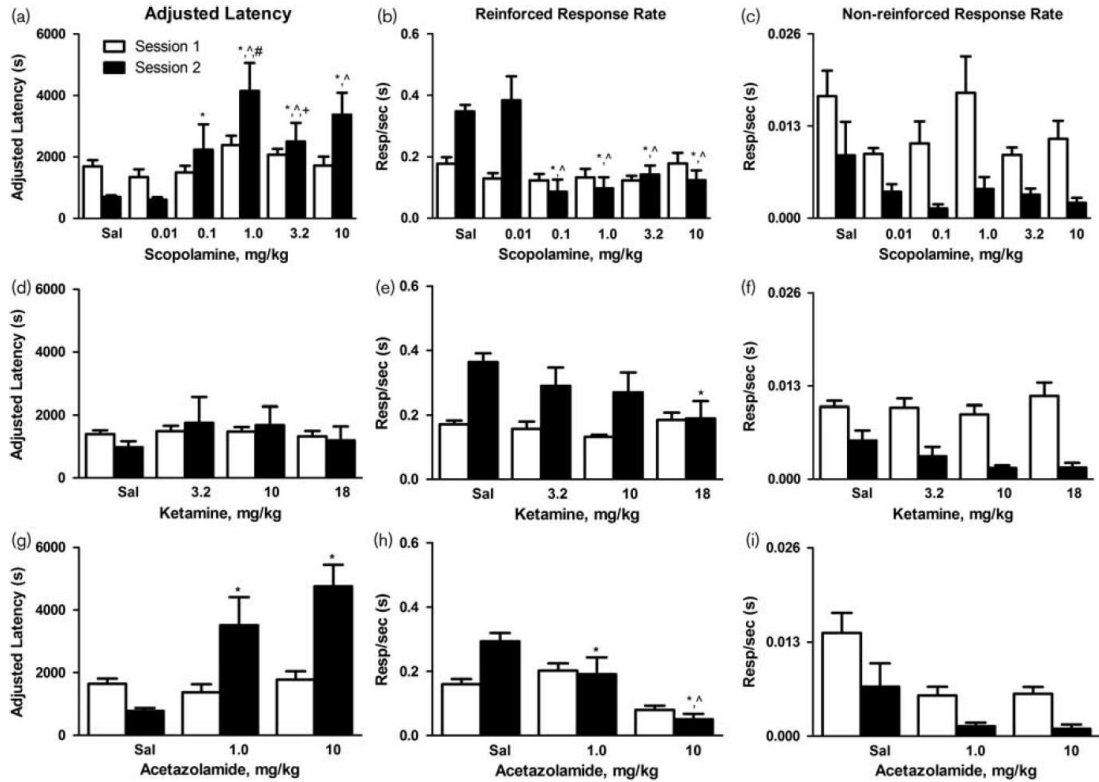


**Figure 23.** Scopolamine, ketamine, and acetazolamide produce different patterns of acquisition and retrieval disruption in mice. Vertical axes: (a,d,g) mean adjusted latencies calculated as the time in s from the first to the 10th reinforcer; (b,e,h) mean reinforced response rates calculated as the total number of center-hole, nose-poke responses over session time in s; (c,f,i) mean nonreinforced response rate calculated as the total number of responses in both the left and right nose-poke holes divided by the total session time in s. Horizontal axes: Saline or doses in mg/kg of scopolamine (a–c), ketamine (d–f), or acetazolamide (g–i) injected intraperitoneally immediately after session 1. (a–c) Total number of mice tested/number of mice completing five reinforcers in session 1: Saline (n=16/16), 0.01 mg/kg (n=6/6), 0.1 mg/kg (n= 9/9), 1.0 mg/kg (n= 10/10), 3.2 mg/kg (n=15/15), and 10 mg/kg (n =12/12) scopolamine. Significantly different from saline in session 2 (\*, at least  $P < 0.05$ ); significantly different from 0.01 mg/kg scopolamine in session 2 (^, at least  $P < 0.05$ ) and significantly different from 1.0 mg/kg acetazolamide in session 2 (^, at least  $P < 0.05$ ). Vertical bars represent SEM.

A dose-response curve was determined for **19e (BD117)** (0.03 and 0.3 mg/kg) as these were the doses effective in the NORT and **18c (MAI27)** (3-30 mg/kg) injected to evaluate the efficacy and safety profile of these novel CAAs. We selected these two CAAs due to their activation profile (two isozymes for **18c** and three isozymes for **19e** activated at nanomolar levels) combined with a good lipophilicity profile that guarantees a likely optimum brain penetration. Data from Figure 24 revealed that 0.03 mg/kg **19e (BD117)** and 30 mg/kg **18c (MAI27)** produced no overall dose differences for adjusted latencies, reinforced rates, or nonreinforced rates. Therefore, these two CAAs at these doses did not impair or improve acquisition and retrieval phases and that the pattern of effects was similar to the trend observed for saline-treated mice. These optimal doses were used in subsequent experiments designed to evaluate the novel CA activators to protect mice from memory deficits caused by ketamine and acetazolamide.

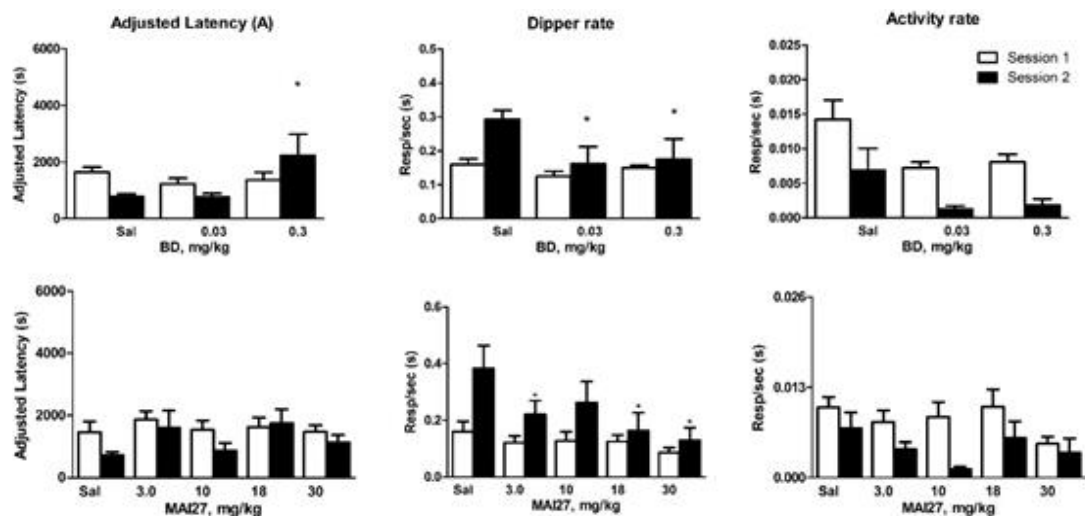


**Figure 24.** Dose response curves of **19e (BD117)** and **18c (MAI27)** in the simple one-day operant task. Horizontal axes: saline or doses in mg/kg **19e (BD117)** (upper panel), **18c (MAI27)** (lower panel) injected intraperitoneally 30 min before session 1. Upper panel for **19e (BD117)**, Total number of mice tested/number of mice completing at least five reinforcers in session 1: Saline (n=23/23), 0.03 mg/kg (n =7/7) and 0.3 mg/kg (n= 8/8). Lower panel for **18c (MAI27)**, Total number of mice tested/number of mice completing at least five reinforcers in session 1: Saline (n=8/6), 3.0 mg/kg (n =14/12), 10 mg/kg (n= 9/5), 18 mg/kg (n =9/9), and 30 mg/kg (n =6/5). Significantly different from saline (\*, at least  $P < 0.05$ ).

To determine if **18c (MAI27)** or **19e (BD117)** would restore the drug-induced deficits produced by ketamine and acetazolamide, we tested 30 mg/kg **18c (MAI27)** combined with 18 mg/kg ketamine and 0.03 mg/kg **19e (BD117)** in combination with acetazolamide (1 and 10 mg/kg). We found that **18c (MAI27)** partially protects the memory deficit caused by ketamine. Importantly, **19e (BD117)** partially protected the memory deficit caused by acetazolamide at 1 mg/kg (Figure 25), similarly to the effect observed in NORT testing.

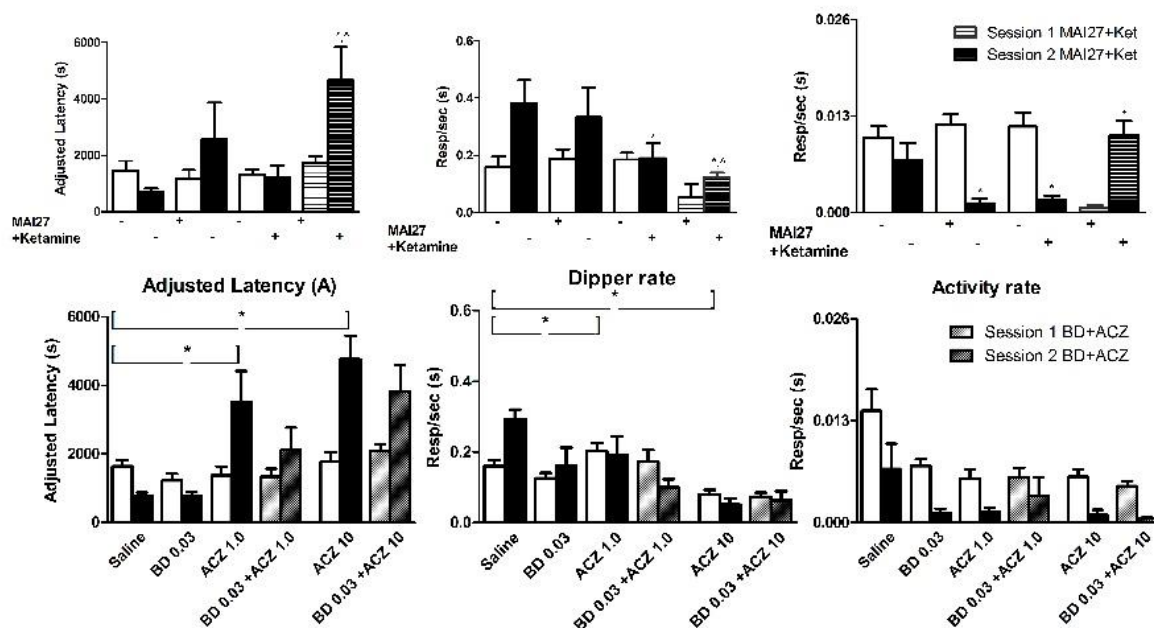


**Figure 25.** Co-administration of **18c (MAI27)** or pretreatment of **19e (BD117)** partially protected the retrieval of a newly learned operant response when administered prior to ketamine and acetazolamide respectively. Horizontal axes, (upper panel): Saline, doses of 30 mg/kg **18c (MAI27)** and 10 mg/kg ketamine alone after session 1, or in combination injected together after session 1. Total number of mice tested/number of mice completing five reinforcers in session: Saline (n= 8/6), 30 mg/kg **18c (MAI27)** (n =6/6), 18 mg/kg ketamine (n =11/11), and 30 mg/kg **18c (MAI27)**+18 mg/kg ketamine (n =8/8). Significantly different from saline (\*, at least  $P < 0.05$ ) or 18 mg/kg ketamine (^, at least  $P < 0.05$ ) in session 2. Horizontal axes, (lower panel): Saline, doses of 0.03 mg/kg **19e (BD117)** injected 30 min prior to session 1, 1 and 10 mg/kg ACZ injected immediately after session 1, or in combination injected 30 min before session 1 **19e (BD117)** and immediately after session 1 (ACZ). Total number of mice tested/number of mice completing five reinforcers in session: Saline (n= 23/23), 0.03 mg/kg **19e (BD117)** (n =7/7), 1 mg/kg ACZ (n =12/12), 10 mg/kg ACZ (n=17/17), 0.03 mg/kg **19e (BD117)**+ 1 mg/kg ACZ (n=11/11) and 0.03 mg/kg **19e (BD117)** + 10 mg/kg ACZ (n=12/12). Significantly different from saline (\*, at least  $P < 0.05$ ) in session 2

## Conclusions

Following our physicochemical profiling strategy, we have determined the cLogP, TPSA and solubility of the novel CAAs series **19** and **20**, which were fitting the general requirements of a good profile for CNS drugs. All CAAs were subsequently screened for toxicity in vitro and were found to be non-toxic. CAA **19e** (**BD117**) was the least toxic out of all CAAs tested in vitro and became our lead activator. The selection of CAA **19e** (**BD117**) was also based on high lipophilicity and on nanomolar potency against three different CA isozymes namely CA IV, CA VA and CA IX. Microsomal stability testing of **19e** (**BD117**) revealed a suitable stability profile that further supported the advancement of this CAA into in vivo testing as a potential nootropic. Significant brain uptake and lack of obvious adverse effects, even at elevated doses, were further consideration for **19e** testing in mice. Lack of behavioral toxicity for a full dose-response curve for **19e** was confirmed in the NORT and the simple 1-day operant task – two tests for memory and learning. To further explore potential roles for the different isozymes, we extended in vivo testing to other representatives of series **19** and **20**, validating our structure-activity design. Importantly, some of CAAs were able to prevent memory deficits induced by scopolamine, ketamine and acetazolamide in NORT (recognition memory) and partially in simple 1- day operant task that likely includes a dopaminergic component as this particular assay has a motivational component to earn a positive reinforcer. NORT results suggest that activation of both CA IV and CA VA are required to prevent memory deficits generated through the cholinergic pathway, while co-activation of CA VA and CA IX seem to be important in preventing recognition memory

deficits generated via GABAergic pathway, in good correlation with the isozyme distribution and function in the mammal brain.

## CHAPTER 4

### DEVELOPMENT AND BIOLOGICAL EVALUATION OF CARBONIC ANHYDRASE INHIBITORS AS POTENTIAL ANTI-CANCER AGENTS

The main goal of the research described in this chapter was to correlate the structure of novel carbonic anhydrase inhibitors with their physicochemical properties, inhibition profile against different CA isozymes, and with their ability to kill cancer cells. We hypothesized that in order to be able to elicit significant cancer cell killing, the CA inhibitors (CAIs) need to combine medium solubility and lipophilicity with a good inhibition profile against specific CA isozymes. Recent studies have shown that two carbonic anhydrase isozymes, CA IX and CA XII are over-expressed in many tumors where they are involved in pH regulation, cell adhesion, and tumor progression [5, 176, 177].

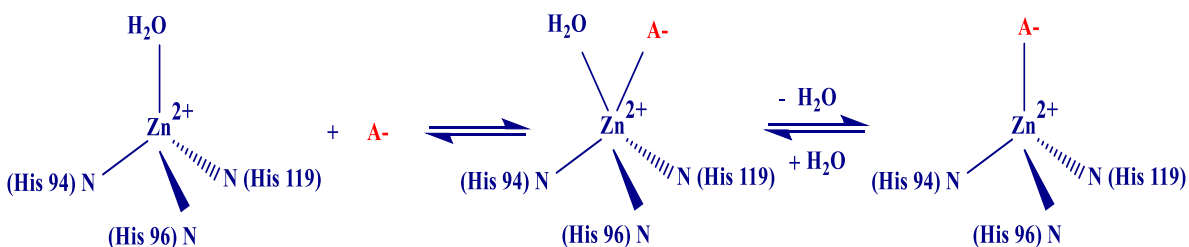
Despite substantial synthetic efforts, achieving a high isozyme selectivity in vitro with classical designs incorporating aromatic/heterocyclic primary sulfonamides is rather difficult due to a relatively high sequence homology that exists between different CA isozymes. This elevated sequence homology translates into extensive structural similarities of their active sites, which makes the design of isozyme-selective CAIs a difficult task [5, 176, 177]. Strategies to enhance the selectivity for membrane-bound isozymes in vivo involve conjugation of CAI pharmacophores with charged groups, with sugars, or with polymeric moieties that will make the inhibitors membrane-impermeant and therefore unable to access the intracellular CA isozymes [177].

## 4.1 Background and Rationale

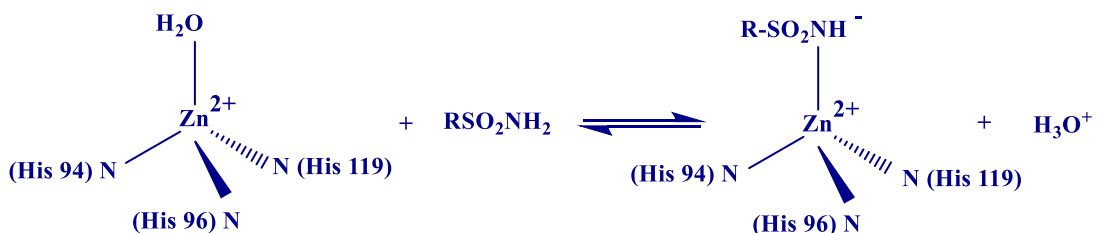
### 4.1.1 Classes of carbonic anhydrase inhibitors

Two main classes of CA inhibitors are known to date [5]:

- 1) First category includes small anions  $\text{CN}^-$ ,  $\text{ClO}_4^-$ ,  $\text{CNO}^-$ ,  $\text{HS}^-$ ,  $\text{HSO}_3^-$ ,  $\text{N}_3^-$ ,  $\text{NO}_3^-$ ,  $\text{R-COO}^-$ ,  $\text{SCN}^-$ ,  $\text{SO}_4^{2-}$  and  $\text{X}^-$  ( $\text{X} = \text{F}, \text{Cl}, \text{Br}, \text{I}$ ). These ions bind directly to the  $\text{Zn}^{2+}$  with different affinities, forming tetra- and penta-coordinated species:



- 2) Second category of CAIs includes organic ligands, mainly sulfonamides, sulfamates, sulfamides, hydroxamates, and some phenols, polyamines, and xanthates discovered recently. These compounds bind to the Zn ion displacing the zinc-bound water and generating tetra coordinated species:



Among the various classes of inhibitors, sulfonamides are the most investigated and used physiological, pharmacological, and clinical use. They bind to the  $\text{Zn}^{2+}$  ion, displacing the  $\text{OH}_2$  or  $\text{OH}$  ligands to generate a stable tetra coordinated Zn species. Early

inhibition studies established that only **aromatic and heterocyclic** primary sulfonamides (R-SO<sub>2</sub>NH<sub>2</sub>, R = Aryl, Hetaryl) are potent CA inhibitors [5].

After the initial discovery of the inhibitory effect of aromatic/heterocyclic primary sulfonamides, many representatives were synthesized and investigated as CAIs. Rigorous selection of the most efficient aromatic and heterocyclic systems and further optimizations of the substituent moieties yielded clinically used inhibitors acetazolamide (**ACZ**), methazolamide (**MTZ**), ethoxzolamide (**ETZ**), dichlorphenamide (**DCP**), benzolamide (**BZA**), zonisamide (**ZNA**) and topiramate (**TPM**) (Chart 2).

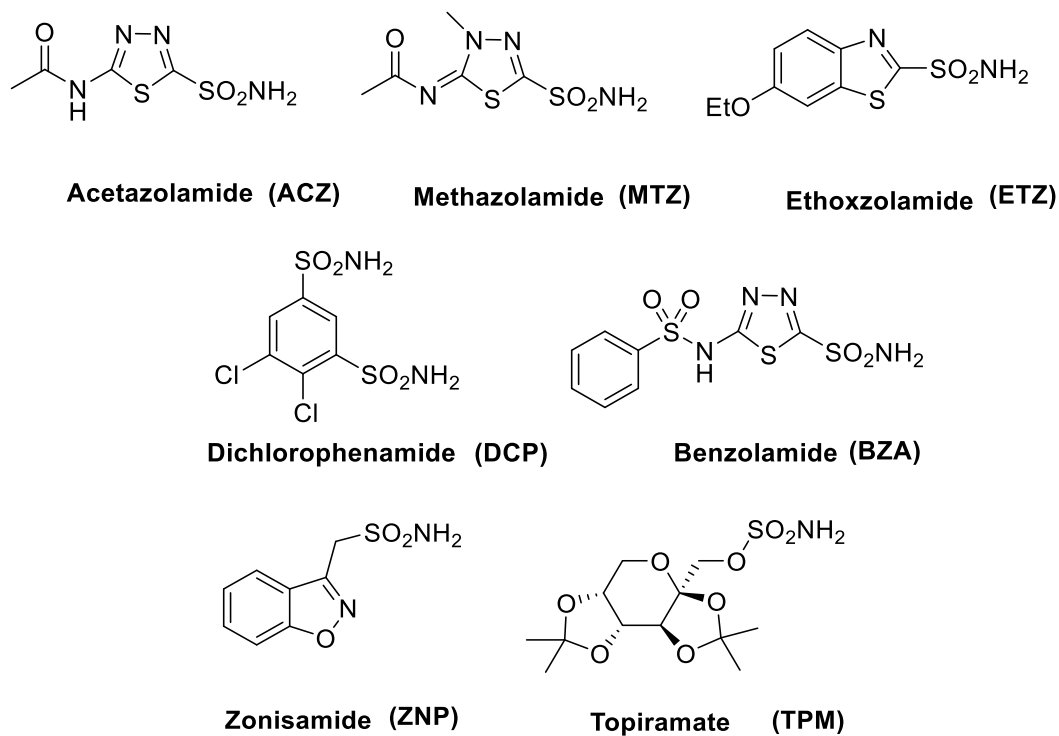


**Chart 2:** CA inhibitors in clinical use, designed either for systemic use (**ACZ-BZA**) or for topical administration into the eye (**ZNP** and **TPM**).

CAIs are used in clinic as diuretics, antiglaucoma agents and antiepileptics [178]. Other uses include the management of mountain sickness, osteoporosis, gastric and duodenal ulcers [5]. The inhibitory effects against different over expressed CA isozymes have been recently investigated in various disease states, including cancer.

#### **4.1.2 Cancer and its metabolic shift**

In the last two decades of oncology research, two membrane bound CA isozymes, namely CA IX and CA XII, are predominantly associated with cancer, where they are involved in pH regulation and tumor progression [14, 71, 72, 176, 179-183].

Cancer cells are characterized by their upregulated glucose metabolism [184, 185]. This hallmark metabolic shift governs cancer cells proliferation, differentiation, survival, and special expression of some cell surface antigens that may be fatal to normal cells [180, 186, 187]. In normal cells, glucose is converted to glucose-6-phosphate which is later converted to pyruvate. This pyruvate is then subsequently oxidized in the mitochondria to carbon dioxide and water. This entire process of oxidative phosphorylation, releases 38 moles of ATP per molecule of glucose (Figure 26 A). Exponential proliferation of cancer cells and the poor associated vasculature can lead to inadequate oxygen supply to some regions of tumors, making them hypoxic [180, 186, 187]. This restricts oxidative phosphorylation as this process requires oxygen supply. To cope up the energy needs, hypoxic tumor cells shift their regular metabolism towards glycolysis. To regenerate the  $\text{NAD}^+$  required in glycolysis, the pyruvate is reduced to lactate with NADH. Glycolysis generates only 2 moles of ATP per single mole of glucose (Figure 26 B). Though this is a very energy-inefficient process compared to

oxidative phosphorylation, glycolysis does not require oxygen [188]. Furthermore, even after reoxygenation of these cancerous cells, glycolysis persists because the obtained metabolic intermediates like lactate and pyruvate are used for the biosynthesis of nucleotides, amino acids and lipids. This provides a selective advantage to proliferating cancer cells. **The over-expression of glycolysis in cancerous cells was first observed by Warburg and it's known as the Warburg effect** (Figure 26B) [188].

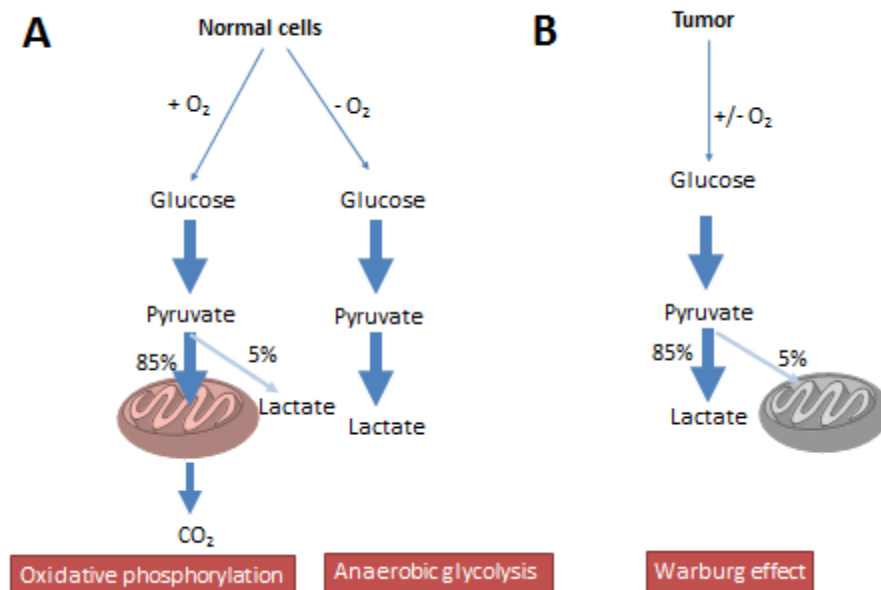


**Figure 26.** Differences between metabolisms of normal cells (A), as compared to tumors (B). Normal cells in the presence of oxygen perform oxidative phosphorylation, while the cancer cells either in the presence or absence of oxygen overexpress glycolysis for their energetic and biosynthetic needs.

#### **4.1.3 Overexpression of CA IX, CA XII in hypoxic tumor cells.**

The overexpression of glycolysis generates large amounts of protons ( $H^+$ ). These protons cannot be neutralized through mitochondrial oxidative phosphorylation process, significantly reduced under hypoxic conditions [189-193]. Thus, malignant cells have evolved various mechanisms to cope with the acidic and hypoxic stress caused by this oncogenic metabolism. Hypoxia triggers the expression of Hypoxia Inducible Factor-1 (HIF-1), which in turn triggers the expression of nearly 500 genes [180, 186, 187]. These genes are translated into different biochemical entities such as pumps, transporters, enzymes that are needed for cancerous cells to survive in the hypoxic and acidic environment. Among the proteins needed to support hypoxic metabolism and pH homeostasis of tumorous cells is the membrane bound carbonic anhydrase (CA), namely CA IX (Figure 27).

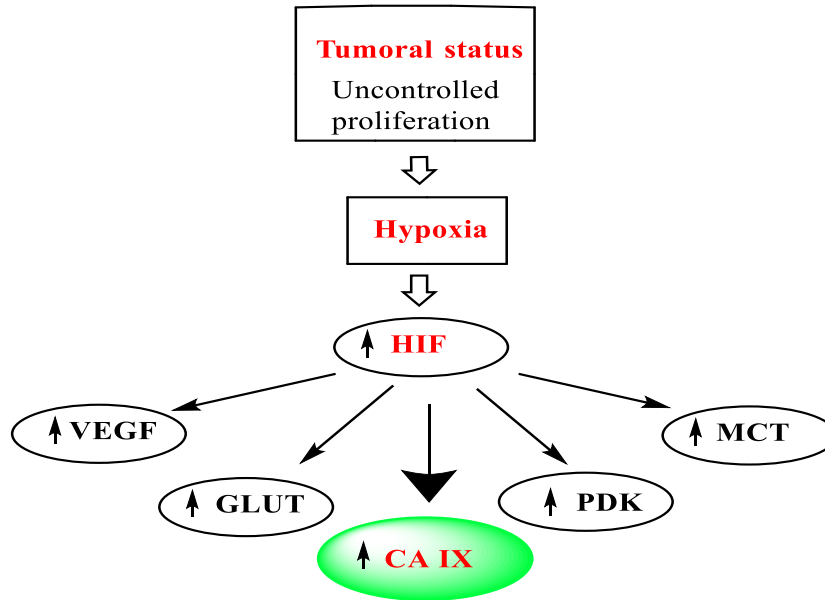


**Figure 27:** Uncontrolled proliferation and poor vasculature of cancer cells leads to the hypoxia. Hypoxia upregulates the HIF pathway which in turn upregulates the expression of transmembrane CA isozyme CA IX.

In cancerous cells, CA IX acts in co-ordination with the cytosolic CA isozymes (CA I and CA II) to maintain internal pH within normal limits (around 7.2). At the same time, they move the protons generated in glycolysis from interior to the exterior of the malignant cells. In cytoplasm,  $H^+$  ions produced through glycolysis are combined with intracellular  $HCO_3^-$  ions in the active sites of cytosolic CA isozymes CA I and CA II to yield carbon dioxide and water.  $CO_2$  diffuses through the cells membrane and is rehydrated outside the tumor cell by membrane bound, over-expressed tumor isozyme CA IX. Bicarbonate ion ( $HCO_3^-$ ) is imported into the cells interior via exchange with  $Cl^-$  through anion exchanger (AE2). This replenishes the cytoplasmic  $HCO_3^-$  levels at the same time allowing continuous  $H^+$  transport outside cell. Thus, malignant cells can maintain their internal pH within normal limits despite intense glycolysis and hypoxic stress (Figure 28).

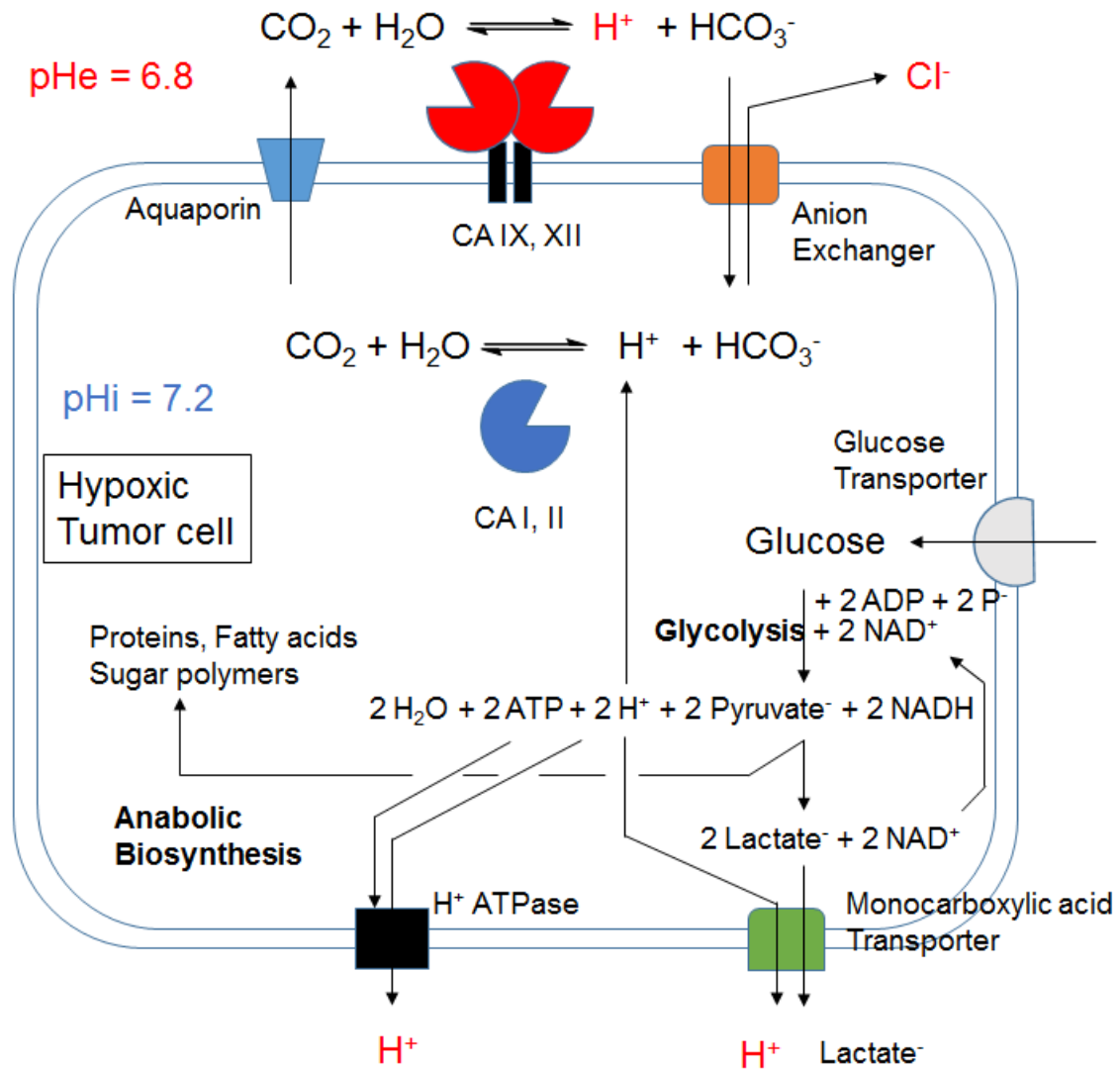


**Figure 28:** The central role played by overexpressed transmembrane CA isozymes CA IX, CA XII in tumor cells metabolism.  $\text{H}^+$  ions produced via glycolysis are transported outside the cell with the help of cytosolic CA Isozymes (CA I and CA II) and transmembrane, tumor overexpressed CA isozyme CA IX.

Proton export through this mechanism leads to a reduction in the extracellular pH (pHe = 6.8) [180, 186, 187]. This is a salient feature of the tumor microenvironment and gives a substantial growth advantage to cancerous cells over normal cells, as normal cells

undergo apoptosis in response to prolonged exposure to acidic environment. Hypoxia also constitutes a detrimental feature for radiotherapy, as oxygen is necessary to generate free radicals to damage tumor cells DNA in radiotherapy. Therefore, there is a need for new pharmaceutical agents that can selectively bind and inhibit tumor overexpressed proteins such as CAIX [194].

#### **4.1.4 Anti-tumor activity of carbonic anhydrase IX inhibitors**

Interfering with tumor cell pH homeostasis through the selective inhibition of CA IX has the potential to control, suppress and kill these proliferative cancer cells [195]. The membrane-bound CA IX is normally found only in the epithelium lining of stomach and small intestine, where the isozyme is involved in pH regulation of the extracellular environment. The tumor expression pattern of CA IX, in comparison with the corresponding normal tissue expression is shown in Figure 29. One can appreciate that CA IX is over expressed in a large variety of cancers, while being absent in the corresponding normal tissues. CA XII was subsequently shown to be co-expressed with CA IX in several tumor tissues but was also found in a wide range of normal tissues. Pharmaceutical agents that can selectively inhibit over expressed CA IX may have therapeutic value for detection, imaging and treatment of a large variety of hypoxic tumors. **In this context, it was shown by our lab and by others that selective inhibition of these tumor-overexpressed CA isozymes constitutes a viable strategy to fight these aggressive metastatic tumors** [14, 176, 177, 180, 196-199].

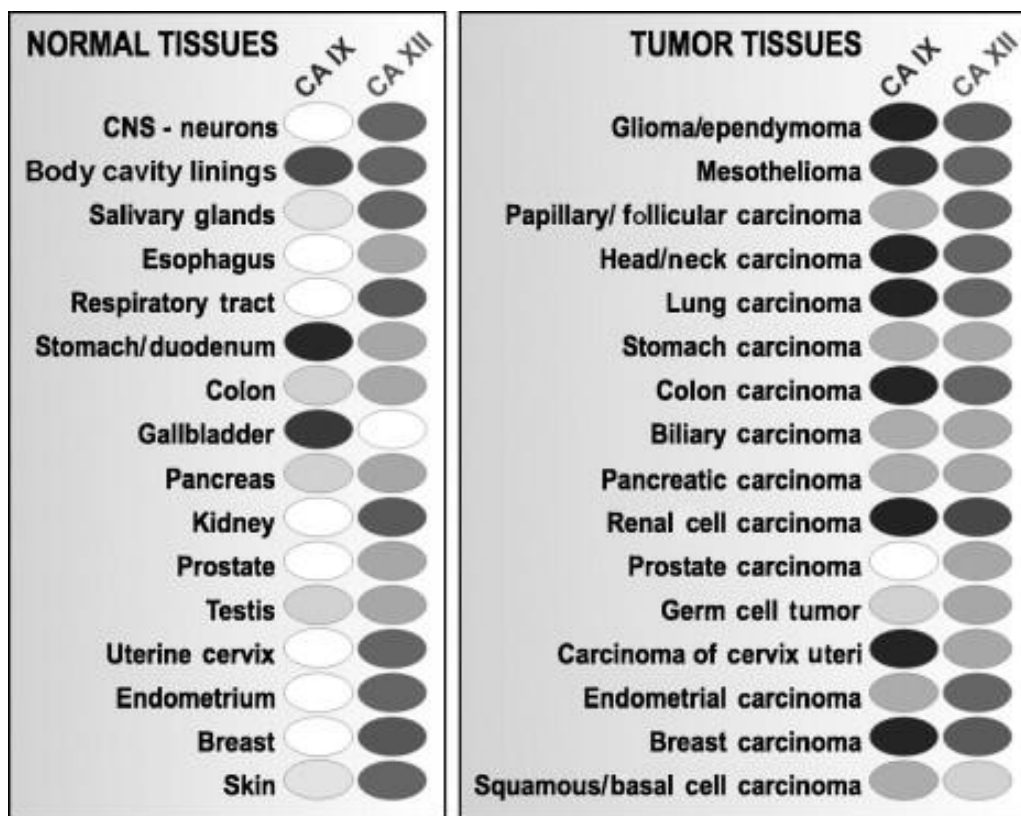


**Figure 29:** Overview of the distribution of CA IX and CA XII in normal human tissues and in corresponding tumors. The intensity of the gray color reflects the presence of that particular CA isoform and its expression level [200].

## 4.2 Approach

### CAIs Design

As mentioned above, efficient strategies to enhance the selectivity for membrane-bound isozymes *in vivo* involve conjugation of CAI pharmacophores with charged groups, with sugar moieties, or with polymeric moieties that will make the inhibitors membrane-impermeant and therefore unable to access the intracellular CA isozymes. The first and last strategies were addressed in following sections.

### **CAI Series 1: PEGylated bis-sulfonamides as carbonic anhydrase inhibitors**

Our first strategy to generate CAI with selectivity for membrane-bound CA isozymes, including CA IX was to attach known CA pharmacophores to polyethylene glycol (PEG). This strategy was explored before for other water-soluble polymeric backbones such as dextran and aminoethyl-dextran, [23, 201]. There are additional benefits arising from polyethylene glycol conjugation (PEGylation) of drugs, which include improved drug solubility, stability and retention time of the drug in the bloodstream, decreased drug immunogenicity, proteolysis and renal excretion, and optimized drug pharmacokinetics [202]. Building on these premises and taking into account that CA IX and XII are dimers in vivo [183], we decided to synthesize bifunctional PEGylated CAIs **24-26** by attaching known CAI pharmacophores (aminobenzenesulfonamide, 5-amino-1,3,4-thiadiazole-2-sulfonamide, aminobenzamide) on a PEG2000 polymeric backbone (PEG2K). We also synthesized the corresponding oligoethyleneglycol analogs **21-23**, bearing just three EG units (Chart 3). The synthesis was performed by Dr. Suleyman Akocak and Mr. Raqib Alam, two former members of our lab. The compounds were purified via preparative liquid chromatography and were characterized by standard methods that included <sup>1</sup>H- and <sup>13</sup>C-NMR, COSY, LC-MS and MALDI-TOF [195].

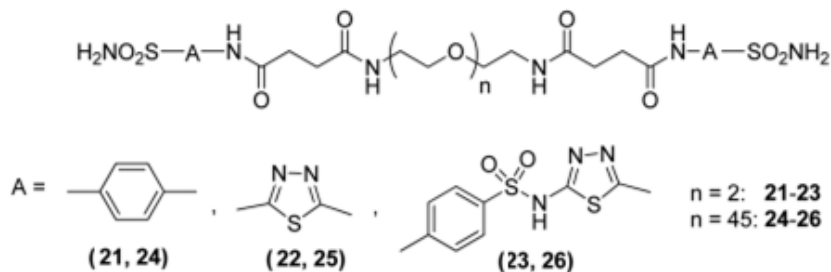


**Chart 3:** Bis-sulfonamide CA Inhibitors **21-26** synthesized for this study

The bis-sulfonamides **21-26** were tested for their ability to inhibit cytosolic (CA I, II) and membrane-bound (CA IV, IX, XII, XIV) isoforms of carbonic anhydrase by our collaborator Dr. Claudiu T. Supuran, at University of Florence. The results are tabulated in Table 5.

Data from Table 5 revealed an excellent inhibitory profile of compounds **21-26** against all membrane-bound isoforms CA IV, IX, XII, XIV, with nanomolar potency of most representatives against these targets. Their inhibitory potency matched or surpassed the potency of acetazolamide **ACZ**, thus validating the proposed design. The most susceptible to inhibition with compounds **21-26** were the tumor over-expressed isoforms CA IX and XII, followed closely by CA XIV and CA IV. Cytosolic isoform CA II was less susceptible to inhibition by compounds **21-26** than CA IV, although nanomolar inhibitors for this target were identified. The proposed CAIs displayed only moderate inhibitory potency against the second cytosolic isoform, CA I, similarly to acetazolamide (Table 15). Bis-sulfonamide **22** was identified as a potent pan-inhibitor with nanomolar potency against all isoforms tested except CA I. We also identified selective inhibitors for membrane-bound isoforms versus cytosolic ones, with either medium selectivity (compounds **21** and **25**) or high selectivity – sulfonamide **24**.

**Table 5:** Inhibition data of human CA isoforms hCA I, II, IV, IX, XII and XIV with derivatives **21-26** reported here and the standard sulfonamide inhibitor acetazolamide (**ACZ**) by a stopped flow CO<sub>2</sub> hydrase assay.

Comp	<b>K<sub>i</sub> (nM)</b>					
	hCA I	hCA II	hCA IV	hCA IX	hCA XII	hCA XIV
<b>21</b>	221	37.1	7.8	2.9	2.6	6.2
<b>22</b>	180	8.7	5.0	9.6	5.9	4.6
<b>23</b>	192	8.6	6.4	24.1	2.8	4.6
<b>24</b>	272	1764	9.5	4.8	3.2	7.3
<b>25</b>	225	66.6	5.8	2.5	5.4	6.8
<b>26</b>	181	12.9	4.4	1.7	3.7	4.4
<b>ACZ</b>	250	12	74	25	5.7	41

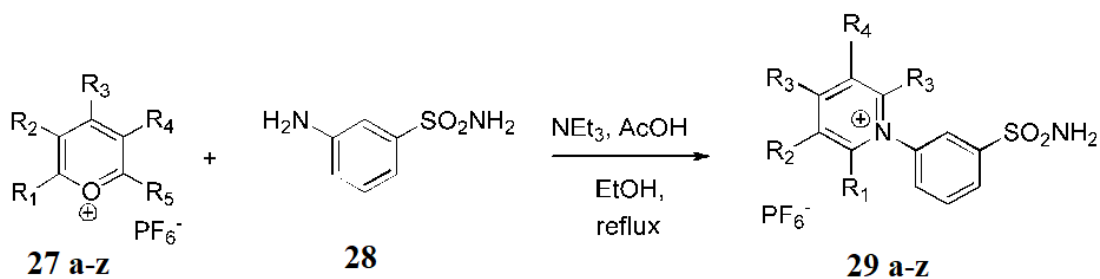
\* Mean from 3 different assays, by a stopped flow technique (errors were in the range of  $\pm$  5-10 % of the reported values). Monomeric (recombinant) human enzymes were used in all cases.

Thus, the most selective inhibitors could be generated from the benzenesulfonamide scaffold, while benzolamides generated potent pan-inhibitors. Interestingly, the long PEG linker increased the selectivity of the bis-sulfonamides **24-26** for the membrane-bound isozymes versus the cytosolic ones (especially against CA II), as compared with their oligoethylene glycol congeners **21-23**. Bis-sulfonamide **24** displayed the highest selectivity between membrane-bound isozymes and their cytosolic counterparts (Table 5). Considering the membrane-impermeant nature of the PEGylated bis-sulfonamides **24-26**, we expected that this selectivity will increase in vivo. Moreover, since tumor-overexpressed CA IX and CA XII isozymes are dimeric, we expected that the bis-

sulfonamides **24-26** will have a more pronounced effect on these targets in vivo, due to cooperative binding and bivalent association of the two-pronged inhibitor with the two neighboring active sites, as shown by Whitesides [203].

### CAI Series 2: Pyridinium sulfonamides as carbonic anhydrase inhibitors and their complexes with sulfocalixarenes and cyclodextrins

As mentioned above, a second strategy used by our team to improve the potency of CAIs and to make them selective for membrane-bound isozymes was through conjugation of CAI pharmacophores with pyridinium moieties, achieved via reaction of pyrylium salts with amino sulfonamides. For example, our team demonstrated the possibility of generating membrane-impermeant inhibitors through conjugation of primary aromatic and heterocyclic sulfonamides with positively charged pyrylium salts [204-207]. Compounds such as **29** and congeners were generated this way by Dr. Suleyman Akocak (Scheme 1). Pyridinium substitution was used to modulate potency and selectivity of novel carbonic anhydrase inhibitors through specific interactions with key amino acids on the active site of the enzyme. The activity of selected compounds from this series is presented in Table 6 [208].



**Scheme 1.** Synthesis of new pyridinium 3-aminobenzene sulfonamide series [208]

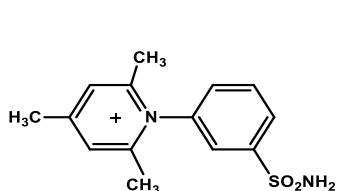
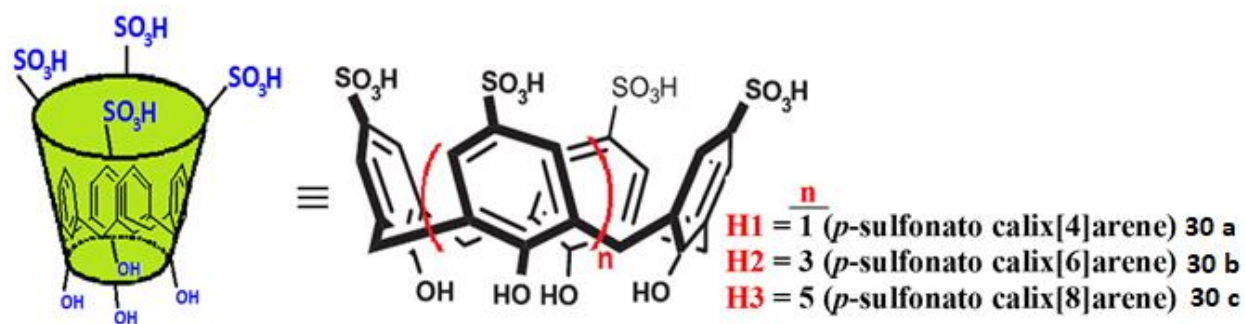
From the series of compounds synthesized in this study [208] we have selected three representatives, **29a**, **29d**, and **29m**, with different substituents on the pyridinium ring. The inhibition profile of these compounds is presented in Table 6 [208].

**Table 6.** Inhibition of tumor-associated hCA IX and hCA XII and off-target cytosolic hCA I and hCA II, with selected pyridinium benzenesulfonamides **29**, and with clinically used CAinhibitor acetazolamide **1**, using the CO<sub>2</sub> hydration assay.

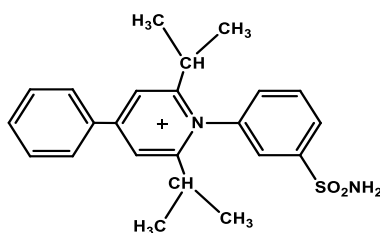
No.	R1	R2	R3	R4	R5	K <sub>i</sub> (nM)			
						hCA I	hCA II	hCA IX	hCA XII
<b>ACZ</b>						250	12	25	5.7
<b>29a</b>	Me	H	Me	H	Me	82.1	1.0	3.2	0.9
<b>29d</b>	iPr	H	Me	H	iPr	33.8	9.6	6.1	5.5
<b>29m</b>	iPr	H	Ph	H	iPr	41.8	9.3	6.4	5.8

\* Mean from 3 different assays, by a stopped flow technique (errors were in the range of ± 5-10 % of the reported values). Monomeric (recombinant) human enzymes used in all cases.

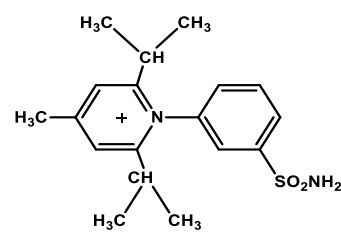
All three pyridinium CAIs (**29a** = G1, **29d** = G2 and **29m** = G3) displayed nanomolar potency against CA IX and CA XII, with a low selectivity against cytosolic isozymes CA I and CA II. Solubility of the compounds was expected to decrease from **29a** to **29m** as their lipophilicity increased to the presence of substituents with increased lipophilicity on the pyridinium ring. In order to solubilize them and to deliver them to tumor cells, we have selected a series of *p*-sulfonated calix[*n*]arenes (H1, H2, H3, *n*=4, 6, 8 Figure 30) and cyclodextrins such as  $\alpha$ -cyclodextrin ( $\alpha$ -CD) **31**,  $\beta$ -cyclodextrin ( $\beta$ -CD) **32** and hydroxypropyl-  $\beta$ -cyclodextrin (HP- $\beta$ -CD) **33** (denoted in what follows as H4, H5 and H6 respectively).



G1 **29a**



G2 **29b**



G3 **29c**

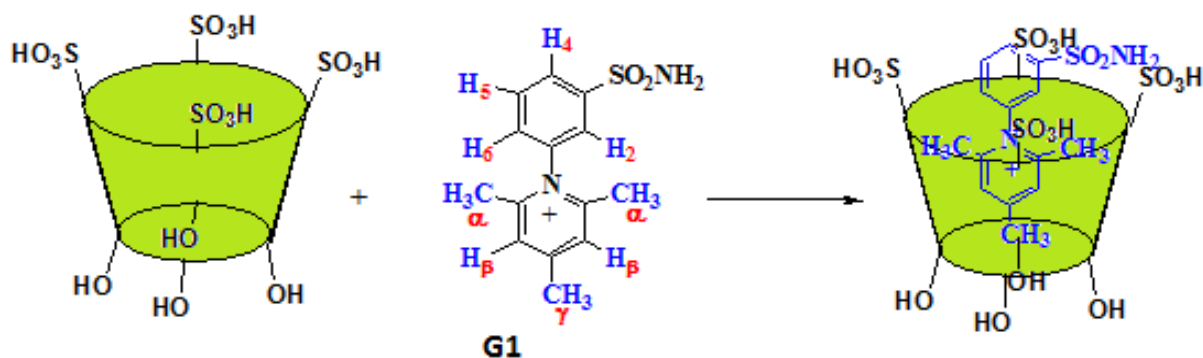


**Figure 30:** Schematic representation of *p*-sulfonated calix[*n*]arenes (H1, H2, H3, *n* = 4, 6, 8) selected as hosts in our complexation study, together with the three pyridinium CAIs **29a** = G1, **29d** = G2 and **29m** = G3 used as complexation guests in this study and the proposed structure of the inclusion complex between **H1** and **G2**.

### **4.3. Materials and methods**

#### **Materials**

Solvents (methanol, ethanol, dichloromethane, acetone, acetonitrile, trifluoroethanol, all HPLC quality) were purchased from EMD (Gibbstown, NJ), Fisher Scientific (Hampton, NH) or VWR International (Radnor, PA) and were used as received. Deionized water produced from a Millipore MilliQ system was used in all experiments that required it. Acetazolamide from Sigma-Aldrich (St. Louis, MO), human colon adenocarcinoma cell line (HT 29), human ovary cancer cell line (SKOV-3), and human breast cancer cell line (MDA-MB231) were purchased from ATCC (Manassas, VA), Dulbecco's Modified Eagle's medium (DMEM), RPMI-1640, and McCoy's 5A media were from Mediatech-Corning (Manassas, VA), fetal bovine serum (FBS), and 3-(4,5-Dimethylthiazol-2-yl)-2,5-diphenyltetrazolium bromide (MTT), phosphate-buffered saline (PBS), dimethyl sulfoxide (DMSO) and water-soluble tetrazolium salt-8 (WST-8) were purchased from VWR International (West Chester, PA).

#### **Methods**

##### **4.3.1 Cytotoxicity evaluation in 2D cell cultures**

Three cell lines namely HT-29, MDA-MB-231 and SKOV3 were cultured at 37°C and 5% CO<sub>2</sub> using RPMI-1640, Dulbecco's Modified Eagle's medium (DMEM) and McCoy's 5A Medium respectively supplemented with 10% fetal bovine serum. When the cells were about 75 % confluent in 75 cm<sup>2</sup> flasks, they were trypsinized with trypsin-EDTA, counted, and plated in 96-well plates at a density of 10<sup>4</sup> cells/well with a final volume of 200 µL in each well. Two plates were made for each cell line. After 24 h

incubation in a 5% humidified incubator at 37 °C, one plate from each cell line was placed in the hypoxia chamber and purged for 10 min with the hypoxia gas mixture (1% O<sub>2</sub>, 5% CO<sub>2</sub>, balance N<sub>2</sub>). After 1h the chamber was purged again with hypoxic gas mixture and placed back in the incubator. After a 24 h incubation in the incubator at 37 °C, both the normoxic and hypoxic plates were retrieved, and media was removed from all wells. Cells were washed with 5 % sterile dextrose and treated with different solutions of different concentrations of CAI **21-26** in media, or with three calixarenes complexes with CAI **29** prepared in 5% sterile dextrose, all pre-filtered through a 0.2 µm sterile nylon filter. Each assay was done at least in triplicate. After 24 h incubation time with CAIs, supernatant was discarded, cells were washed with phosphate-buffered saline (PBS) and, after removal of PBS, each well received 120 µL of MTT/media solution (prepared from 5 mg/mL MTT in sterile PBS, added to media in the ratio 1:6). Plates were incubated 4 h at 37 °C, MTT/media was aspirated off and 150 µL of DMSO was added to each well to dissolve formazan crystals. Plates were stored in the incubator for 5 min at 37 °C and absorbance was read at 570 nm using the 630 nm wavelength as reference.

#### **4.3.2 Cytotoxicity evaluation in 3D cell cultures**

Three cell lines, namely HT-29, MDA-MB-231 and SKOV3, were cultured at 37°C and at 5% CO<sub>2</sub> using RPMI-1640, Dulbecco's Modified Eagle's medium (DMEM) and McCoy's 5A medium respectively, supplemented with 10% fetal bovine serum. When the cells were about 75 % confluent in 75 cm<sup>2</sup> flasks they were trypsinized with trypsin-EDTA, counted, and plated in 96-well plates with round bottom at a density of

10<sup>3</sup> cells/well, in a final volume of 100 µL. After 7 days of incubation in a 5% CO<sub>2</sub> humidified incubator at 37 °C plates were treated with the same solutions/complexes of CAI presented above. Each assay was done at least in triplicate. After 24 h incubation, cells are treated with 10% WST-8 in media. The plate was stored in the incubator for 4 h and the plate was subsequently read for absorbance at 450 nm with a reference at 650 nm.

#### 4.4 Results and discussion

Based on the methods described above, we proceeded in assessing the anticancer activity of PEGylated bis-sulfonamides **24-26**, pyridinium CAIs **29** and their host-guest complexes

Thus, for 2D testing of bis-sulfonamides **24-26**, cells were grown subconfluent in 96-well plates in normal conditions (37 °C, 5% CO<sub>2</sub> in air), with half of the plates from each cell line incubated in normal (normoxic) conditions and the other half subjected to hypoxic conditions (1% O<sub>2</sub>, 5% CO<sub>2</sub> and 94% N<sub>2</sub>) to induce the expression of CA isozymes. After 24 h treatment with CAIs **21-26** solutions in media at three different concentrations (1 mM, 100 μM, and 10 μM) in either normoxic/hypoxic conditions, viability of cells was measured using an MTT assay. In the case of 3D testing, tumor spheroids become naturally hypoxic in about 7 days due to their 3D growth that isolates spheroid core cells from oxygen perfusion. We assessed their susceptibility to treatment with CAIs **21-26** at 1 mM and 100 μM concentration, for 24 h incubation time. Viability of the spheroids was assessed via a WST-8 assay (Figure 31).

Data from Figure 31 revealed that all inhibitors impacted tumor cell viability, with a greater impact elicited in hypoxic conditions where CA IX are overexpressed. All three cell lines were affected by the CAI treatment in a concentration-dependent manner, as expected, with colon HT-29 and breast MDA-MB231 cancer cells slightly more sensitive to CAI treatment than ovarian cancer cell line SKOV-3.

Significant decreases in tumor cell viability were obtained with inhibitors **21**, **22** and **25**, with the rest of inhibitors being generally less efficient even at high concentrations. Some exceptions occurred, such as inhibitor **23** that proved efficient only in MDA-MB231

cell line. These data are in contrast with the rather uniform inhibition profile of the series against CA IX and XII (Table 5) and *demonstrate that besides inhibition profile physicochemical properties of the inhibitor (lipophilicity, solubility) together with the cellular penetrability and other factors are essential for achieving efficient tumor cell killing*. The interplay of these factors generated CAIs with efficient in vitro cell killing from all three scaffolds selected. The most efficient CAI against all three cell lines in both normoxia and hypoxia proved to polymeric bis-sulfonamide **25**, bearing the classical 1,3,4-thiadiazole-2-sulfonamide “warhead”. It displayed robust cell killing, with cell viabilities as low as 30-40% at 1 mM, 50% at 100  $\mu$ M and 60-70% at 10  $\mu$ M, being influenced by the cell type and presence of hypoxia.

The above-mentioned data revealed the impact of in vitro models of tumor proliferation for the evaluation of potency of CAI as a pre-requisite for in vivo testing. Along these lines, we decided to quantify the CAI effects in 3D cell cultures, which take into account the tissue penetrability of the inhibitor and are thus closer to the environment encountered in vivo. Thus, tumor spheroids were grown using the same HT-29, MDA-MB231 and SKOV-3 cell lines, maintained in normoxic conditions. Tumor spheroids become naturally hypoxic in about 7 days due to their 3D growth that isolates spheroid core cells from oxygen perfusion. We subsequently assessed their susceptibility to treatment with CAIs **18-26** at 1 mM and 100  $\mu$ M concentration, for 24 h incubation time. Viability of the spheroids was assessed via the WST-8 assay in this case (Figure 31). Inhibition data depicted in Figure 31 revealed that the most efficient cell killing by CAIs was observed in tumor spheroids derived from HT-29 and SKOV-3 cell lines, with MDA-MB231 cell line being less affected. Polymeric bis-sulfonamide **25** was the most

efficient CAI in this assay too, decreasing the viability to about 50%/80% in SKOV-3, 60%/70% in HT-29 and 80%/90% in MDA-MB231 at 1 mM/100  $\mu$ M respectively. Other efficient CAIs in this in vitro 3D cell model were **21** and **23**, but with a less consistent, cell-dependent inhibition profile.

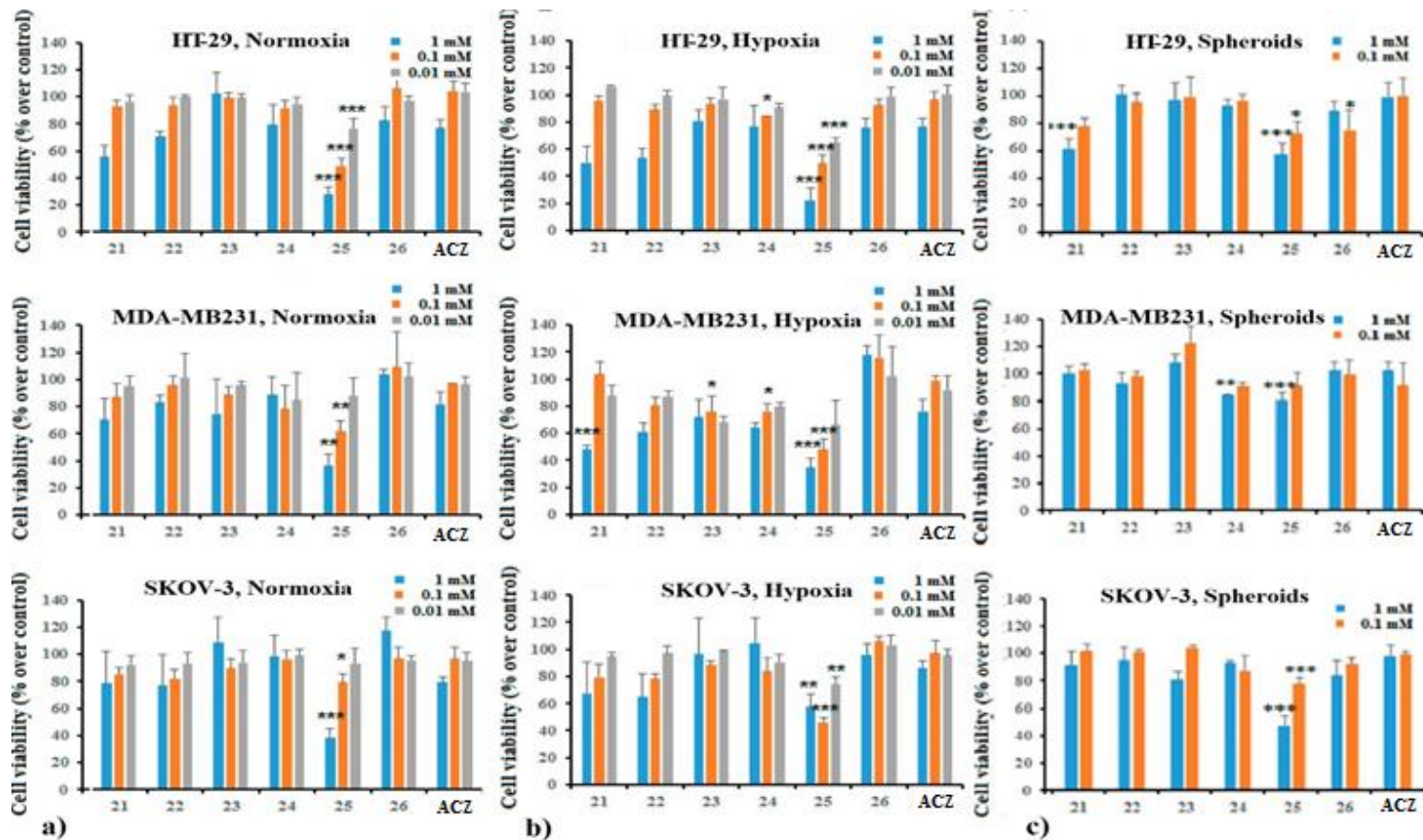


**Figure 31.** Effect of PEGylated bis-sulfonamide carbonic anhydrase inhibitors 21-26 and acetazolamide (ACZ), at different concentrations, on the viability of colon HT-29, breast MDA-MB231 and ovarian SKOV-3 cancer cell lines under a) normoxic (b) hypoxic and (c) 3D cell cultures (tumor spheroids) conditions. P values were determined by one-way ANOVA, comparing the value with the acetazolamide (ACZ) (\*P < 0.05, \*\*P < 0.01, \*\*\*P < 0.001). Only the statistical significant differences were shown.

The evaluation of the cytotoxicity of pyridinium CAIs **29** was performed using the same procedures used for CAIs **21-26**, after generation of their host-guest complexes with sulfocalixarenes **30a-c**, and cyclodextrins **31-33**. All host and guest molecules solutions (2 mM) were prepared at in D<sub>2</sub>O. Inclusion complexes were generated by Dr. Ozlem Karakus by mixing 300 μL Host (**H**) and Guest (**G**) solutions at 1:1 molar ratio. Formation of complexes was confirmed by <sup>1</sup>H-NMR (data not shown).

Thus, complexes from sulfocalixarenes and cyclodextrin hosts (**H1-H6**) and guest molecules **29** (**29a** = G1, **29d** = G2 and **29m** = G3), were assessed for their ability to kill the same three tumor cell lines HT-29, MDA-Mb231, SKOV-3 in both 2D (hypoxic and normoxic) and 3D (tumor spheroids) models, as described previously. We also used acetazolamide, as reference CAI, and we assessed the toxicity of the hosts in parallel (Figure 32,33). Data from Figure 32 and Figure 33 revealed that all host molecules are non-toxic. All complexes showed better activity towards cancer cell lines than acetazolamide control. Among all complexes the **H3-G1**, **H3-G2** and **H3-G3** formulations showed robust killing especially on cells grown in hypoxic conditions and on tumor spheroid (Figures 32, 33). The cytotoxicity properties of the complexes formed by all guest molecules with the calixarene carrier **H3** was superior to all other complexes formed with other hosts.

Moreover, data form Figure 32 and Figure 33 revealed that complexes of CAIs **29** with the calixarene hosts (**H1-H3**) were more efficient stronger than those of the same guests with cyclodextrins (**H4-H6**). Although it has lower complexation properties with respect to **H1**, calixarene carrier **H3** appeared to be best candidate for a delivery system for CAIs **29**. We postulate that the reason behind this behavior is the optimum balance

between complexation and decomplexation processes achieved by this host, which enables the efficient binding and delivery of pyridinium sulfonamides **29**, with subsequent CA IX inhibition and killing of the tumor cells.

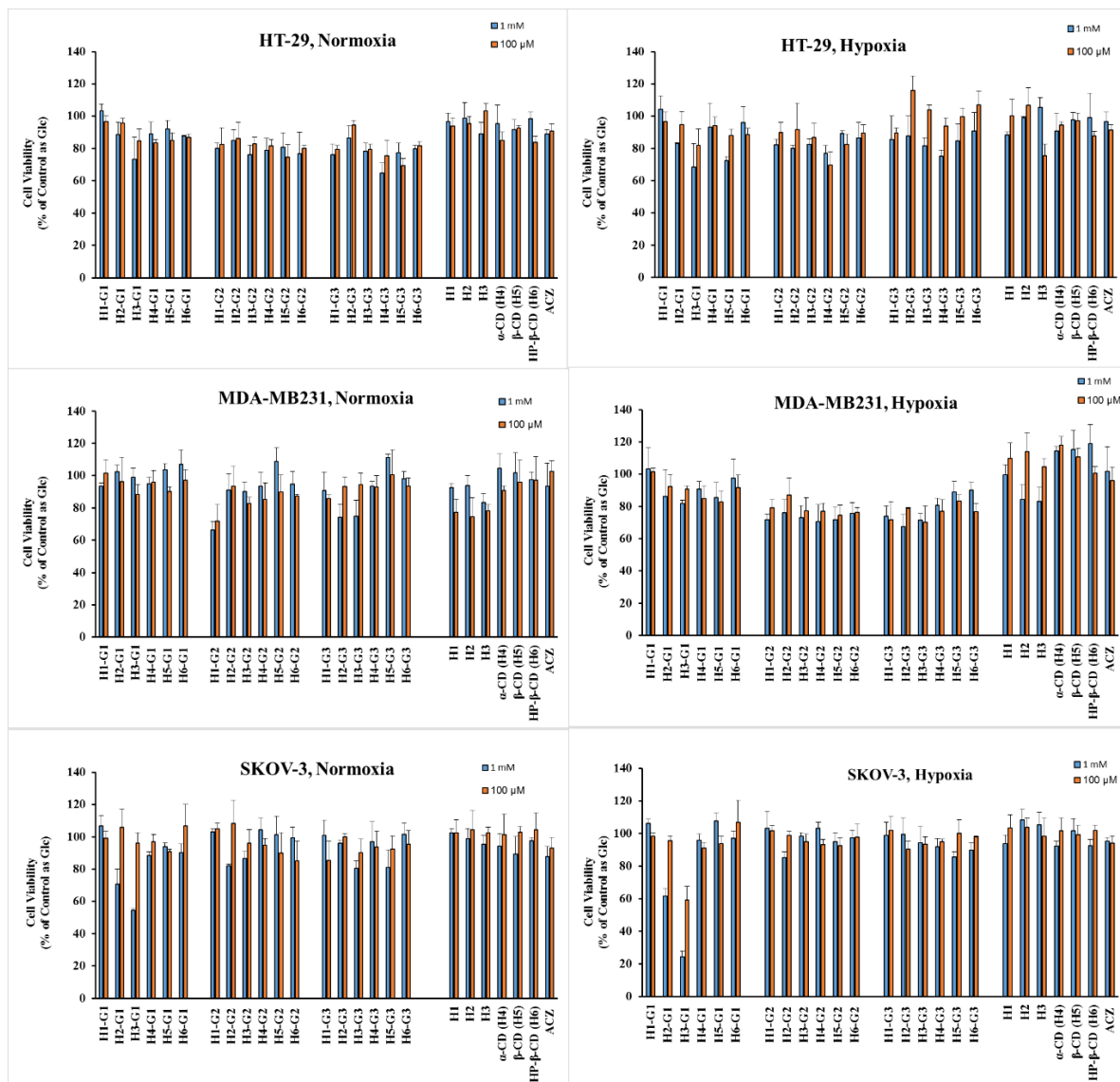


**Figure 32.** Comparative cytotoxicity of complexes generated from calixarenes **H1-H3** and cyclodextrins **H4-H6** with guest CAIs **29 G1-G3** against normoxic (left panels), and hypoxic (right panels) 2D cell cultures. Acetazolamide (ACZ) was used as control.

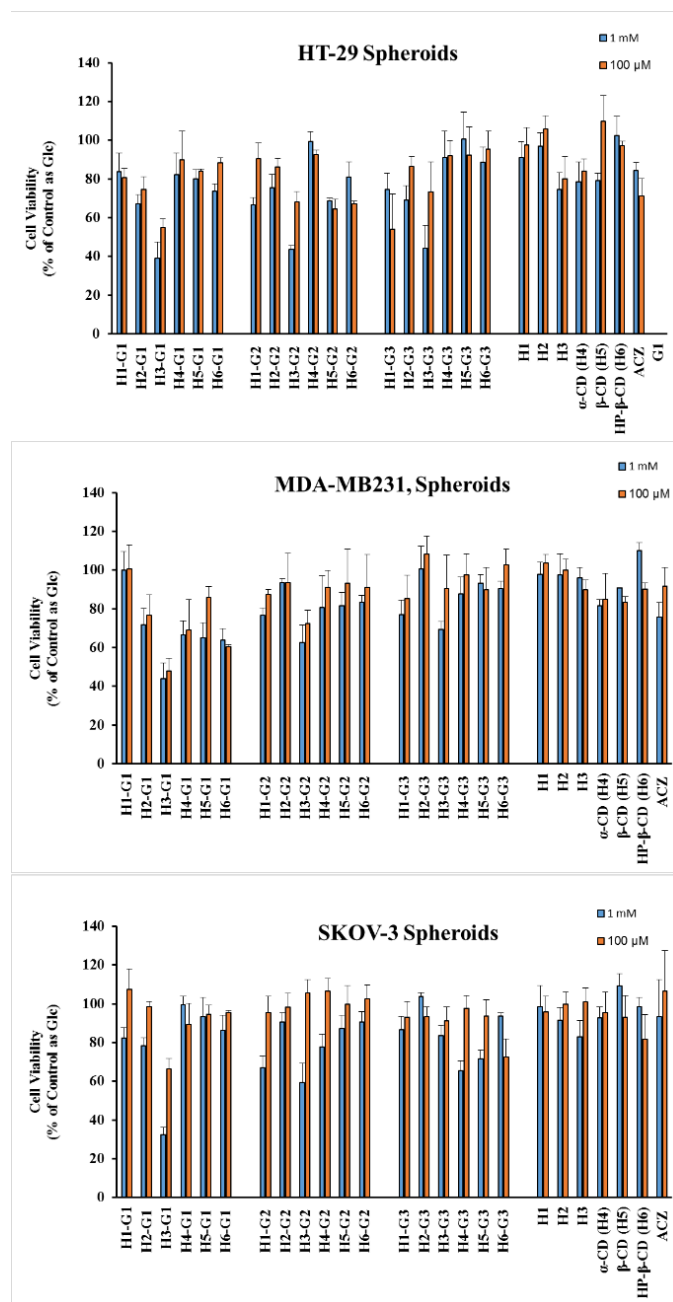


**Figure 33.** Comparative cytotoxicity of complexes generated from calixarenes **H1-H3** and cyclodextrins **H4-H6** with guest CAIs **29 G1-G3** against tumor spheroids. Acetazolamide (ACZ) was used as control.

## 4.5 Conclusions

A detailed structure–activity relationship study was carried out within a series of new bis-sulfonamides **21–26** from three different established carbonic anhydrase inhibitor “warheads”. These CAIs were profiled against a set of membrane-bound and cytosolic CA isoforms, including the tumor overexpressed CA IX and XII. We have identified potent pan-inhibitors, together with CAIs with selectivity for membrane-bound isozymes. This CAI set was also assessed *in vitro*, in 2D and 3D tumor cellular models expressing CA IX and XII, and we have successfully identified several potent CAIs that can significantly kill the tumor cells under both normoxic and hypoxic conditions. The most efficient CAI proved to be polymeric bis-sulfonamide **25**, which showed nanomolar potency against purified CA IX and XII isozymes and consistent and significant cancer cell killing at concentrations of 10–100  $\mu\text{M}$  across different tumors expressing these CA isozymes. The findings presented in this work may help the identification of other similar candidates, possibly with improved properties.

We were also able to mirror these positive results with our host-guest complexes of pyridinium sulfonamides **29**. All complexes showed better activity towards cancer cell lines than acetazolamide control, with complexes H3-G1, H3-G2 and H3-G3 showing robust killing especially on cells grown in hypoxic conditions and on tumor spheroids. Complexes of CAIs **29** with the calixarene hosts (H1-H3) were more efficient stronger than those of the same guests with cyclodextrins (H4-H6). Calixarene carrier H3 was found to be the best delivery system for pyridinium sulfonamides **29**.

## CHAPTER 5

### SUMMARY AND FUTURE STUDIES OF CA MODULATORS

For CAA project, the present study provides several novel insights into the CAs involvement in cognition. We have proposed a novel set of nanomolar CA activators that act selectively on CA IV, CA VA and/or CA IX, key CA isozymes involved in brain metabolism. Their potency and selectivity against other CA isozymes present at the level of the brain, together with their optimum lipophilicity validated our initial design and recommend them as novel probes for elucidation of the role of these isozymes in brain physiology and potential modulators of learning, memory and cognition. The use of the CAAs in NORT and 1-day operant task assays revealed the ability of select CAAs to prevent memory deficits induced by known amnesics scopolamine, ketamine and acetazolamide, and representing the importance of the cholinergic pathway, glutamatergic pathway and GABAergic pathway in the learning and retrieval of memory in these specific tasks in mice.

The study evidenced an important contribution of CA IV and CA VA co-activation in preventing memory deficits caused through the cholinergic pathway and of co-activation of CA VA and CA IX in preventing memory deficits caused through the GABAergic pathway.

Future studies will allow the evolution of these lead compounds into CAAs with different activation profiles and subsequent nootropic activity to allow the continuation of our triangulation of CA isozymes involved in learning and memory, to be further developed into potential drugs for efficient management of MCI and perhaps other more advanced forms of dementia such as early Alzheimer's disease as our understanding of

the role of carbonic anhydrase in normal and pathological states in the brain continues to develop.

For CAI project, sulfonamides proved to be a CAI with good tumor suppression revealed from our in vitro toxicity tests. As sulfonamide (**SLC-0111**) targeting isoforms IX/XII is currently in Phase II clinical trials as an antitumor/antimetastatic agent, the findings presented in this work may help the identification of other similar candidates, possibly with improved properties. This research also reveals that in addition to the established role of CAIs as diuretics and antiglaucoma drugs, CAIs have the potential to act as novel anticancer drugs.

## BIBLIOGRAPHY

1. Xiang, Q., et al., *Kinetics of the Reversible Reaction of CO<sub>2</sub>(aq) and HCO<sub>3</sub><sup>-</sup> with Sarcosine Salt in Aqueous Solution*. The Journal of Physical Chemistry A, 2012. **116**(42): p. 10276-10284.
2. Keilin, D. and T. Mann, *Carbonic anhydrase. Purification and nature of the enzyme*. Biochemical Journal, 1940. **34**(8-9): p. 1163-1176.
3. Van Slyke, D.D. and J.A. Hawkins, *studies of gas and electrolyte equilibria in blood xvi. The evolution of carbon dioxide from blood and buffer solutions*. Journal of Biological Chemistry, 1930. **87**(2): p. 265-279.
4. Meldrum, N.U. and F.J.W. Roughton, *Carbonic anhydrase. Its preparation and properties*. The Journal of Physiology, 1933. **80**(2): p. 113-142.
5. Supuran, C.T., *Carbonic anhydrases: novel therapeutic applications for inhibitors and activators*. Nat Rev Drug Discov, 2008. **7**(2): p. 168-81.
6. Bradfield, J.R., *Plant carbonic anhydrase*. Nature, 1947. **159**(4040): p. 467.
7. Smith, K.S., et al., *Carbonic anhydrase is an ancient enzyme widespread in prokaryotes*. Proc Natl Acad Sci U S A, 1999. **96**(26): p. 15184-9.
8. Krishnamurthy, V.M., et al., *Carbonic anhydrase as a model for biophysical and physical-organic studies of proteins and protein-ligand binding*. Chem Rev, 2008. **108**(3): p. 946-1051.
9. Supuran, C.T. and C. Capasso, *The eta-class carbonic anhydrases as drug targets for antimalarial agents*. Expert Opin Ther Targets, 2015. **19**(4): p. 551-63.

10. Ozensoy Guler, O., C. Capasso, and C.T. Supuran, *A magnificent enzyme superfamily: carbonic anhydrases, their purification and characterization*. *J Enzyme Inhib Med Chem*, 2016. **31**(5): p. 689-94.
11. Ferry, J.G., *The gamma class of carbonic anhydrases*. *Biochim Biophys Acta*, 2010. **1804**(2): p. 374-81.
12. Xu, Y., et al., *Structure and metal exchange in the cadmium carbonic anhydrase of marine diatoms*. *Nature*, 2008. **452**(7183): p. 56-61.
13. Lane, T.W., et al., *Biochemistry: a cadmium enzyme from a marine diatom*. *Nature*, 2005. **435**(7038): p. 42.
14. Alterio, V., et al., *Multiple binding modes of inhibitors to carbonic anhydrases: how to design specific drugs targeting 15 different isoforms?* *Chem Rev*, 2012. **112**(8): p. 4421-68.
15. Draghici, B., et al., *Ethylene bis-imidazoles are highly potent and selective activators for isozymes VA and VII of carbonic anhydrase, with a potential nootropic effect*. *Chem Commun (Camb)*, 2014. **50**(45): p. 5980-3.
16. Supuran, C.T., *Carbonic anhydrases: from biomedical applications of the inhibitors and activators to biotechnological use for CO<sub>2</sub> capture*. 2013, Taylor & Francis.
17. Supuran, C.T., *Structure-based drug discovery of carbonic anhydrase inhibitors*. *J Enzyme Inhib Med Chem*, 2012. **27**(6): p. 759-772.
18. Truppo, E., et al., *Carbonic anhydrase VII is S-glutathionylated without loss of catalytic activity and affinity for sulfonamide inhibitors*. *Bioorganic & Medicinal Chemistry Letters*, 2012. **22**(4): p. 1560-1564.

19. Parkkila, S., *An overview of the distribution and function of carbonic anhydrase in mammals*. *Exs*, 2000(90): p. 79-93.
20. Maren, T.H., *The kinetics of HCO<sub>3</sub><sup>-</sup> synthesis related to fluid secretion, pH control, and CO<sub>2</sub> elimination*. *Annu Rev Physiol*, 1988. **50**: p. 695-717.
21. Vogh, B.P., *The relation of choroid plexus carbonic anhydrase activity to cerebrospinal fluid formation: study of three inhibitors in cat with extrapolation to man*. *J Pharmacol Exp Ther*, 1980. **213**(2): p. 321-31.
22. Chesler, M., *Regulation and modulation of pH in the brain*. *Physiol Rev*, 2003. **83**(4): p. 1183-221.
23. Maren, T.H., et al., *Renal and cerebrospinal fluid formation pharmacology of a high molecular weight carbonic anhydrase inhibitor*. *J Pharmacol Exp Ther*, 1997. **280**(1): p. 98-104.
24. Wang, B., *Drug design of zinc-enzyme inhibitors: functional, structural, and disease applications*. Vol. 14. 2009: John Wiley & Sons.
25. Tong, C.K., et al., *Interstitial carbonic anhydrase (CA) activity in brain is attributable to membrane-bound CA type IV*. *J Neurosci*, 2000. **20**(22): p. 8247-53.
26. Shah, G.N., et al., *Carbonic anhydrase IV and XIV knockout mice: roles of the respective carbonic anhydrases in buffering the extracellular space in brain*. *Proc Natl Acad Sci U S A*, 2005. **102**(46): p. 16771-6.
27. Supuran, C.T., *Carbonic anhydrases: novel therapeutic applications for inhibitors and activators*. *Nat Rev Drug Discov*, 2008. **7**(2): p. 168-181.

28. Supuran, C.T., *Bacterial Carbonic Anhydrases as Drug Targets: Toward Novel Antibiotics?* *Frontiers in Pharmacology*, 2011. **2**: p. 34.
29. Parkkila, S., et al., *Expression of membrane-associated carbonic anhydrase XIV on neurons and axons in mouse and human brain.* *Proc Natl Acad Sci U S A*, 2001. **98**(4): p. 1918-1923.
30. Agnati, L.F., et al., *On the cellular localization and distribution of carbonic anhydrase II immunoreactivity in the rat brain.* *Brain Res*, 1995. **676**(1): p. 10-24.
31. So, A.K., et al., *A novel evolutionary lineage of carbonic anhydrase (epsilon class) is a component of the carboxysome shell.* *J Bacteriol*, 2004. **186**(3): p. 623-30.
32. Tripp, B.C., K. Smith, and J.G. Ferry, *Carbonic anhydrase: new insights for an ancient enzyme.* *J Biol Chem*, 2001. **276**(52): p. 48615-8.
33. Sawaya, M.R., et al., *The structure of beta-carbonic anhydrase from the carboxysomal shell reveals a distinct subclass with one active site for the price of two.* *J Biol Chem*, 2006. **281**(11): p. 7546-55.
34. Nair, S.K. and D.W. Christianson, *Unexpected pH-dependent conformation of His-64, the proton shuttle of carbonic anhydrase II.* *Journal of the American Chemical Society*, 1991. **113**(25): p. 9455-9458.
35. Lindskog, S. and D. N. Silverman, *The Carbonic Anhydrases New Horizons: The catalytic Mechanism of Mammalian Carbonic Anhydrases.* Vol. 90. 2000. 175-95.
36. Sly, W.S. and P.Y. Hu, *Human carbonic anhydrases and carbonic anhydrase deficiencies.* *Annu Rev Biochem*, 1995. **64**: p. 375-401.

37. Sly, W.S., et al., *Carbonic anhydrase II deficiency identified as the primary defect in the autosomal recessive syndrome of osteopetrosis with renal tubular acidosis and cerebral calcification*. Proc Natl Acad Sci U S A, 1983. **80**(9): p. 2752-6.
38. Maren, T.H., *Carbonic anhydrase: chemistry, physiology, and inhibition*. Physiol Rev, 1967. **47**(4): p. 595-781.
39. Limozin, N., et al., [*Radioimmunoassay of carbonic anhydrase I and II in rats. Application to the central nervous system during ontogeny*]. Biochimie, 1979. **61**(1): p. 115-9.
40. Kumpulainen, T., et al., *A single-step solid phase radioimmunoassay for quantifying human carbonic anhydrase I and II in cerebrospinal fluid*. Clin Chim Acta, 1985. **150**(3): p. 205-12.
41. Liu, X., et al., *Expression of Carbonic Anhydrase I in Motor Neurons and Alterations in ALS*. Int J Mol Sci, 2016. **17**(11).
42. Sultana, R., et al., *Identification of nitrated proteins in Alzheimer's disease brain using a redox proteomics approach*. Neurobiology of Disease, 2006. **22**(1): p. 76-87.
43. Sultana, R., et al., *Redox proteomics identification of oxidized proteins in Alzheimer's disease hippocampus and cerebellum: An approach to understand pathological and biochemical alterations in AD*. Neurobiology of Aging, 2006. **27**(11): p. 1564-1576.
44. Supuran, C.T., A. Scozzafava, and J. Conway, *Carbonic anhydrase: its inhibitors and activators*. Vol. 1. 2004: CRC Press.

45. Ghandour, M.S., et al., *Double labeling immunohistochemical technique provides evidence of the specificity of glial cell markers*. *J Histochem Cytochem*, 1979. **27**(12): p. 1634-7.
46. Ghandour, M.S., et al., *Immunochemical and immunohistochemical study of carbonic anhydrase II in adult rat cerebellum: a marker for oligodendrocytes*. *Neuroscience*, 1980. **5**(3): p. 559-71.
47. Langley, O.K., et al., *Carbonic anhydrase: an ultrastructural study in rat cerebellum*. *Histochem J*, 1980. **12**(4): p. 473-83.
48. Roussel, G., et al., *Demonstration of a specific localization of carbonic anhydrase C in the glial cells of rat CNS by an immunohistochemical method*. *Brain Res*, 1979. **160**(1): p. 47-55.
49. Kumpulainen, T. and L.K. Korhonen, *Immunohistochemical localization of carbonic anhydrase isoenzyme C in the central and peripheral nervous system of the mouse*. *J Histochem Cytochem*, 1982. **30**(4): p. 283-92.
50. Kumpulainen, T., et al., *Immunolabeling of carbonic anhydrase isoenzyme C and glial fibrillary acidic protein in paraffin-embedded tissue sections of human brain and retina*. *J Histochem Cytochem*, 1983. **31**(7): p. 879-86.
51. Kimelberg, H.K., P.E. Stieg, and J.E. Mazurkiewicz, *Immunocytochemical and biochemical analysis of carbonic anhydrase in primary astrocyte cultures from rat brain*. *J Neurochem*, 1982. **39**(3): p. 734-42.
52. Snyder, D.S., et al., *Carbonic anhydrase, 5'-nucleotidase, and 2',3'-cyclic nucleotide-3'-phosphodiesterase activities in oligodendrocytes, astrocytes, and neurons isolated from the brains of developing rats*. *J Neurochem*, 1983. **40**(1): p. 120-7.

53. Cammer, W. and F.A. Tansey, *The astrocyte as a locus of carbonic anhydrase in the brains of normal and dysmyelinating mutant mice*. J Comp Neurol, 1988. **275**(1): p. 65-75.
54. Cammer, W. and H. Zhang, *Carbonic anhydrase in distinct precursors of astrocytes and oligodendrocytes in the forebrains of neonatal and young rats*. Brain Res Dev Brain Res, 1992. **67**(2): p. 257-63.
55. Jeffrey, M., G.A. Wells, and A.W. Bridges, *Carbonic anhydrase II expression in fibrous astrocytes of the sheep*. J Comp Pathol, 1991. **104**(4): p. 337-43.
56. Nogradi, A., *Differential expression of carbonic anhydrase isozymes in microglial cell types*. Glia, 1993. **8**(2): p. 133-42.
57. Nogradi, A., C. Kelly, and N.D. Carter, *Localization of acetazolamide-resistant carbonic anhydrase III in human and rat choroid plexus by immunocytochemistry and in situ hybridisation*. Neurosci Lett, 1993. **151**(2): p. 162-5.
58. Ruusuvuori, E., et al., *Neuronal carbonic anhydrase VII provides GABAergic excitatory drive to exacerbate febrile seizures*. Embo j, 2013. **32**(16): p. 2275-86.
59. Ghandour, M.S., et al., *Carbonic anhydrase IV on brain capillary endothelial cells: a marker associated with the blood-brain barrier*. Proc Natl Acad Sci U S A, 1992. **89**(15): p. 6823-7.
60. Svichar, N. and M. Chesler, *Surface carbonic anhydrase activity on astrocytes and neurons facilitates lactate transport*. Glia, 2003. **41**(4): p. 415-9.
61. Fujikawa-Adachi, K., et al., *Human mitochondrial carbonic anhydrase VB. cDNA cloning, mRNA expression, subcellular localization, and mapping to chromosome x*. J Biol Chem, 1999. **274**(30): p. 21228-33.

62. Ghandour, M.S., et al., *Mitochondrial carbonic anhydrase in the nervous system: expression in neuronal and glial cells*. J Neurochem, 2000. **75**(5): p. 2212-20.
63. Price, T.O., et al., *Topiramate treatment protects blood-brain barrier pericytes from hyperglycemia-induced oxidative damage in diabetic mice*. Endocrinology, 2012. **153**(1): p. 362-72.
64. Ruusuvuori, E., et al., *Carbonic anhydrase isoform VII acts as a molecular switch in the development of synchronous gamma-frequency firing of hippocampal CA1 pyramidal cells*. J Neurosci, 2004. **24**(11): p. 2699-707.
65. Aspatwar, A., et al., *Carbonic anhydrase related protein VIII and its role in neurodegeneration and cancer*. Curr Pharm Des, 2010. **16**(29): p. 3264-76.
66. Taniuchi, K., et al., *Developmental expression of carbonic anhydrase-related proteins VIII, X, and XI in the human brain*. Neuroscience, 2002. **112**(1): p. 93-99.
67. Taniuchi, K., et al., *cDNA cloning and developmental expression of murine carbonic anhydrase-related proteins VIII, X, and XI*. Brain Res Mol Brain Res, 2002. **109**(1-2): p. 207-15.
68. Pan, P.W., et al., *Brain phenotype of carbonic anhydrase IX-deficient mice*. Transgenic Res, 2012. **21**(1): p. 163-76.
69. Ivanov, S., et al., *Expression of hypoxia-inducible cell-surface transmembrane carbonic anhydrases in human cancer*. Am J Pathol, 2001. **158**(3): p. 905-19.
70. Hilvo, M., et al., *Expression of carbonic anhydrase IX in mouse tissues*. J Histochem Cytochem, 2004. **52**(10): p. 1313-22.

71. Pastorek, J., et al., *Cloning and characterization of MN, a human tumor-associated protein with a domain homologous to carbonic anhydrase and a putative helix-loop-helix DNA binding segment*. *Oncogene*, 1994. **9**(10): p. 2877-88.
72. Tureci, O., et al., *Human carbonic anhydrase XII: cDNA cloning, expression, and chromosomal localization of a carbonic anhydrase gene that is overexpressed in some renal cell cancers*. *Proc Natl Acad Sci U S A*, 1998. **95**(13): p. 7608-13.
73. Parkkila, S., et al., *Expression of membrane-associated carbonic anhydrase XIV on neurons and axons in mouse and human brain*. *Proc Natl Acad Sci U S A*, 2001. **98**(4): p. 1918-23.
74. Nagelhus, E.A., et al., *Carbonic anhydrase XIV is enriched in specific membrane domains of retinal pigment epithelium, Muller cells, and astrocytes*. *Proc Natl Acad Sci U S A*, 2005. **102**(22): p. 8030-5.
75. De Simone, G., A. Scozzafava, and C.T. Supuran, *Which carbonic anhydrases are targeted by the antiepileptic sulfonamides and sulfamates?* *Chem Biol Drug Des*, 2009. **74**(3): p. 317-21.
76. Meier-Ruge, W., P. Iwangoff, and K. Reichlmeier, *Neurochemical enzyme changes in Alzheimer's and Pick's disease*. *Arch Gerontol Geriatr*, 1984. **3**(2): p. 161-5.
77. Sultana, R., et al., *Redox proteomics identification of oxidized proteins in Alzheimer's disease hippocampus and cerebellum: an approach to understand pathological and biochemical alterations in AD*. *Neurobiol Aging*, 2006. **27**(11): p. 1564-76.

78. Sultana, R., et al., *Identification of nitrated proteins in Alzheimer's disease brain using a redox proteomics approach*. Neurobiol Dis, 2006. **22**(1): p. 76-87.
79. Sultana, R., M. Perluigi, and D.A. Butterfield, *Oxidatively modified proteins in Alzheimer's disease (AD), mild cognitive impairment and animal models of AD: role of Abeta in pathogenesis*. Acta neuropathologica, 2009. **118**(1): p. 131.
80. Feldman, H.H. and C. Jacova, *Mild cognitive impairment*. Am J Geriatr Psychiatry, 2005. **13**(8): p. 645-55.
81. Tabert, M.H., et al., *Neuropsychological prediction of conversion to Alzheimer disease in patients with mild cognitive impairment*. Arch Gen Psychiatry, 2006. **63**(8): p. 916-24.
82. Smith, A.D., et al., *Homocysteine-lowering by B vitamins slows the rate of accelerated brain atrophy in mild cognitive impairment: a randomized controlled trial*. PLoS One, 2010. **5**(9): p. e12244.
83. Ravaglia, G., et al., *Homocysteine and folate as risk factors for dementia and Alzheimer disease*. Am J Clin Nutr, 2005. **82**(3): p. 636-43.
84. Squire, L.R. and J.T. Wixted, *The cognitive neuroscience of human memory since H.M.* Annu Rev Neurosci, 2011. **34**: p. 259-88.
85. Squire, L.R., *Memory and the hippocampus: a synthesis from findings with rats, monkeys, and humans*. Psychol Rev, 1992. **99**(2): p. 195-231.
86. Winkler, J., et al., *Essential role of neocortical acetylcholine in spatial memory*. Nature, 1995. **375**(6531): p. 484-7.

87. Banks, M.I., J.A. White, and R.A. Pearce, *Interactions between distinct GABA(A) circuits in hippocampus*. *Neuron*, 2000. **25**(2): p. 449-57.
88. Makani, S. and M. Chesler, *Endogenous alkaline transients boost postsynaptic NMDA receptor responses in hippocampal CA1 pyramidal neurons*. *J Neurosci*, 2007. **27**(28): p. 7438-46.
89. Chen, X.H., I. Bezprozvanny, and R.W. Tsien, *Molecular basis of proton block of L-type Ca<sup>2+</sup> channels*. *J Gen Physiol*, 1996. **108**(5): p. 363-74.
90. Prod'homme, B., D. Pietrobon, and P. Hess, *Direct measurement of proton transfer rates to a group controlling the dihydropyridine-sensitive Ca<sup>2+</sup> channel*. *Nature*, 1987. **329**(6136): p. 243-6.
91. Traynelis, S.F. and S.G. Cull-Candy, *Proton inhibition of N-methyl-D-aspartate receptors in cerebellar neurons*. *Nature*, 1990. **345**(6273): p. 347-50.
92. Tang, C.M., M. Dichter, and M. Morad, *Modulation of the N-methyl-D-aspartate channel by extracellular H<sup>+</sup>*. *Proc Natl Acad Sci U S A*, 1990. **87**(16): p. 6445-9.
93. Sinning, A. and C.A. Hübner, *Minireview: pH and synaptic transmission*. *FEBS Lett*, 2013. **587**(13): p. 1923-1928.
94. Makani, S. and M. Chesler, *Rapid Rise of Extracellular pH Evoked by Neural Activity Is Generated by the Plasma Membrane Calcium ATPase*. *J Neurophysiol*, 2010. **103**(2): p. 667-676.
95. Makani, S., et al., *NMDA receptor-dependent afterdepolarizations are curtailed by carbonic anhydrase 14: regulation of a short-term postsynaptic potentiation*. *J Neurosci*, 2012. **32**(47): p. 16754-62.

96. Gu, F., et al., *Translational responses of NR2B overexpression in the cerebral cortex of transgenic mice: a liquid chromatography-based proteomic approach*. Brain Res, 2009. **1250**: p. 1-13.
97. Mori, H. and M. Mishina, *Structure and function of the NMDA receptor channel*. Neuropharmacology, 1995. **34**(10): p. 1219-37.
98. Ferris, K.E., R.D. Clark, and E.L. Coates, *Topical inhibition of nasal carbonic anhydrase affects the CO<sub>2</sub> detection threshold in rats*. Chem Senses, 2007. **32**(3): p. 263-71.
99. Swenson, E.R. and L.J. Teppema, *Prevention of acute mountain sickness by acetazolamide: as yet an unfinished story*. J Appl Physiol (1985), 2007. **102**(4): p. 1305-7.
100. Sommer, B.R., E.L. Mitchell, and T.E. Wroolie, *Topiramate: Effects on cognition in patients with epilepsy, migraine headache and obesity*. Ther Adv Neurol Disord, 2013. **6**(4): p. 211-27.
101. Sun, M.K. and D.L. Alkon, *Pharmacological enhancement of synaptic efficacy, spatial learning, and memory through carbonic anhydrase activation in rats*. J Pharmacol Exp Ther, 2001. **297**(3): p. 961-7.
102. Sun, M.K. and D.L. Alkon, *Carbonic anhydrase gating of attention: memory therapy and enhancement*. Trends Pharmacol Sci, 2002. **23**(2): p. 83-9.
103. Hamidi, S. and M. Avoli, *Carbonic anhydrase inhibition by acetazolamide reduces in vitro epileptiform synchronization*. Neuropharmacology, 2015. **95**: p. 377-387.

104. Canto de Souza, L., et al., *Carbonic anhydrase activation enhances object recognition memory in mice through phosphorylation of the extracellular signal-regulated kinase in the cortex and the hippocampus*. *Neuropharmacology*, 2017. **118**: p. 148-156.
105. Sun, M., D. Dahl, and D.L. Alkon, *Heterosynaptic transformation of GABAergic gating in the hippocampus and effects of carbonic anhydrase inhibition*. *J Pharmacol Exp Ther*, 2001. **296**(3): p. 811-7.
106. Sun, M.K., et al., *Theta rhythm of hippocampal CA1 neuron activity: gating by GABAergic synaptic depolarization*. *J Neurophysiol*, 2001. **85**(1): p. 269-79.
107. Leiner, M. and G. Leiner, *The activators of carbonic acid anhydratase*. *Naturwissenschaften*, 1941. **29**: p. 195-197.
108. Mann, T. and D. Keilin, *Sulphanilamide as a specific inhibitor of carbonic anhydrase*. *Nature*, 1940. **146**: p. 164-165.
109. Ho, C. and J.M. Sturtevant, *Activation of bovine carbonic anhydrase by ethylenediamine tetraacetic acid*. *Biochemical and Biophysical Research Communications*, 1960. **3**(1): p. 20-23.
110. Ilies, M.A., et al., *Carbonic anhydrase activators. Part 17. Synthesis and activation study of a series of 1-(1,2,4-triazole-(1H)-3-yl)-2,4,6-trisubstituted-pyridinium salts against isozymes I, II and IV*. *European Journal of Medicinal Chemistry*, 1997. **32**(11): p. 911-918.
111. Silverman, D.N., C. Tu, and G.C. Wynns, *Proton transfer between hemoglobin and the carbonic anhydrase active site*. *J Biol Chem*, 1978. **253**(8): p. 2563-7.

112. Silverman, D.N., L. Backman, and C. Tu, *Role of hemoglobin in proton transfer to the active site of carbonic anhydrase*. J Biol Chem, 1979. **254**(8): p. 2588-91.
113. Paranawithana, S.R., et al., *Enhancement of the catalytic activity of carbonic anhydrase III by phosphates*. J Biol Chem, 1990. **265**(36): p. 22270-4.
114. Parkes, J.L. and P.S. Coleman, *Enhancement of carbonic anhydrase activity by erythrocyte membranes*. Arch Biochem Biophys, 1989. **275**(2): p. 459-68.
115. Supuran, C.T. and A. Scozzafava, *Activation of carbonic anhydrase isozymes*. Exs, 2000(90): p. 197-219.
116. Silverman, D.N. and S. Lindskog, *The catalytic mechanism of carbonic anhydrase: implications of a rate-limiting protolysis of water*. Accounts of Chemical Research, 1988. **21**(1): p. 30-36.
117. Supuran, C.T., et al., *Carbonic anhydrase activators. Part 14. Syntheses of mono and bis pyridinium salt derivatives of 2-amino-5-(2-aminoethyl)- and 2-amino-5-(3-aminopropyl)-1,3,4-thiadiazole and their interaction with isozyme II*. European Journal of Medicinal Chemistry, 1996. **31**(7): p. 597-606.
118. Supuran, C.T., et al., *Carbonic anhydrase activators. VII. Isozyme II activation by bisazolyl-methanes, -ethanes and related azoles*. Biol Pharm Bull, 1993. **16**(12): p. 1236-9.
119. Supuran, C.T., et al., *Carbonic anhydrase activators. XV. A kinetic study of the interaction of bovine isozyme II with pyrazoles, bis- and tris-azolyl-methanes*. Biol Pharm Bull, 1996. **19**(11): p. 1417-22.

120. Christianson, D.W. and C.A. Fierke, *Carbonic Anhydrase: Evolution of the Zinc Binding Site by Nature and by Design*. Accounts of Chemical Research, 1996. **29**(7): p. 331-339.
121. Ilies, M., et al., *Carbonic anhydrase activators: design of high affinity isozymes I, II, and IV activators, incorporating tri-/tetrasubstituted-pyridinium-azole moieties*. J Med Chem, 2002. **45**(2): p. 504-10.
122. Scozzafava, A. and C.T. Supuran, *Carbonic anhydrase activators: high affinity isozymes I, II, and IV activators, incorporating a beta-alanyl-histidine scaffold*. J Med Chem, 2002. **45**(2): p. 284-91.
123. Supuran, C.T. and A. Scozzafava, *Carbonic anhydrase activators: amino acyl/dipeptidyl histamine derivatives bind with high affinity to isozymes I, II and IV and act as efficient activators*. Bioorg Med Chem, 1999. **7**(12): p. 2915-23.
124. Dave, K., et al., *Pyridinium derivatives of histamine are potent activators of cytosolic carbonic anhydrase isoforms I, II and VII*. Org Biomol Chem, 2011. **9**(8): p. 2790-800.
125. Briganti, F., et al., *Carbonic anhydrase activators: X-ray crystallographic and spectroscopic investigations for the interaction of isozymes I and II with histamine*. Biochemistry, 1997. **36**(34): p. 10384-92.
126. Temperini, C., et al., *Carbonic anhydrase activators: X-ray crystal structure of the adduct of human isozyme II with L-histidine as a platform for the design of stronger activators*. Bioorg Med Chem Lett, 2005. **15**(23): p. 5136-41.
127. Temperini, C., A. Scozzafava, and C.T. Supuran, *Carbonic anhydrase activators: the first X-ray crystallographic study of an adduct of isoform I*. Bioorg Med Chem Lett, 2006. **16**(19): p. 5152-6.

128. Temperini, C., et al., *Carbonic anhydrase activators. Activation of isozymes I, II, IV, VA, VII, and XIV with l- and d-histidine and crystallographic analysis of their adducts with isoform II: engineering proton-transfer processes within the active site of an enzyme.* Chemistry - An European Journal, 2006. **12**(27): p. 7057-66.
129. Dave, K., et al., *An inhibitor-like binding mode of a carbonic anhydrase activator within the active site of isoform II.* Bioorg Med Chem Lett, 2011. **21**(9): p. 2764-8.
130. Duda, D., et al., *Structural and kinetic analysis of the chemical rescue of the proton transfer function of carbonic anhydrase II.* Biochemistry, 2001. **40**(6): p. 1741-8.
131. Elder, I., et al., *Proton transfer from exogenous donors in catalysis by human carbonic anhydrase II.* Arch Biochem Biophys, 2005. **437**(1): p. 106-14.
132. Aggarwal, M., et al., *Structural insight into activity enhancement and inhibition of H64A carbonic anhydrase II by imidazoles.* IUCrJ, 2014. **1**: p. 129-135.
133. Lounsbury, N., et al., *Heterocyclic chalcone activators of nuclear factor (erythroid-derived 2)-like 2 (Nrf2) with improved in vivo efficacy.* Bioorg Med Chem, 2015. **23**(17): p. 5352-9.
134. Zhou, L., et al., *Development of a high throughput equilibrium solubility assay using miniaturized shake-flask method in early drug discovery.* J Pharm Sci, 2007. **96**(11): p. 3052-71.
135. Lopes, F.M., et al., *Comparison between proliferative and neuron-like SH-SY5Y cells as an in vitro model for Parkinson disease studies.* Brain Res, 2010. **1337**: p. 85-94.

136. Encinas, M., et al., *Sequential treatment of SH-SY5Y cells with retinoic acid and brain-derived neurotrophic factor gives rise to fully differentiated, neurotrophic factor-dependent, human neuron-like cells*. J Neurochem, 2000. **75**(3): p. 991-1003.
137. Matsumoto, K., et al., *Expression of brain-derived neurotrophic factor and p145TrkB affects survival, differentiation, and invasiveness of human neuroblastoma cells*. Cancer Res, 1995. **55**(8): p. 1798-806.
138. Wilson, M.S., J.R. Graham, and A.J. Ball, *Multiparametric High Content Analysis for assessment of neurotoxicity in differentiated neuronal cell lines and human embryonic stem cell-derived neurons*. Neurotoxicology, 2014. **42**: p. 33-48.
139. Delcour, M., et al., *Impact of prenatal ischemia on behavior, cognitive abilities and neuroanatomy in adult rats with white matter damage*. Behav Brain Res, 2012. **232**(1): p. 233-44.
140. Nagar, S. and K. Korzekwa, *Commentary: nonspecific protein binding versus membrane partitioning: it is not just semantics*. Drug Metab Dispos, 2012. **40**(9): p. 1649-52.
141. McGinnity, D.F., et al., *Evaluation of human pharmacokinetics, therapeutic dose and exposure predictions using marketed oral drugs*. Curr Drug Metab, 2007. **8**(5): p. 463-79.
142. Bisen-Hersh, E.B., P.N. Hineline, and E.A. Walker, *Effects of early chemotherapeutic treatment on learning in adolescent mice: implications for cognitive impairment and remediation in childhood cancer survivors*. Clin Cancer Res, 2013. **19**(11): p. 3008-18.

143. Dodart, J.C., C. Mathis, and A. Ungerer, *Scopolamine-induced deficits in a two-trial object recognition task in mice*. Neuroreport, 1997. **8**(5): p. 1173-8.
144. Han, R.W., et al., *Neuropeptide S enhances memory and mitigates memory impairment induced by MK801, scopolamine or Abeta(1)(-)(4)(2) in mice novel object and object location recognition tasks*. Neuropharmacology, 2013. **70**: p. 261-7.
145. Sik, A., et al., *Performance of different mouse strains in an object recognition task*. Behav Brain Res, 2003. **147**(1-2): p. 49-54.
146. Ben-Azu, B., et al., *Involvement of GABAergic, BDNF and Nox-2 mechanisms in the prevention and reversal of ketamine-induced schizophrenia-like behavior by morin in mice*. Brain Res Bull, 2018. **139**: p. 292-306.
147. Foley, J.J., R.B. Raffa, and E.A. Walker, *Effects of chemotherapeutic agents 5-fluorouracil and methotrexate alone and combined in a mouse model of learning and memory*. Psychopharmacology (Berl), 2008. **199**(4): p. 527-38.
148. Walker, E.A. and J.J. Foley, *Acquisition session length modulates consolidation effects produced by 5-HT<sub>2C</sub> ligands in a mouse autoshaping-operant procedure*. Behav Pharmacol, 2010. **21**(2): p. 83-9.
149. Walker, E.A., *Animal models*. Adv Exp Med Biol, 2010. **678**: p. 138-46.
150. Machatha, S.G. and S.H. Yalkowsky, *Comparison of the octanol/water partition coefficients calculated by ClogP, ACDlogP and KowWin to experimentally determined values*. Int J Pharm, 2005. **294**(1-2): p. 185-92.

151. Lipinski, C.A., et al., *Experimental and computational approaches to estimate solubility and permeability in drug discovery and development settings*. Adv Drug Deliv Rev, 2001. **46**(1-3): p. 3-26.
152. Blake, J.F., *Cheminformatics - predicting the physicochemical properties of 'drug-like' molecules*. Curr Opin Biotechnol, 2000. **11**(1): p. 104-7.
153. Ertl, P., B. Rohde, and P. Selzer, *Fast calculation of molecular polar surface area as a sum of fragment-based contributions and its application to the prediction of drug transport properties*. J Med Chem, 2000. **43**(20): p. 3714-7.
154. van de Waterbeemd, H., et al., *Estimation of blood-brain barrier crossing of drugs using molecular size and shape, and H-bonding descriptors*. J Drug Target, 1998. **6**(2): p. 151-65.
155. Pajouhesh, H. and G.R. Lenz, *Medicinal Chemical Properties of Successful Central Nervous System Drugs*. NeuroRx, 2005. **2**(4): p. 541-553.
156. Ginouves, M., et al., *Comparison of Tetrazolium Salt Assays for Evaluation of Drug Activity against Leishmania spp.* Journal of Clinical Microbiology, 2014. **52**(6): p. 2131-2138.
157. Lutter, A.H., et al., *Applying XTT, WST-1, and WST-8 to human chondrocytes: A comparison of membrane-impermeable tetrazolium salts in 2D and 3D cultures*. Clinical Hemorheology and Microcirculation, 2017. **67**(3-4): p. 327-342.
158. Antunes, M. and G. Biala, *The novel object recognition memory: neurobiology, test procedure, and its modifications*. Cognitive Processing, 2012. **13**(2): p. 93-110.

159. Antunes, M. and G. Biala, *The novel object recognition memory: neurobiology, test procedure, and its modifications*. Cogn Process, 2012. **13**(2): p. 93-110.
160. Rajagopal, L., et al., *The novel object recognition test in rodents in relation to cognitive impairment in schizophrenia*. Curr Pharm Des, 2014. **20**(31): p. 5104-14.
161. Bevins, R.A. and J. Besheer, *Object recognition in rats and mice: a one-trial non-matching-to-sample learning task to study 'recognition memory'*. Nat Protoc, 2006. **1**(3): p. 1306-11.
162. Vogel-Ciernia, A. and M.A. Wood, *Examining object location and object recognition memory in mice*. Curr Protoc Neurosci, 2014. **69**: p. 8.31.1-17.
163. Leger, M., et al., *Object recognition test in mice*. Nat Protoc, 2013. **8**: p. 2531.
164. Lueptow, L.M., *Novel Object Recognition Test for the Investigation of Learning and Memory in Mice*. J Vis Exp, 2017(126).
165. Meneses, A., *Stimulation of 5-HT1A, 5-HT1B, 5-HT2A/2C, 5-HT3 and 5-HT4 receptors or 5-HT uptake inhibition: short- and long-term memory*. Behav Brain Res, 2007. **184**(1): p. 81-90.
166. Nazir, N., et al., *Phytochemical analysis, molecular docking and anti-amnesic effects of methanolic extract of Silybum marianum (L.) Gaertn seeds in scopolamine induced memory impairment in mice*. Journal of Ethnopharmacology, 2018. **210**: p. 198-208.
167. Brown, P.L. and H.M. Jenkins, *Auto-shaping of the pigeon's key-peck*. Journal of the Experimental Analysis of Behavior, 1968. **11**(1): p. 1-8.

168. Manuel-Apolinar, L. and A. Meneses, *8-OH-DPAT facilitated memory consolidation and increased hippocampal and cortical cAMP production*. Behav Brain Res, 2004. **148**(1-2): p. 179-84.
169. Meneses, A., *A Pharmacological Analysis of an Associative Learning Task: 5-HT(1) to 5-HT(7) Receptor Subtypes Function on a Pavlovian/Instrumental Autoshaped Memory*. Learning & Memory, 2003. **10**(5): p. 363-372.
170. Vanover, K.E. and J.E. Barrett, *An automated learning and memory model in mice: pharmacological and behavioral evaluation of an autoshaped response*. Behav Pharmacol, 1998. **9**(3): p. 273-83.
171. Barrett, J.E. and K.E. Vanover, *Assessment of learning and memory using the autoshaping of operant responding in mice*. Curr Protoc Neurosci, 2004. **Chapter 8**: p. Unit 8.5F.
172. Meneses, A., et al., *5-HT7 receptor activation: procognitive and anti-amnesic effects*. Psychopharmacology (Berl), 2015. **232**(3): p. 595-603.
173. Foley, J.J., R.B. Raffa, and E.A. Walker, *Effects of chemotherapeutic agents 5-fluorouracil and methotrexate alone and combined in a mouse model of learning and memory*. Psychopharmacology, 2008. **199**(4): p. 527-538.
174. Bisen-Hersh, E.B., P.N. Hineline, and E.A. Walker, *Effects of Early Chemotherapeutic Treatment on Learning in Adolescent Mice: Implications for Cognitive Impairment and Remediation in Childhood Cancer Survivors*. Clinical cancer research : an official journal of the American Association for Cancer Research, 2013. **19**(11): p. 3008-3018.
175. Walker, E.A., et al., *Effects of repeated administration of chemotherapeutic agents tamoxifen, methotrexate, and 5-fluorouracil on the acquisition and*

- retention of a learned response in mice.* Psychopharmacology (Berl), 2011. **217**(4): p. 539-548.
176. Neri, D. and C.T. Supuran, *Interfering with pH regulation in tumours as a therapeutic strategy.* Nat Rev Drug Discov, 2011. **10**(10): p. 767-77.
177. Akocak, S. and M.A. Ilies, *Next-generation primary sulfonamide carbonic anhydrase inhibitors,* in *Targeting carbonic anhydrases,* C.T. Supuran and C. Capasso, Editors. 2014, Future Science: London. p. 35-51.
178. Supuran, C.T. and A. Scozzafava, *Carbonic anhydrase inhibitors and their therapeutic potential.* Expert Opinion on Therapeutic Patents, 2000. **10**(5): p. 575-600.
179. Supuran, C.T., *Carbonic anhydrase inhibitors.* Bioorg Med Chem Lett, 2010. **20**(12): p. 3467-74.
180. Supuran, C.T., *Carbonic anhydrases: novel therapeutic applications for inhibitors and activators.* Nature Reviews Drug Discovery, 2008. **7**: p. 168-181.
181. Supuran, C.T., *How many carbonic anhydrase inhibition mechanisms exist? J Enzyme Inhib Med Chem,* 2016. **31**(3): p. 345-60.
182. Alterio, V., et al., *Crystal structure of the catalytic domain of the tumor-associated human carbonic anhydrase IX.* Proc Natl Acad Sci U S A, 2009. **106**(38): p. 16233-8.
183. Whittington, D.A., et al., *Crystal structure of the dimeric extracellular domain of human carbonic anhydrase XII, a bitopic membrane protein overexpressed in certain cancer tumor cells.* Proc Natl Acad Sci U S A, 2001. **98**(17): p. 9545-50.

184. Chaffer, C.L. and R.A. Weinberg, *How does multistep tumorigenesis really proceed?* *Cancer Discov*, 2015. **5**(1): p. 22-4.
185. Hanahan, D. and R.A. Weinberg, *Hallmarks of cancer: the next generation*. *Cell*, 2011. **144**(5): p. 646-74.
186. McDonald, P.C., S.C. Chafe, and S. Dedhar, *Overcoming Hypoxia-Mediated Tumor Progression: Combinatorial Approaches Targeting pH Regulation, Angiogenesis and Immune Dysfunction*. *Front Cell Dev Biol*, 2016. **4**: p. 27.
187. Parks, S.K., J. Chiche, and J. Pouyssegur, *pH control mechanisms of tumor survival and growth*. *J Cell Physiol*, 2011. **226**(2): p. 299-308.
188. Vander Heiden, M.G., L.C. Cantley, and C.B. Thompson, *Understanding the Warburg effect: the metabolic requirements of cell proliferation*. *Science*, 2009. **324**(5930): p. 1029-33.
189. Wykoff, C.C., et al., *Hypoxia-inducible expression of tumor-associated carbonic anhydrases*. *Cancer Res*, 2000. **60**(24): p. 7075-83.
190. Saarnio, J., et al., *Immunohistochemical study of colorectal tumors for expression of a novel transmembrane carbonic anhydrase, MN/CA IX, with potential value as a marker of cell proliferation*. *Am J Pathol*, 1998. **153**(1): p. 279-85.
191. Dubois, L., et al., *Imaging the hypoxia surrogate marker CA IX requires expression and catalytic activity for binding fluorescent sulfonamide inhibitors*. *Radiother Oncol*, 2007. **83**(3): p. 367-73.
192. De Simone, G. and C.T. Supuran, *Carbonic anhydrase IX: Biochemical and crystallographic characterization of a novel antitumor target*. *Biochim Biophys Acta*, 2010. **1804**(2): p. 404-9.

193. Swietach, P., et al., *Tumor-associated carbonic anhydrase 9 spatially coordinates intracellular pH in three-dimensional multicellular growths*. J Biol Chem, 2008. **283**(29): p. 20473-83.
194. Donovan, L., et al., *Hypoxia—implications for pharmaceutical developments*. Sleep & breathing = Schlaf & Atmung, 2010. **14**(4): p. 291-298.
195. Akocak, S., et al., *PEGylated Bis-Sulfonamide Carbonic Anhydrase Inhibitors Can Efficiently Control the Growth of Several Carbonic Anhydrase IX-Expressing Carcinomas*. J Med Chem, 2016. **59**(10): p. 5077-88.
196. Supuran, C.T., *Inhibition of carbonic anhydrase IX as a novel anticancer mechanism*. World J Clin Oncol, 2012. **3**(7): p. 98-103.
197. Supuran, C.T., *Structure-based drug discovery of carbonic anhydrase inhibitors*. J Enzyme Inhib Med Chem, 2012. **27**(6): p. 759-72.
198. Ilies, M.A., et al., *Carbonic anhydrase inhibitors. Inhibition of tumor-associated isozyme IX by halogenosulfanilamide and halogenophenylaminobenzolamide derivatives*. J Med Chem, 2003. **46**(11): p. 2187-96.
199. Akocak, S., et al., *Synthesis and biological evaluation of novel aromatic and heterocyclic bis-sulfonamide Schiff bases as carbonic anhydrase I, II, VII and IX inhibitors*. Bioorg Med Chem, 2017. **25**(12): p. 3093-3097.
200. Pastorekova, S., S. Parkkila, and J. Zavada, *Tumor-associated Carbonic Anhydrases and Their Clinical Significance*. Advances in Clinical Chemistry, 2006. **42**: p. 167-216.

201. Tinker, J.P., R. Coulson, and I.M. Weiner, *Dextran-bound inhibitors of carbonic anhydrase*. *Journal of Pharmacology and Experimental Therapeutics*, 1981. **218**(3): p. 600-607.
202. Veronese, F.M. and A. Mero, *The impact of PEGylation on biological therapies*. *BioDrugs*, 2008. **22**(5): p. 315-29.
203. Mack, E.T., et al., *Dependence of Avidity on Linker Length for a Bivalent Ligand-Bivalent Receptor Model System*. *Journal of the American Chemical Society*, 2012. **134**(1): p. 333-345.
204. Supuran, C.T., M.A. Ilies, and A. Scozzafava, *Carbonic anhydrase inhibitors — Part 29 I: Interaction of isozymes I, II and IV with benzolamide-like derivatives*. *European Journal of Medicinal Chemistry*, 1998. **33**(9): p. 739-751.
205. Supuran, C.T., et al., *Carbonic anhydrase inhibitors — Part 53. Synthesis of substituted-pyridinium derivatives of aromatic sulfonamides: The first non-polymeric membrane-impermeable inhibitors with selectivity for isozyme IV*. *European Journal of Medicinal Chemistry*, 1998. **33**(7): p. 577-594.
206. Supuran, C.T., et al., *Carbonic anhydrase inhibitors: synthesis of sulfonamides incorporating 2,4,6-trisubstituted-pyridinium-ethylcarboxamido moieties possessing membrane-impermeability and in vivo selectivity for the membrane-bound (CA IV) versus the cytosolic (CA I and CA II) isozymes*. *J Enzyme Inhib*, 2000. **15**(4): p. 381-401.
207. Scozzafava, A., et al., *Carbonic Anhydrase Inhibitors: Synthesis of Membrane-Impermeant Low Molecular Weight Sulfonamides Possessing in Vivo Selectivity for the Membrane-Bound versus Cytosolic Isozymes*. *J Med Chem*, 2000. **43**(2): p. 292-300.

208. Akocak, S., *Design and delivery of selective inhibitors of tumor-overexpressed isozymes of carbonic anhydrase - towards new theranostic systems for cancer detection and treatment, Dissertation defense in Pharmaceutical Sciences, School of Pharmacy*. 2014, Temple University: Philadelphia. p. 121.